Application of Microwave Heating to Thermogravimetric Analysis and Synthesis of Functional Particulate Materials

（熱重量分析と機能性粉体材料合成へのマイクロ波加熱法の利用）

By

Achmad Dwitama Karisma

D153372

HIROSHIMA UNIVERSITY

SEPTEMBER 2018

Application of Microwave Heating to Thermogravimetric Analysis and Synthesis of Functional Particulate Materials

（熱重量分析と機能性粉体材料合成へのマイクロ波加熱法の利用）

A Thesis submitted to
The Department of Chemical Engineering
Graduate School of Engineering
Hiroshima University

By
Achmad Dwitama Karisma
D153372

In Partial Fulfillment of Requirements
For the Degree of
Doctor Engineering

Hiroshima University
SEPTEMBER 2018

Approved by

Professor Kunihiro Fukui
Advisor

ABSTRACT

Microwave heating technology has an increasing attention for miscellaneous purposes, especially in the material synthesis field, because of their advantages in rapidly heating rate, selectivity material in heating process, and improving the quality of product. The interaction between electromagnetic energy and the materials in the microwave heating process is related to the dielectric properties and the characteristics of the materials. It is expected that the dielectric properties of the materials are changed by the temperature condition during the microwave heating process. Therefore, the understanding in the mechanism of the microwave heating and its application in the material synthesis should be clarified.

In this dissertation, the microwave heating mechanism using the developed single mode type of microwave thermogravimetric and its application on the material synthesis was investigated. The potassium-type zeolite, NiCuZn ferrite, and Cu-Ce-Zr oxide nanoparticles were synthesized by microwave heating method.

Chapter 1 describes the background and the motivation of current research. Basic theoretical explanation of microwave heating technology and microwave dielectric properties were provided. Further, the review of previous researches on microwave heating application on the material synthesis was also discussed in this chapter.

Chapter 2 explains the mechanism of the microwave heating process throughout the development of the single-mode type microwave heating thermogravimetry (MWTG) apparatus. The temperature distribution, microwave absorption efficiency, and permittivity loss of copper oxide (CuO) pellet heated by microwave irradiation were investigated to clarify the validation of the developed single-mode type MWTG apparatus. The result shows that the numerically determined dependency of the CuO microwave absorption efficiency and permittivity loss at various temperature condition were found to be in good agreement with the published data.

In chapter 3 to chapter 5, the application of the microwave heating to the synthesis of functional particulate materials was investigated. Chapter 3 investigates the synthesis of potassium-type zeolite (K-zeolite) from the coal fly ash and biomass incineration fly ash by microwave heating hydrothermal treatment. The effect of microwave heating on

the crystalline zeolite synthesis rate was investigated by comparison with external heating method. It was found that the zeolite crystal formation rate obtained by microwave heating method was higher than that by the external heating method. Further, the ammonium adsorption capacity of the K-zeolite synthesized by both method was almost the same, indicating that the heating method did not affect the properties of the obtained zeolite.

Chapter 4 explain the synthesis of NiCuZn ferrite nanoparticle by the microwave direct denitration reaction (MDD) method. $Ni_{0.5}Cu_{0.1}Zn_{0.4}Fe_2O_3$ could be synthesized from a mixture of metal nitrate hydrate solutions. The result shows that MDD method could provide the single phase of NiCuZn ferrite powder with an average particle diameter of about 30 nm at a reaction temperature of 900^{o}C. The particle diameter was less than one-fifth of that by the solid state reaction (SSR) method from the mixture of metal oxide powder at the same reaction temperature. The saturation magnetization of product synthesized by MDD method was found 25.08 emu/g, which was more than three time that by SSR method. On the other hand, the coercivity of the product synthesized by MDD, 55.21 Oe was found about half of that obtained by SSR method. This result suggests that the MDD method could provide more attractive magnetic characteristics of NiCuZn ferrite nanoparticle to the product powder.

The MDD method was also applied to the synthesis of Cu-Ce-Zr oxide, which investigated in chapter 5. The $Ce_{0.6}Zr_{0.4}O_2$:Cu catalyst (CCZ catalyst) nanoparticles were synthesized by MDD method and compared their properties with those by the citric acid method. As a result, the CCZ catalyst could be obtained below 20% of Cu doping ratio by both methods. The MDD method could provide the larger specific surface area of CCZ catalyst product than those by the citric acid method, i.e. 68.0 m^2/g and 30 m^2/g, respectively. However, the CCZ nanoparticles synthesized by citric acid method had a little higher oxygen storage capacity (OSC) value than those by MDD method.

Chapter 6 contains the summary of all chapters and direction for further investigation.

Contents

List of Figures

List of Tables

CHAPTER 1

INTRODUCTION

1.1 Microwave Heating Technology

The microwave is the electromagnetic radiation with the wavelengths ranging from 1 mm to 1 m, and the frequencies range between 300 MHz and 300 GHz. The frequencies 915 MHz and 2.45 GHz are the most common among those dedicated to power applications for industrial, scientific, and medical purpose because these frequencies correspond to significant penetration depth within most of the materials. Microwave can be generated by various devices, such as a magnetron, klystrons, power grid tubes, and gyrotron. The most common devices used as a source is magnetron which is more efficient, reliable, and available at lower cost than other sources[1].

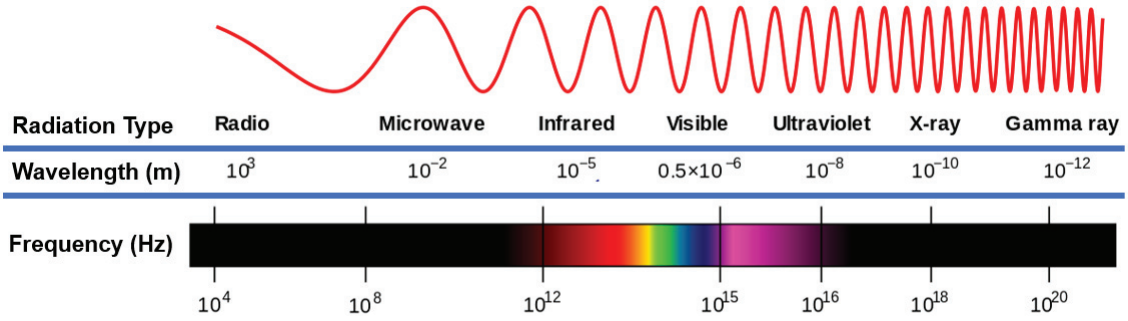

Figure 1.1 Diagram of the electromagnetic spectrum

Firstly, microwave technology adopted for communications and remote sensing scopes such as broadcasting, radar, and navigation. An increasing attention to microwave application as a thermal purpose has been gained since World War II. Since then, microwave heating has been used for miscellaneous purposes, such as food processing [2–8], drying process [9–15], synthesis of materials [16–22], ceramics processing [23–27], chemical organic reaction[28–30], etc. The reason for high interest in the microwave heating research field is because of its some advantages compared with the conventional heating, such as a higher heating rate, clean energy, selected heating, and improve the quality of the product powder, such as the particle size and crystallinity in the synthesis of materials field.

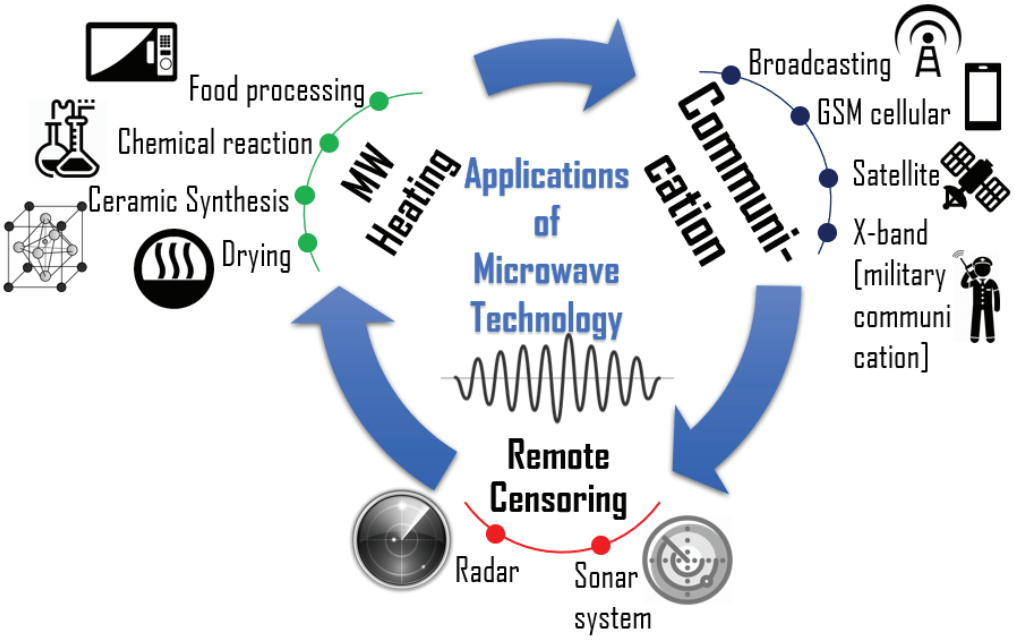

Figure 1.2 Applications of microwave technology

The mechanism of microwave heating is different from the conventional heating. At the conventional heating, the heat transfer involves the conduction or the convection from the surface to the center of the material. On the other hand, the microwave heating involves the conversion from the electromagnetic energy to thermal energy. The electromagnetic radiation will be heated up the material because of the ion and molecule of material are oscillated by the penetrated microwave. The heat generation was throughout the volume of material, resulting in the volumetric heating[31]. Therefore, the microwave heating could provide the higher heating rate than conventional heating.

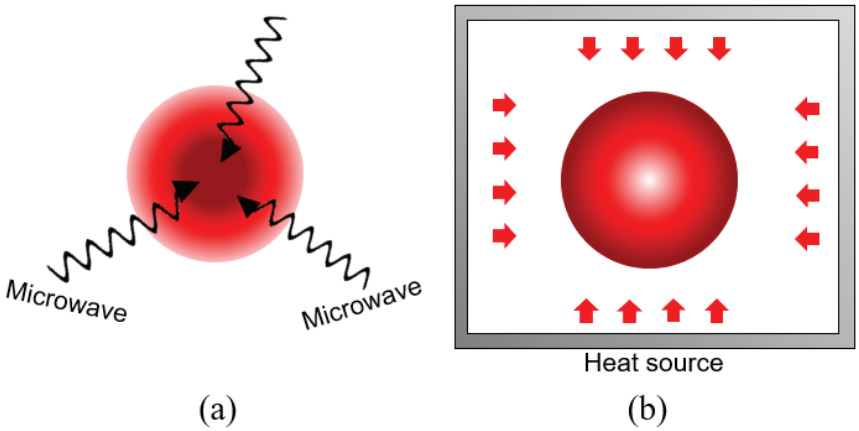

Figure 1.3 The difference of heating pattern between (a) microwave heating and (b) conventional heating

There are two types of commonly used microwave cavity systems, single-mode type and multimode type. The volume of the cavity in multimode type microwave is large, causes the multiple electromagnetic field distribution due to the scattering from walls and through the sample at random angles[8]. These are broadly similar to the domestic microwave oven in operation. The single mode type, the sample material is heated by one-way traveling microwave. The sample is positioned to be at peak maximum of the electric component of the microwave field[32].

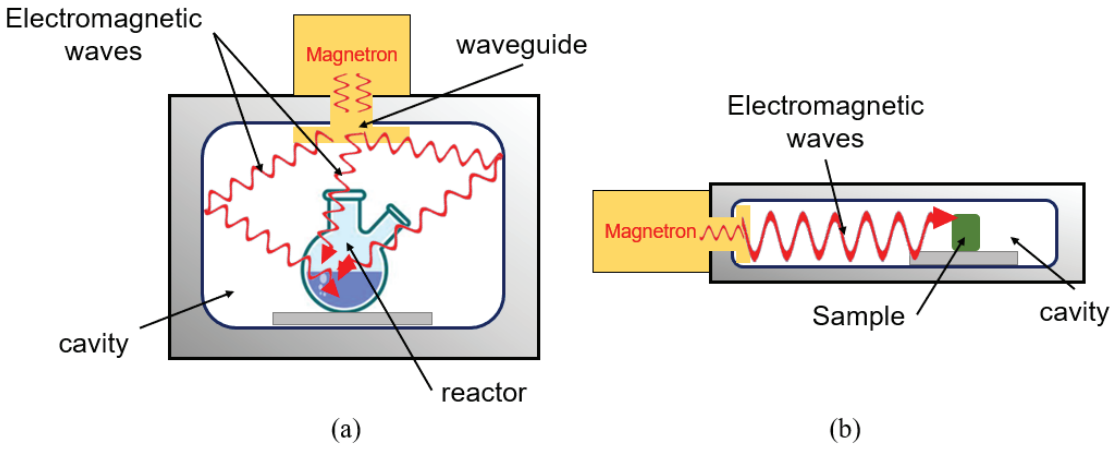

Figure 1.4 Schematic of (a) multimode and (b) single mode type of microwave system

In some previous works, the study about microwave thermal analysis has been investigated. Karmazsin first developed the concept of applying microwave heating to thermal analysis[33,34]. Recently, Parkes et al, have developed the microwave thermal analysis instrument utilizing multimode microwave type[35] and single mode type[36,37]. However, the mechanism of microwave heating, such as microwave absorption, dielectric properties, and temperature distribution in the sample material during microwave heating has not been clarified sufficiently.

1.2 Microwave dielectric properties

The microwave heating is depended on the ability of the material to absorb the irradiation microwave. Based on the interaction with microwave, the material can be classified into three types: (1) Electrical conductor material, where the microwave is reflected and unabsorbed, typified by bulk metals and alloys. (2) Transparent or low dielectric loss material, in which the microwave is neither reflected, nor absorbed, typified by fused quartz, Teflon, and several glasses. (3) Absorbers or high dielectric loss material, which absorb the microwave energy to a certain degree based on the value of permittivity loss factor and convert it to heat energy, e.g. an aqueous solution, a polar solvent, etc.[38].

The interaction between material and electromagnetic energy is related to the dielectric properties (complex permittivity, ε) of the material. Complex permittivity is consisted of real permittivity, ε' and imaginary permittivity, ε''. The complex permittivity could be expressed as,

$$\varepsilon = \varepsilon' + j\varepsilon'' \tag{1.1}$$

Real permittivity, or usually called dielectric constant, is a measure of how much energy from an external electric field is stored in the material. On the other hand, imaginary permittivity, known as dielectric loss, represents the ability of the material to convert the absorbed energy into heat.

$$\varepsilon'' = \varepsilon' + \frac{\sigma}{\omega\varepsilon_0} \tag{1.2}$$

Where σ is the electrical conductivity of the material, ω is the angular frequency of the radiation ($\omega = 2\pi f$, where f is the microwave frequency. The ratio of the dielectric loss to the dielectric constant is known as the loss tangent (tan δ) which given,

$$\tan\delta = \frac{\kappa''}{\kappa'} = \frac{\varepsilon''}{\varepsilon'} \tag{1.3}$$

κ' and κ'' are relative dielectric constant and relative dielectric loss respectively, which are given as $\kappa' = \frac{\varepsilon'}{\varepsilon_0}$ and $\kappa'' = \frac{\varepsilon''}{\varepsilon_0}$, where ε_0 is the vacuum permittivity ($\varepsilon_0 = 8.85 \cdot 10^{-12} F/m$).

The power dissipated per unit volume of material p can be derived using the equation,

$$p = \frac{\omega}{2}(\varepsilon_0 \varepsilon'' \|\boldsymbol{E}\|^2 + \mu_0 \mu'' \|\boldsymbol{H}\|^2) \tag{1.4}$$

Here, $\boldsymbol{H}$ and $\boldsymbol{E}$ are the magnetic and electric field vector, respectively. μ'' and μ_0 are relative permeability and vacuum permeability, respectively[39].

1.3 Material synthesis by microwave heating treatment

Recently, the material synthesis using microwave heating treatment has attracted much attention from the researchers. With all of its advantages and unique performance characteristics as mentioned above, microwave heating treatment has a promising potential to be applied in the synthesize of some functional particulate materials.

1.3.1 Synthesis of organic materials

One of microwave heating application is the synthesis of organic materials. Under the microwave irradiation, the organic reaction can be accelerated and the selectivities of products can be obtained by control the microwave parameters. Since the 1986[28], the microwave heating become an interesting preparation methods on the synthesis of organic chemistry.

Palombi et al. [40] in 1997 reported the oxidation of alcohol using t-butyl hydroperoxide (TBHP) supported on zeolite under the microwave irradiation. The application of microwave heating and molecular catalysis has allowed the advantage in simplicity of the process, cheap, and environmentally safe in oxidative procedure. Moreover, the microwave assisted method can provide the short reaction times under solvent free conditions.

Chighine et.al.[41] has been synthesized carboxylic esters via reaction of carboxylic acid with O-alkylisoureas using microwave-assisted method. The result shows that microwave-assisted method produce excellent ester formation yield with clean inversion of configuration. Moreover, microwave-assisted method could shorten

the reaction time become only for 5 min or less, even without additional reagent or catalyst.

1.3.2 Synthesis of zeolite from coal fly ash

The research about microwave synthesis of zeolite has been started at the end of 80's and began the increased year by year especially after the middle of 90's [42]. Zeolite is crystalline aluminosilicates consist of a tetrahedral framework of $[SiO_4]^{4+}$ and $[AlO_4]^{5-}$ linked to each other at the corner by sharing oxygen atoms[43]. It has wide applications as an adsorption, catalytic activity, air purification, and so on.

Zeolite can be synthesized from many different materials. Querol et al. synthesized the zeolite material from fly ash by conventional and microwave-assisted hydrothermal method[44]. The synthesized yield and zeolite type obtained from the microwave-assisted and conventional method were very similar. However, the activation time was drastically reduced by the microwave-assisted method, from 24-48 h to 30 min. This result shows that the microwave heating could provide the synthesized zeolite from fly ash effectively. Moreover, it also has an important potential for the recycling of solid wastes, for example, coal fly ash, in industrial application.

Coal fly ash is an industrial byproduct and could be obtained by the electrostatic or mechanical precipitation of dust-like particles from the flue gases of furnaces fired with pulverized coal. The use of coal fly ash as a raw material of synthesized zeolite has been focused in the last few years. The interest in the zeolite synthesis from coal fly ash was increased due to the relationship between the environmental issue and the waste/ byproduct utilization.

Fukui et al. reported that the phillipsite zeolite could be synthesized by hydrothermal with microwave heating method[45,46]. The microwave heating reduces the particle size of synthesized phillipsite and makes the waiting time for the beginning of crystallization much shorter than conventional heating. Moreover, the microwave heating treatment enhances the rate and constant value of the adsorption capacity of the product powder.

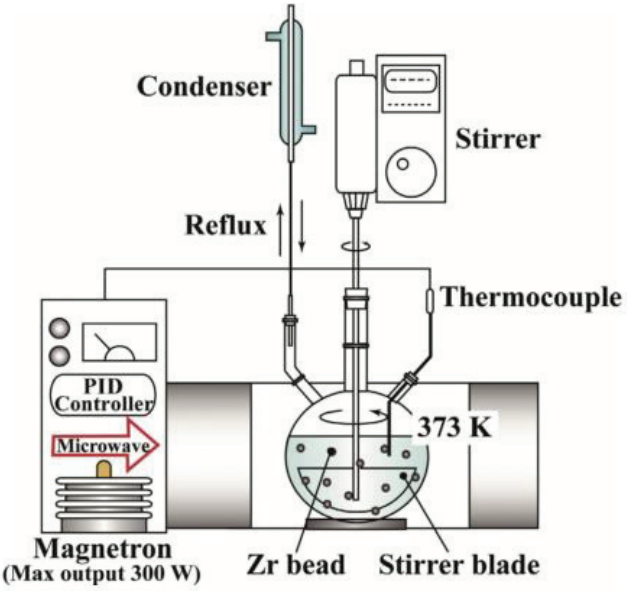

Figure 1.5 Schematic of experimental setup microwave hydrothermal treatment with pulverization process[47]

Fukasawa et al. also synthesized the zeolite from coal fly ash by microwave hydrothermal treatment with pulverization process[47]. The slurry of coal fly ash was pulverized by zirconia bead before and during the microwave hydrothermal treatment. Figure 1.5 shows the schematic of the experimental setup for the pulverization process during microwave hydrothermal treatment. The pulverization of the slurry before thermal treatment promoted the generation of byproduct hydroxysodalite than phillipsite. On the other hand, the partial pulverization during only the first hour of the microwave hydrothermal treatment can improve the ammonium-ion adsorption capacity of the product, correspond to the generation rate of phillipsite. Moreover, partial pulverization is effective in reducing of treatment time because it increases the dissolution mass per unit time of aluminate and silicate ions from coal fly ash.

1.3.3 Synthesis of the material by denitration reaction

The microwave heating application also appropriate to synthesize the material that involves the chemical reaction. Fukui et al. have reported the mechanism of synthesis of metallic oxide powder from metallic nitrate solution by microwave denitration method[48]. The CuO powder can be synthesized from $Cu(NO_3)_2 \cdot 3H_2O$ solution by microwave heating treatment. It was found that the route of denitration reaction by

microwave heating is the same as those by conventional external heating. Figure 1.4 shows the XRD pattern of the synthesized products at various reaction temperature. As the reaction temperature increases, the crystal water is gradually evaporated and at the temperature of 150 ^{o}C, the crystalline phase of $Cu(NO_3)_2 \cdot 2.5H_2O$ is obtained. Then it decomposes to the intermediate product $Cu_3(NO_3)(OH)_3$ and nitrogen oxide gas at 250 ^{o}C. Finally, at the reaction temperature of 600 ^{o}C, the final product of CuO powder was formed. From these result, the sequence for the denitration reaction of $Cu(NO_3)_2 \cdot 3H_2O$ by microwave heating could be expressed as follows:

$Cu(NO_3)_2 \cdot 3H_2O \rightarrow Cu(NO_3)_2 \cdot 2.5H_2O \rightarrow Cu_3(NO_3)(OH)_3 \rightarrow CuO$

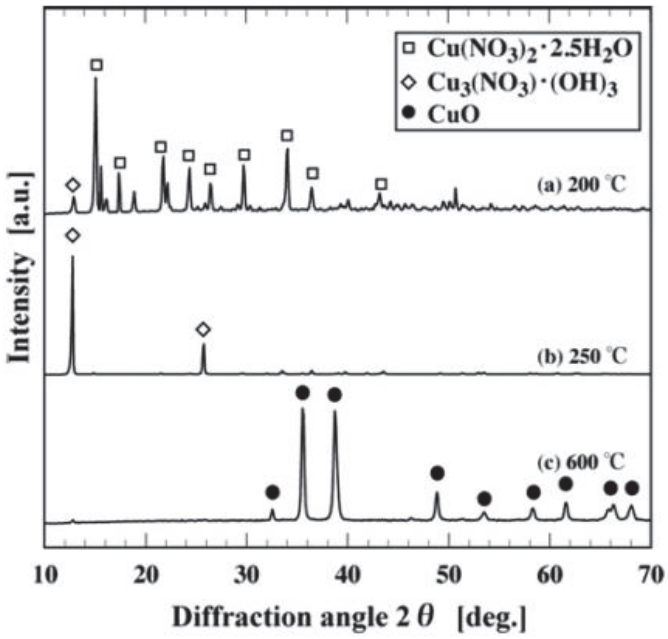

Figure 1.6 XRD pattern of the intermediate and final product obtained from $Cu(NO_3)_2 \cdot 3H_2O$

On the other hand, in case of $Ni(NO_3)_2 \cdot 6H_2O$ solution irradiated by microwave, the reaction temperature could not be increased more than 270 ^{o}C, and a little of nitrogen oxide gas was detected. Moreover, the intermediate product $Ni_3(NO_3)_2(OH)_4$ was obtained at this reaction temperature. It was thought that the intermediate product $Ni_3(NO_3)_2(OH)_4$ has low microwave absorptivity, therefore, as shown in figure 1.7, the temperature could not reach the denitration reaction temperature, then it could not decompose to the NiO product. From these results, it is indicated that the denitration reaction by microwave heating method was not only depended on the microwave

absorptivity of the intermediate and final product but also the temperature difference between the completion of the intermediate conversion and the beginning of the final product conversion.

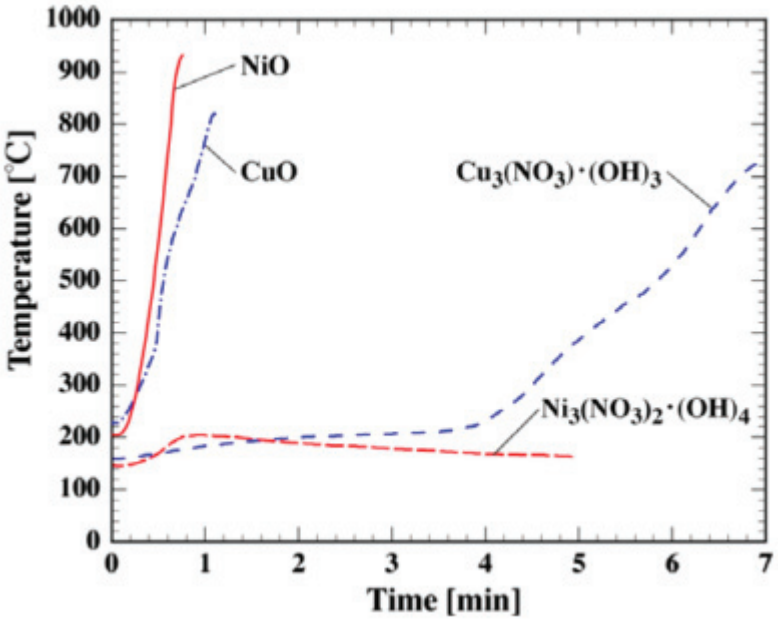

Figure 1.7 Change in temperature with microwave irradiation time for the metallic oxides and the acquired intermediates[48]

Segawa et al. have successfully synthesized the NiO powder from $Ni(NO_3)_2 \cdot 6H_2O$ solution by microwave denitration method with the addition of NiO powder reagent in the raw material solution[49]. The addition of NiO powder in the raw material to function as a microwave acceptor. NiO powder was chosen to be the addition material because it has high microwave absorptivity. Moreover, it was expected that the addition of NiO powder could not affect the final product of the denitration reaction. With the addition of NiO powder, the reaction temperature could be increased over 270 ^{o}C monotonically and the denitration reaction to NiO powder can be successfully completed by microwave heating method without any by-product in the final reaction.

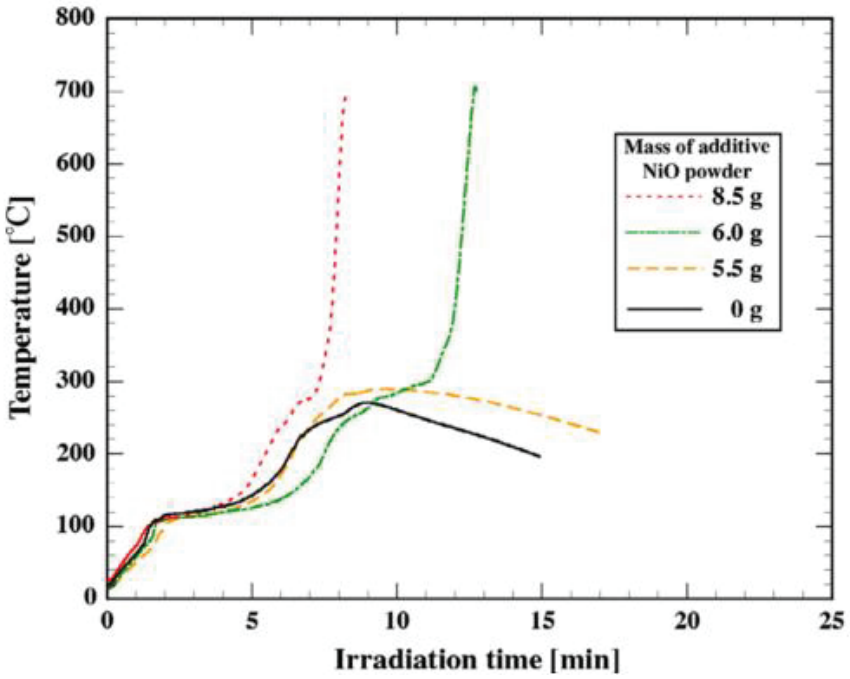

Figure 1.8 Change in temperature with microwave irradiation time for the $Ni(NO_3)_2 \cdot 6H_2O$ aqueous solution or suspension[49]

1.3.4 Synthesis of ceramics

The synthesis of ceramic materials by microwave heating assisted has been investigated by some previous works. Spinel ferrites ceramics (MFe_2O_4, where M is divalent cation) which considered as important electronic material, have been prepared by conventional ceramic and wet chemical methods. The wet chemical methods with hydrothermal process appear to have much attention for preparing fine crystallized ferrite powder[50]. For this reason, the introducing microwave heating assisted in the hydrothermal process is advantageous due to it can reduce processing time and energy cost.

In 1998, Komarneni et al.[51] prepared some spinel ferrite ceramics, such as $ZnFe_2O_4$, $NiFe_2O_4$, $MnFe_2O_4$, and $CoFe_2O_4$ by microwave-assisted synthesis method. The nitrates of zinc, nickel, manganese, and cobalt solutions were mixed with ferric nitrate as a raw material and neutralized with ammonia to a specific pH, then irradiated with the microwave using a microwave digestion system. Nanophase ferrites with high surface areas, in range of 72-247 m^2/g can be synthesized in a few minutes at a low temperature of 164ºC. This rapid synthesis of nanophase ferrites is expected to lead to energy savings.

Kim et al. also synthesized Co-Zn ferrite and Ni-Zn ferrite powders by microwave-hydrothermal method[52]. The reagent of $FeCl_3 \cdot 6H_2O$, $NiCl_2 \cdot 6H_2O$, $CoCl_2 \cdot 6H_2O$, and $ZnCl_2$ was used as the starting materials. It has been reported that the nanoparticles spinel ferrite powders with average particle about 10 nm have been successfully synthesized at the relatively low reaction temperature. They also obtained that the conventional hydrothermal method requires a relatively higher temperature and longer reaction time than the microwave method to promote crystallization. In microwave method, the crystallization of the spinel ferrites was promoted by the increase in reaction temperature and time. However, the magnetic properties of the products have not been investigated yet.

Recently, Farinas et al. prepared the Cobalt ferrites powder from the mixture of $Fe(NO_3)_3 \cdot 9H_2O$ and $Co(NO_3)_2 \cdot 6H_2O$, with NH_4OH and TPAH as a precipitating reagent by microwave-assisted hydrothermal method[53]. The nanocrystalline $CoFe_2O_4$ with the size of 5-10 nm could be synthesized by microwave-assisted method with both precipitating reagents. The nanoparticles of the products also have a uniform structure and highly dispersed without hard agglomerates. Moreover, the sintering process improves the crystallinity and enhanced the magnetic saturation properties of the product samples. It shows that microwave synthesis method is a promising technique to produce the spinel ferrite with a high quality in microstructure and the magnetic properties.

From these previous works, it was thought that with all of the advantages and unique characteristics, the microwave heating treatment is a promising method to synthesize the important material, such as ceramics and catalysts, that involves the chemical reactions. In this study, the synthesis of some particulate material which involves the denitration reaction by microwave heating method was investigated. The NiCuZn ferrite and Cu-Ce-Zr oxide nanoparticles were synthesized from the mixed metallic nitrate hydrate solution by microwave heating method.

1.4 Objectives and Outline of the Dissertation

The main objectives of this dissertation are to investigate the microwave heating mechanism using the developed single mode type of microwave thermogravimetric and its application on the material synthesis. The potassium-type zeolite, NiCuZn ferrite, and Cu-Ce-Zr oxide nanoparticles were synthesized by microwave heating method. The

schematic diagram of dissertation organization is shown in Figure 1.9. The brief descriptions of each chapter are shown below.

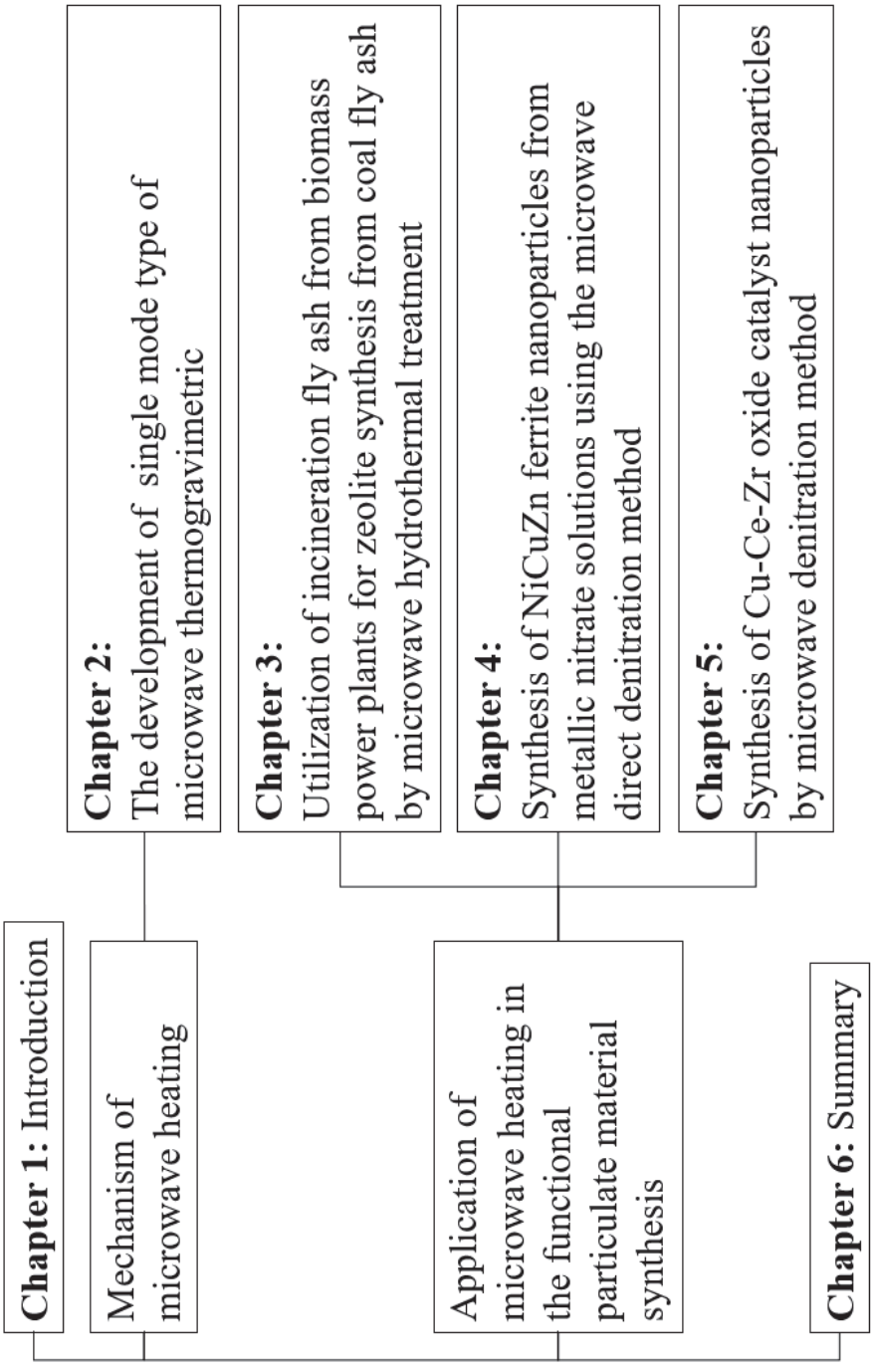

Figure 1.9 Organization and structure of chapters in the present dissertation

Chapter 1 describes the background and the motivation of current research. Basic theoretical explanation of microwave heating technology and microwave dielectric

properties were provided. Further, the review of previous researches on microwave heating application on the material synthesis was also discussed in this chapter.

Chapter 2 explains the mechanism of the microwave heating process throughout the development of the single-mode type microwave heating thermogravimetry (MWTG) apparatus. The temperature distribution, microwave absorption efficiency, and dielectric properties of copper oxide (CuO) pellet heated by microwave irradiation were investigated to clarify the validation of the developed single-mode type MWTG apparatus. The result shows that the numerically determined dependency of the CuO microwave absorption efficiency and dielectric properties, i.e. permittivity loss at various temperature condition were found to be in good agreement with the published data.

In chapter 3 to chapter 5, the application of the microwave heating to the synthesis of functional particulate materials was investigated. **Chapter 3** investigates the synthesis of potassium-type zeolite (K-zeolite) from the coal fly ash and biomass incineration fly ash by microwave heating hydrothermal treatment. The effect of microwave heating on the crystalline zeolite synthesis rate was investigated by comparison with the external heating method. It was found that the zeolite crystal formation rate obtained by microwave heating method was higher than that by the external heating method. Further, the ammonium adsorption capacity of the K-zeolite synthesized by both method was almost the same, indicating that the heating method did not affect the properties of the obtained zeolite.

Chapter 4 explain the synthesis of NiCuZn ferrite nanoparticle by the microwave direct denitration reaction (MDD) method. $Ni_{0.5}Cu_{0.1}Zn_{0.4}Fe_2O_4$ could be synthesized from a mixture of metal nitrate hydrate solutions. The result shows that MDD method could provide the single phase of NiCuZn ferrite powder with an average particle diameter of about 30 nm at a reaction temperature of 900ºC. The particle diameter was less than one-fifth of that by the solid state reaction (SSR) method from the mixture of metal oxide powder at the same reaction temperature. The saturation magnetization of product synthesized by MDD method was found 25.08 emu/g, which was more than three time that by SSR method. On the other hand, the coercivity of the product synthesized by MDD, 55.21 Oe was found about half of that obtained by SSR method. This result suggests that the MDD method could provide more attractive magnetic characteristics of NiCuZn ferrite nanoparticle to the product powder.

The MDD method was also applied to the synthesis of Cu-Ce-Zr oxide, which investigated in **chapter 5**. The $Ce_{0.6}Zr_{0.4}O_2$:Cu catalyst (CCZ catalyst) nanoparticles were synthesized by MDD method and compared their properties with those by the citric acid method. As a result, the CCZ catalyst could be obtained below 20% of Cu doping ratio by both methods. The MDD method could provide the larger specific surface area of CCZ catalyst product than those by the citric acid method, i.e. 68 m^2/g and 30 m^2/g, respectively. However, the CCZ nanoparticles synthesized by citric acid method had a little higher oxygen storage capacity (OSC) value than those by MDD method.

Chapter 6 contains the summary of all chapters and direction for further investigation.

1.5 References

[1] D.F. Stein, Microwave processing of materials, 1994. doi:https://doi.org/10.17226/2266.

[2] R. Vadivambal, D.S. Jayas, Non-uniform temperature distribution during microwave heating of food materials-A review, Food Bioprocess Technol. 3 (2010) 161–171. doi:10.1007/s11947-008-0136-0.

[3] P. Puligundla, Potentials of Microwave Heating Technology for Select Food Processing Applications - a Brief Overview and Update, J. Food Process. Technol. 04 (2013). doi:10.4172/2157-7110.1000278.

[4] R. Akarapu, B.Q. Li, Y. Huo, J. Tang, F. Liu, Integrated Modeling of Microwave Food Processing and Comparison With Experimental Measurements, J. Microw. Power Electromagn. Energy. 39 (2004) 171–184.

[5] H.W. Yang, S. Gunasekaran, Temperature Profiles in a Cylindrical Model Food During Pulsed Microwave Heating, J. Food Sci. 66 (2001) 998–1004. doi:10.1111/j.1365-2621.2001.tb08225.x.

[6] H.W. Yang, S. Gunasekaran, Comparison of temperature distribution in model food cylinders based on Maxwell's equations and Lambert's law during pulsed microwave heating, J. Food Eng. 64 (2004) 445–453. doi:10.1016/j.jfoodeng.2003.08.016.

[7] S. Gunasekaran, H.W. Yang, Effect of experimental parameters on temperature distribution during continuous and pulsed microwave heating, J. Food Eng. 78

(2007) 1452–1456. doi:10.1016/j.jfoodeng.2006.01.017.

[8] D. Kybartas, E. Ibenskis, R. Surna, Single mode circular waveguide applicator for microwave heating of oblong objects in food research, Elektron. Ir Elektrotechnika. 8 (2011) 79–82.

[9] M.A. Abdelghani-Idrissi, Experimental investigations of occupied volume effect on the microwave heating and drying kinetics of cement powder in a mono-mode cavity, Appl. Therm. Eng. 21 (2001) 955–965. doi:10.1016/S1359-4311(00)00099-5.

[10] A. Idris, K. Khalid, W. Omar, Drying of silica sludge using microwave heating, Appl. Therm. Eng. 24 (2004) 905–918. doi:10.1016/j.applthermaleng.2003.10.001.

[11] G. Chen, W. Wang, A.S. Mujumdar, Theoretical study of microwave heating patterns on batch fluidized bed drying of porous material, Chem. Eng. Sci. 56 (2001). doi:10.1016/S0009-2509(01)00320-7.

[12] E.C.M. Sanga, A.S. Mujumdar, G.S. V Raghavan, Simulation of convection-microwave drying for a shrinking material, Chem. Eng. Process. 41 (2002) 487–499. doi:10.1016/S0255-2701(01)00170-2.

[13] I. Turner, The effect of dielectric properties on microwave drying kinetics, (n.d.).

[14] P. Rattanadecho, The simulation of microwave heating of wood using a rectangular wave guide: Influence of frequency and sample size, Chem. Eng. Sci. 61 (2006) 4798–4811. doi:10.1016/j.ces.2006.03.001.

[15] C. Liu, L. Zhang, J. Peng, C. Srinivasakannan, B. Liu, H. Xia, J. Zhou, L. Xu, Temperature and moisture dependence of the dielectric properties of silica sand., J. Microw. Power Electromagn. Energy. 47 (2013) 199–209. http://www.ncbi.nlm.nih.gov/pubmed/24779140.

[16] B. Rahmani Vahid, M. Haghighi, Urea-nitrate combustion synthesis of MgO/MgAl2O4 nanocatalyst used in biodiesel production from sunflower oil: Influence of fuel ratio on catalytic properties and performance, Energy Convers. Manag. 126 (2016) 362–372. doi:10.1016/j.enconman.2016.07.050.

[17] C. Ragupathi, L. John Kennedy, J. Judith Vijaya, A new approach: Synthesis, characterization and optical studies of nano-zinc aluminate, Adv. Powder Technol. 25 (2014) 267–273. doi:10.1016/j.apt.2013.04.013.

[18] C.C. Tseng, J.L. Lee, Y.M. Liu, M. Der Ger, Y.Y. Shu, Microwave-assisted hydrothermal synthesis of spinel nickel cobaltite and application for supercapacitors, J. Taiwan Inst. Chem. Eng. 44 (2013) 415–419. doi:10.1016/j.jtice.2012.12.014.

[19] A.S. Vanetsev, Y.D. Tretyakov, Microwave-assisted synthesis of individual and multicomponent oxides, Russ. Chem. Rev. 76 (2007) 397–413. doi:10.1070/RC2007v076n05ABEH003650.

[20] R.D. Peelamedu, R. Roy, D. Agrawal, Anisothermal reaction synthesis of garnets, ferrites, and spinels in microwave field, Mater. Res. Bull. 36 (2001) 2723–2739. doi:10.1016/S0025-5408(01)00743-7.

[21] S. Khalid, C. Cao, L. Wang, Y. Zhu, Microwave Assisted Synthesis of Porous NiCo2O4 Microspheres: Application as High Performance Asymmetric and Symmetric Supercapacitors with Large Areal Capacitance, Sci. Rep. 6 (2016) 22699. doi:10.1038/srep22699.

[22] S. Verma, P.A. Joy, Y.B. Khollam, H.S. Potdar, S.B. Deshpande, Synthesis of nanosized MgFe2O4 powders by microwave hydrothermal method, Mater. Lett. 58 (2004) 1092–1095. doi:10.1016/j.matlet.2003.08.025.

[23] D.K. Agrawal, Microwave processing of ceramics, Curr. Opin. Solid State Mater. Sci. 3 (1998) 480–485. doi:10.1016/S1359-0286(98)80011-9.

[24] I. Ganesh, B. Srinivas, R. Johnson, B.P. Saha, Y.R. Mahajan, Microwave assisted solid state reaction synthesis of MgAl2O4 spinel powders, J. Eur. Ceram. Soc. 24 (2004) 201–207. doi:10.1016/S0955-2219(03)00602-2.

[25] M. Kamel Attar Kar, F. Manteghi, M. Ghahari, Microwave assisted sol-gel auto-combustion synthesis of NiCuFe 2 O 4 nanoparticles using citric acid as an organic chelating agent: structural and optical studies Mahnaz Kamel Attar Kar, Proc. 19th Int. Electron. Conf. Synth. Org. Chem. (2015) 2–7. doi:10.3390/ecsoc-19-c005.

[26] M. Penchal Reddy, W. Madhuri, G. Balakrishnaiah, N. Ramamanohar Reddy, K. V. Siva Kumar, V.R.K. Murthy, R. Ramakrishna Reddy, Microwave sintering of iron deficient Ni-Cu-Zn ferrites for multilayer chip inductors, Curr. Appl. Phys. 11 (2011) 191–198. doi:10.1016/j.cap.2010.07.005.

[27] S. Javadi, S.M. Masoudpanah, A. Zakeri, Conventional versus microwave

combustion synthesis of CoFe2O4 nanoparticles, J. Sol-Gel Sci. Technol. 79 (2016) 176–183. doi:10.1007/s10971-016-4010-7.

[28] R.J. Giguere, T.L. Bray, S.M. Duncan, G. Majetich, Application of commercial microwave ovens to organic synthesis., Tetrahedron Lett. 27 (1986) 4945–4948. doi:10.1016/S0040-4039(00)85103-5.

[29] A. de la Hoz, Á. Díaz-Ortiz, A. Moreno, Microwaves in organic synthesis. Thermal and non-thermal microwave effects, Chem. Soc. Rev. 34 (2005) 164–178. doi:10.1039/B411438H.

[30] M.B. Gawande, S.N. Shelke, R. Zboril, R.S. Varma, Microwave-assisted chemistry: Synthetic applications for rapid assembly of nanomaterials and organics, Acc. Chem. Res. 47 (2014) 1338–1348. doi:10.1021/ar400309b.

[31] J. Sun, W. Wang, Q. Yue, Review on microwave-matter interaction fundamentals and efficient microwave-associated heating strategies, Materials (Basel). 9 (2016). doi:10.3390/ma9040231.

[32] G.M.B. Parkes, G. Bond, P.A. Barnes, E.L. Charsley, Development of a new instrument for performing microwave thermal analysis, Rev. Sci. Instrum. 71 (2000) 168–175. doi:10.1063/1.1150179.

[33] E. Karmazsin, R. Barhoumi, P. Satre, F. Gaillard, Use of microwaves in thermal analysis, J. Therm. Anal. 30 (1985) 43–47. doi:10.1007/BF02128113.

[34] E. Karmazsin, Use of low- and high-power microwave energy for thermal analysis, Thermochim. Acta. 110 (1987) 289–295. doi:10.1016/0040-6031(87)88237-0.

[35] G.M.B. Parkes, H.M. Williams, Development of a microwave thermogravimetric analyser based on a multimode oven, Rev. Sci. Instrum. 76 (2005). doi:10.1063/1.1921506.

[36] G.M.B. Parkes et al., Microwave thermal analysis - A new approach to the study of the thermal and dielectric properties of materials by G parks.pdf, J. Therm. Anal. Cal. 56 (1999) 723–731.

[37] G.M.B. Parkes, P.A. Barnes, E.L. Charsley, G. Bond, Microwave differential thermal analysis in the investigation of thermal transitions in materials, Anal. Chem. 71 (1999) 5026–5032. doi:10.1021/ac990760w.

[38] D.E. Clark, D.C. Folz, J.K. West, Processing materials with microwave energy,

Mater. Sci. Eng. A. 287 (2000) 153–158. doi:10.1016/S0921-5093(00)00768-1.

[39] T. Segawa, T. Fukasawa, A.-N. Huang, Y. Yamada, M. Suzuki, K. Fukui, Influence of the heating method on the particle characteristics of copper oxide powders synthesized from copper nitrate aqueous solutions, Chem. Eng. Sci. 153 (2016) 108–116. doi:10.1016/j.ces.2016.07.008.

[40] L. Palombi, F. Bonadiesa, A. Scettri, Microwave-assisted oxidation of saturated and unsaturated alcohols with t-butyl hydroperoxide and zeolites, Tetrahedron. 53 (1997) 15867–15876. doi:10.1016/S0040-4020(97)10047-3.

[41] A. Chighine, S. Crosignani, M.C. Arnal, M. Bradley, B. Linclau, Microwave-assisted ester formation using O-alkylisoureas: A convenient method for the synthesis of esters with inversion of configuration, J. Org. Chem. 74 (2009) 4753–4762. doi:10.1021/jo900476y.

[42] Y. Li, W. Yang, Microwave synthesis of zeolite membranes: A review, J. Memb. Sci. 316 (2008) 3–17. doi:10.1016/j.memsci.2007.08.054.

[43] X. Querol, N. Moreno, J.C. Umaa, A. Alastuey, E. Hernández, A. López-Soler, F. Plana, Synthesis of zeolites from coal fly ash: an overview, Int. J. Coal Geol. 50 (2002) 413–423. doi:10.1016/S0166-5162(02)00124-6.

[44] X. Querol, A. Alastuey, A. López-Soler, F. Plana, J.M. Andrés, R. Juan, P. Ferrer, C.R. Ruiz, A fast method for recycling fly ash: Microwave-assisted zeolite synthesis, Environ. Sci. Technol. 31 (1997) 2527–2533. doi:10.1021/es960937t.

[45] K. Fukui, K. Arai, K. Kanayama, H. Yoshida, Phillipsite synthesis from fly ash prepared by hydrothermal treatment with microwave heating, Adv. Powder Technol. 17 (2006) 369–382. doi:10.1163/156855206777866164.

[46] K. Fukui, K. Kanayama, T. Yamamoto, H. Yoshida, Effects of microwave irradiation on the crystalline phase of zeolite synthesized from fly ash by hydrothermal treatment, Adv. Powder Technol. 18 (2007) 381–393. doi:10.1163/156855207781389483.

[47] T. Fukasawa, A.D. Karisma, D. Shibata, A.N. Huang, K. Fukui, Synthesis of zeolite from coal fly ash by microwave hydrothermal treatment with pulverization process, Adv. Powder Technol. 28 (2017) 798–804. doi:10.1016/j.apt.2016.12.006.

[48] K. Fukui, Y. Igawa, N. Arimitsu, M. Suzuki, T. Segawa, K.I. Fujii, T. Yamamoto, H. Yoshida, Mechanism of synthesis of metallic oxide powder from aqueous metallic nitrate solution by microwave denitration method, Chem. Eng. J. 211–212 (2012) 1–8. doi:10.1016/j.cej.2012.09.032.

[49] T. Segawa, K. Kawaguchi, K. Ishii, M. Suzuki, N. Arimitsu, H. Yoshida, K. Fukui, Nickel oxide powder synthesis from aqueous solution of nickel nitrate hexahydrate by a microwave denitration method, Adv. Powder Technol. 26 (2015) 983–990. doi:10.1016/j.apt.2015.04.004.

[50] T. Pannaraparayil, High density Mn-Zn ferrites: synthesis and characterization, 54 (1990) 645–650.

[51] S. Komarneni, M.C. D'Arrigo, C. Leonelli, G.C. Pellacani, H. Katsuki, Microwave-Hydrothermal Synthesis of Nanophase Ferrites, J. Am. Ceram. Soc. 81 (1998) 3041–3043. doi:10.1111/j.1151-2916.1998.tb02738.x.

[52] C.K. Kim, J.H. Lee, S. Katoh, R. Murakami, M. Yoshimura, Synthesis of Co-, Co-Zn and Ni-Zn ferrite powders by the microwave-hydrothermal method, Mater. Res. Bull. 36 (2001) 2241–2250. doi:10.1016/S0025-5408(01)00703-6.

[53] J.C. Fariñas, R. Moreno, A. Pérez, M.A. García, M. García-Hernández, M.D. Salvador, A. Borrell, Microwave-assisted solution synthesis, microwave sintering and magnetic properties of cobalt ferrite, J. Eur. Ceram. Soc. 38 (2018) 2360–2368. doi:10.1016/j.jeurceramsoc.2017.12.052.

CHAPTER 2

The development of single mode type of microwave thermogravimetric

2.1 Introduction

Microwave heating has long been used for diverse purposes such as food processing[1], drying[2], coal treatment[3], chemical reaction[4,5], synthesis of organic and inorganic materials[6–8], sintering of ceramics[9], and synthesis of nanoparticles[10]. In the field of nuclear engineering, it is particularly used for the synthesis of mixed-oxide powder (MOX fuel powder) by the direct denitration of mixed aqueous solutions of uranium nitrate and plutonium nitrate[11,12].

Microwave heating enables the direct, rapid, and selective heating of a material with a higher efficiency compared to conventional heating methods. Microwave heating involves the direct interaction between an electromagnetic field and the heated material. In the process, the electric field component of the microwave radiation polarizes the object and generates carriers such as electrons and other ions, which covey an electric current. The current generates heat through the electrical resistance of the material[13]. However, the complex electric permittivity and dielectric loss of the material significantly affect the heating performance and its efficiency, because the permittivity, for example, depends on both the temperature and type of the material.

Although it is well known that microwave heating considerably improves reaction rate and conversion, it may also inhibit the synthesis of byproducts, although the mechanism responsible for this observation is yet to be sufficiently established. To clarify this issue, it is necessary to measure the reaction temperature, the microwave energy absorbed by the material, and the change in the mass of the object, which corresponds to the conversion of the reaction, simultaneously in situ during the progress of the reaction. The relationships among these three parameters may be used to optimize a microwave heating apparatus. A microwave heating thermogravimetry apparatus should thus be developed to enable the accurate measurement of these parameters.

There are two main types of commonly used microwave heating systems, namely, single-mode-type and multimode type. Parkes *et al.* developed a multimode-type microwave heating thermogravimetry apparatus, which produced results that were comparable with those of a conventional heating thermogravimetry system[13]. However, the amount of microwave power absorbed in their multimode apparatus could not be determined.

The single-mode system has certain advantages compared to the multimode system, such as reduced microwave power requirement and a more uniform temperature distribution in the cavity[14]. Moreover, because the sample material is heated by one-way traveling microwaves in the single-mode system, the microwave absorption efficiency and dielectric properties can be evaluated.

In this chapter, the newly developed new single-mode-type microwave heating thermogravimetry apparatus was studied. A copper (II) oxide (CuO) powder pellet, which exhibits little mass change under microwave heating, was used as the heated material. The temperature distribution and microwave absorption efficiency of the pellet were primarily investigated, and the precision of the electromagnetic field measurements was confirmed by comparing the measurements with numerical simulation results. The dependence of the dielectric properties of the CuO on the temperature was also examined based on the acquired data. The dielectric properties of other materials were also investigated.

2.2 Materials and Methods

2.2.1 Experimental

Figure 2.1 is a schematic representation of the newly developed single-mode-type microwave heating thermogravimetry apparatus, which consisted of a magnetron, a waveguide, a radiation thermometer (JS-TMH91; Minori Corp., Kobe), a personal computer (used for control and data logging), power meters (HP 437B; Hewlett Packard Corp., USA), an electric balance (MC-1000; AND, Tokyo), and a dummy load (microwave absorber).

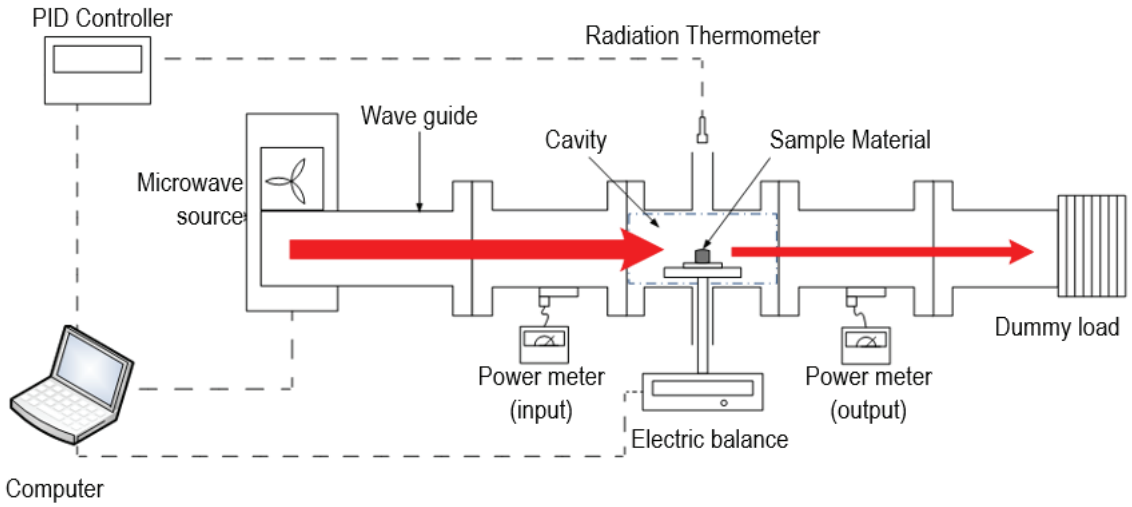

Figure 2.1 Schematic of developed single-mode-type microwave heating thermogravimetry apparatus.

A 2.45 GHz microwave generated by the magnetron was introduced through the waveguide into the measurement section, which measured 260 × 50 × 110 mm. The sample material, which was set on a quartz glass and alumina plate in the measurement section, absorbed the microwave energy and was heated. The temperature of the material was measured by the radiation thermometer through an observation pipe. The microwave outputs at the inlet and outlet of the measurement section were measured by the power meters. The difference between the two measurements corresponded to the microwave energy absorbed by the sample material and was used to determine the microwave absorption efficiency of the material. The microwave absorption efficiency was defined as the ratio of the microwave power absorbed by the sample material to the microwave power at the inlet of the measurement section. It was calculated as follows:

$$\eta_{\exp} = \frac{p_{in} - p_{out}}{p_{in}} \tag{2.1}$$

where $\eta_{\exp}$ is the experimental microwave absorption efficiency, and p_{in} and p_{out} are respectively the microwave powers at the inlet and outlet of the measurement section. Because the microwave power that passed through the measurement section was substantially absorbed by the dummy load, the sample material was only heated one-way by the travelling microwave. An infrared thermal camera (G100EX; Avio Corp., Tokyo) was used to capture the image of the temperature distribution on the surface of the sample material from the top and side.

The sample material was a disk-shaped pellet produced from copper (II) oxide (CuO) powder (ACS reagent, Sigma-Aldrich, Germany). The pellet measured 20.0 mm in diameter and 9.0 mm in height. CuO was selected because it easily absorbs microwave energy[15]; its free thermal reduction energy is also low, and this reduces the microwave power required for heating[16]. The mass and packing fraction of the CuO pellet were 8.0 g and 0.51, respectively.

2.2.2 Numerical simulation in the apparatus

To evaluate the reliability and measurement precision of the newly developed single-mode-type microwave heating apparatus, it was necessary to examine the temperature distribution and microwave absorption efficiency of the sample material. Because the microwave generates heat by its interaction with the dipoles and electric charges in the material, the temperature distribution and microwave absorption efficiency of the material depend on its internal electric and magnetic fields.

Three-dimensional (3D) finite-element simulation of the system in the steady state was conducted using a boundary condition comprising full reflection of the microwave by the metallic wall and full absorption by the dummy load in a rectangular coordinate system[4]. The RF mode was used to determine the power density distribution in the sample material. Figure 2.2 shows the geometry of the measurement section of the apparatus and the calculation mesh. The geometry and dimensions of the measurement section and the sample material used for the simulation were the same as those of the actual objects. The total number of the mesh cells and the cell size were 1,784,214 and 1 mm^3, respectively.

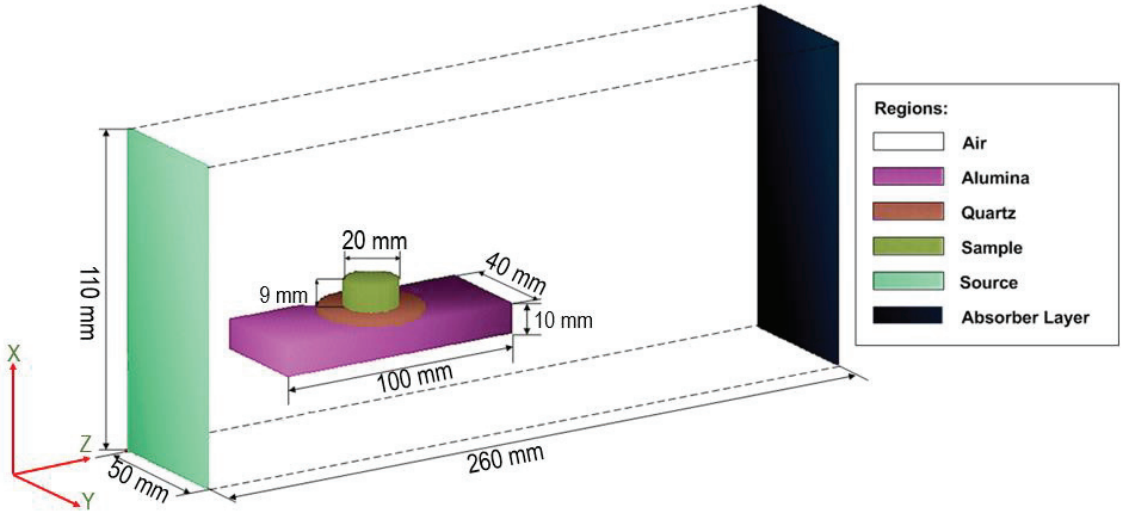

(a)

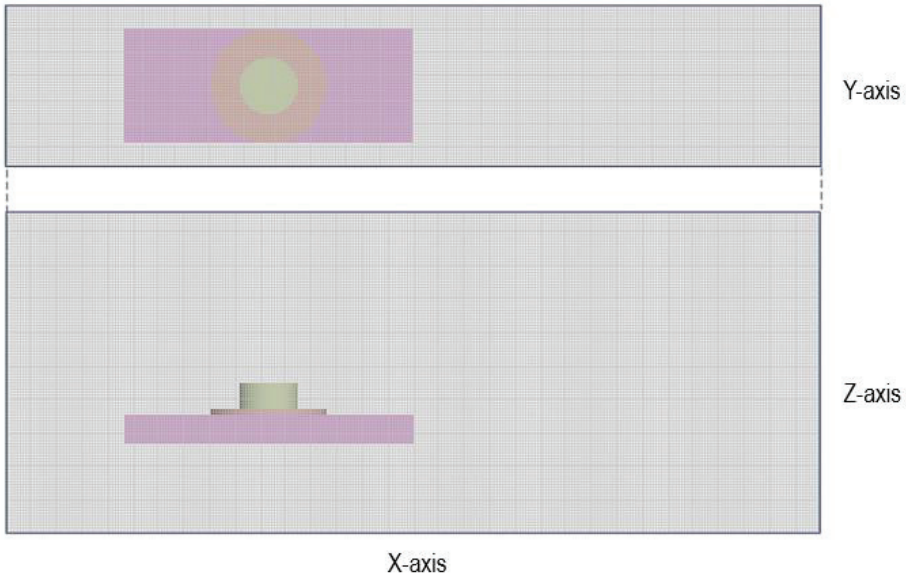

(b)

Figure 2.2 Simulation system of microwave heating. (a) Simulation geometry, (b) Calculation grid.

The electromagnetic field of the apparatus can be expressed by the following Maxwell differential equations, based on Ampere and Faraday's laws[17,18]:

$$\nabla \times \boldsymbol{E} = -\frac{\partial(\mu \boldsymbol{H})}{\partial \boldsymbol{t}} \tag{2.2}$$

$$\nabla \times \boldsymbol{H} = -\frac{\partial(\mu \boldsymbol{E})}{\partial \boldsymbol{t}} + j_0 \tag{2.3}$$

The following Gauss law expressions were also applied[18]:

$$\nabla \cdot \varepsilon E = 0 \tag{2.4}$$

$$\nabla \cdot \mu H = 0 \tag{2.5}$$

where $\boldsymbol{E}$ is the electric field vector, $\boldsymbol{H}$ is the magnetic field vector, $\boldsymbol{j}_0$ is the current density, ε is the complex permittivity, and μ is the complex magnetic permeability.

A combination of these equations gives the following[17]:

$$\nabla \times \boldsymbol{E} = -j\omega\mu\boldsymbol{H} \tag{2.6}$$

$$\nabla \times \boldsymbol{H} = j\omega\varepsilon\boldsymbol{E} + \boldsymbol{j}_0 \tag{2.7}$$

where ω is the angular frequency and j is an imaginary unit. The electromagnetic field of the apparatus can be determined using these equation (2.6) and (2.7).

The sample material is characterized by its complex permittivity and magnetic permeability, the standard expression of which are respectively as follows[19]:

$$\varepsilon = \varepsilon' + j\varepsilon'' \tag{2.8}$$

$$\mu = \mu' + j\mu'' \tag{2.9}$$

where ε' and μ' are the real parts of the permittivity and permeability, and ε'' and μ'' are the imaginary parts, respectively. The real part of the permittivity is a measure of the ability of the material to store electrical energy, while the imaginary part, which is referred to as the permittivity loss, represents the energy lost from the electric field of the material. This lost energy is usually converted into thermal energy[20].

The change in temperature of the material due to microwave irradiation is determined by the time-averaged power density, which represents the microwave power absorbed by the object. The power density p can be determined using equation (2.10), based on the electromagnetic field configuration[21]:

$$p = \frac{\omega}{2}\left(\varepsilon''\|\boldsymbol{E}\|^2 + \mu''\|\boldsymbol{H}\|^2\right) \tag{2.10}$$

In the numerical simulation, the microwave absorption efficiency η_{calc} was calculated using the following:

$$\eta_{calc} = \frac{p_s}{p_s + p_d} \tag{2.11}$$

where p_s and p_d are the power densities of the sample material and the dummy load, respectively.

A dynamic model was used to determine the temperature distribution of the

sample material during the microwave heating. The dynamic thermal transport was analyzed using Fourier's law, which can be expressed as follows[22]:

$$\rho C_p \frac{\partial T}{\partial t} = \nabla(k\nabla T) + q \tag{2.12}$$

where ρ, C_p, and k are respectively the true density, specific heat capacity, and thermal conductivity of the sample material. With the assumption that the time-averaged dissipated power density is converted into heat by thorough microwave irradiation, the power density p is equal to the amount of generated heat q in equation (2.12)[8].

2.3 Results & Discussion

2.3.1 Evaluation of temperature profile

Because the heat generated in the CuO pellet could not be determined by experiment or from the temperature distribution, the numerical simulation of the power density distribution was first conducted. Figure 2.3 shows the simulated power density distribution of the CuO pellet in the measurement section for a source current density $\boldsymbol{j}_0$ of 4.5×10^4 A/m^2. The physical constants at 25 °C (room temperature) used for the present simulation were the same as those in our previous works[8]. The top view of the power density distribution shows that the peripheral part of the pellet near the microwave inlet had the highest power density, with a monotonous decrease in the direction of the outlet. Furthermore, the power density distribution was almost axisymmetric about the center line. Judging from the side view, the microwave was focused on both top and bottom parts closer to the microwave inlet. The minimum power density occurred on the top surface of the CuO pellet closer to the outlet.

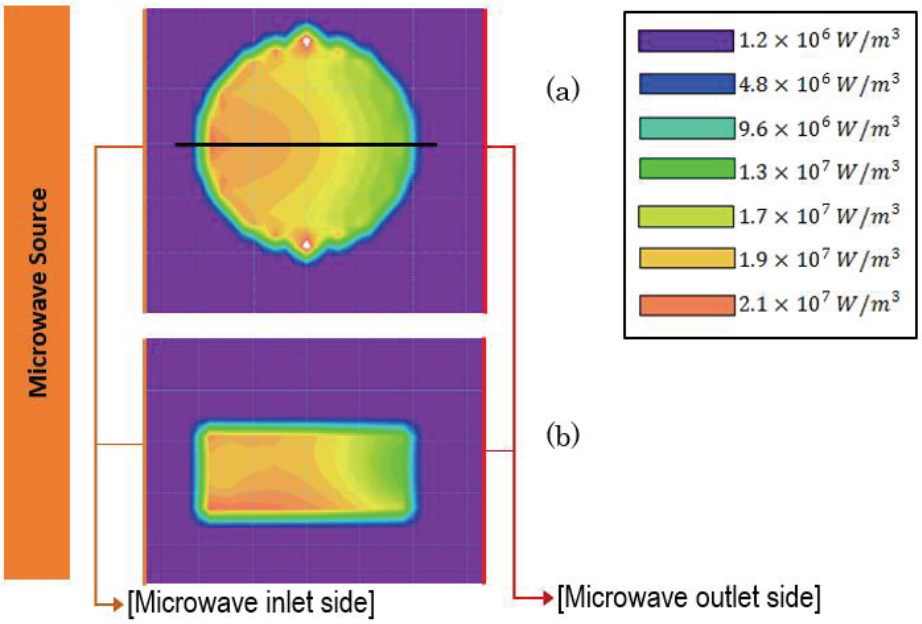

Figure 2.3 Simulated power density distribution in CuO pellet. (a) Top view, (b) Side view

The above pattern of the power density distribution suggests that there was precisely a one-way travel of the microwave from the inlet to the outlet side of the measurement section. Because the power density reflects the microwave energy absorbed by the sample material, the efficiency and uniformity of the microwave heating are dependent on both the power density distribution and the heat conductivity from the heat source to the bulk. The uneven power density distribution in the CuO pellet created a nonhomogeneous temperature distribution.

The temperature distribution in the CuO pellet was numerically obtained for comparison with that determined by experiment. Figure 2.4 shows the top views of the measured and simulated temperature distributions. Here, the current density j_0 was fitted so that measured maximum temperature agreed with the simulation value. Figures 2.4 (a) and (b) show the temperature distribution images of the CuO pellet captured by the thermal camera and that obtained by numerical simulation, respectively. As can be observed, the simulation temperature distribution is almost similar to the power density distribution. This is because the power density reflects the amount of heat generation, as expressed by equation (2.12). The measured and simulated temperature distributions also agree well, with the maximum temperature of the CuO pellet occurring on the side closer

to the microwave source, and a monotonous decrease in the direction of the microwave outlet. These consistencies affirm the one-way travel of the microwave in the developed single-mode-type microwave heating apparatus.

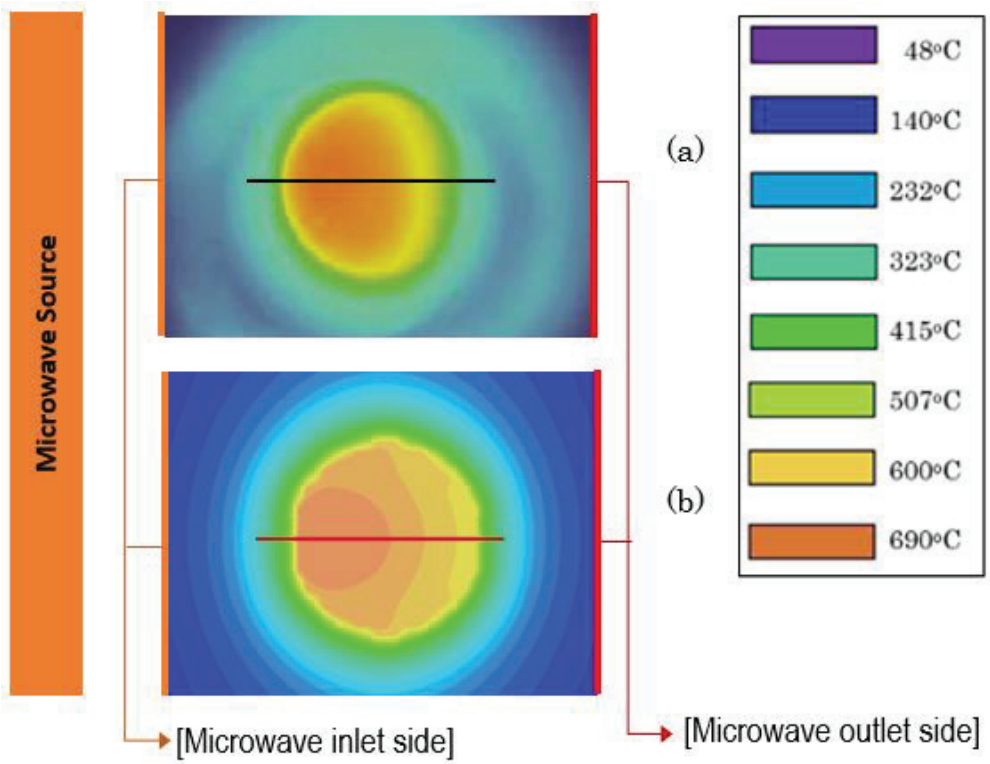

Figure 2.4 Top-view temperature distribution in CuO pellet during microwave heating. (a) Experiment, (b) Simulation.

To verify the temperature distribution, the variation of the temperature along the center line shown in Figure 2.4 was examined. The results of the experiment and simulation are shown in Figure 2.5, where they are represented by the black and red lines, respectively. It can be observed from the results of the experiment that the surface temperature of the CuO pellet increased from about 670 °C to 700 °C in the direction of the outlet side of the apparatus. The maximum temperature occurred at 3 mm from the edge of the pellet closer to the microwave inlet side, after which the temperature decreased monotonously. The simulation results indicate that the temperature at the edges of the pellet closer to the microwave inlet and outlet sides were about 690 and 630 °C, respectively. In agreement with the experimental results, the simulation indicated that the hottest part of the pellet occurred within 2–6 mm from the edge closer to the microwave inlet, the temperature being 710 °C. Considering that the deviation between

the temperature profiles of the experiment and numerical simulation was within 8.2%, it can be concluded that the numerical simulation fairly accurate reproduced the electromagnetic field, power density, and temperature distribution of the CuO pellet.

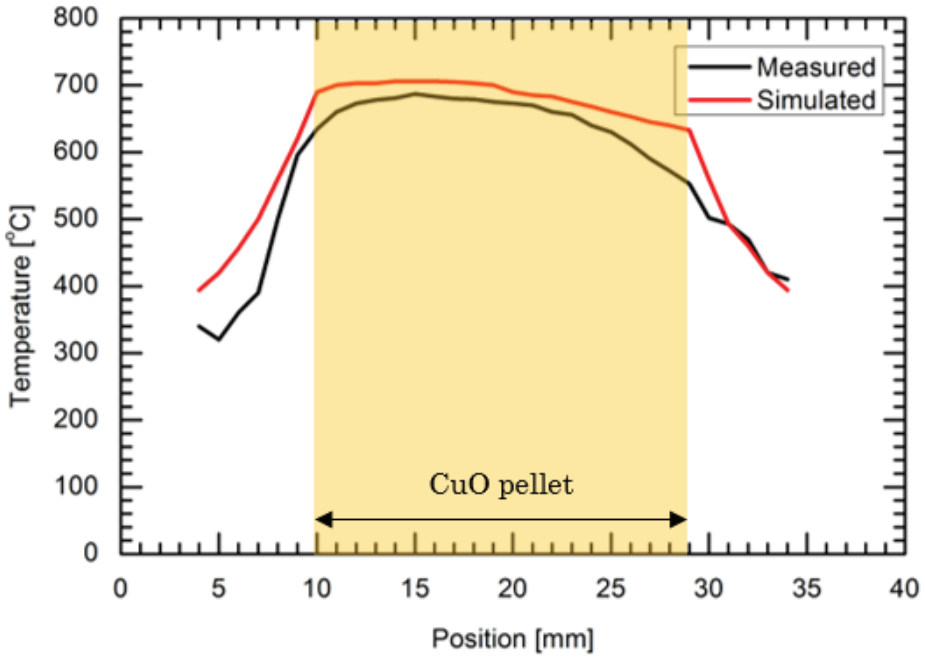

Figure 2.5 Measured and simulated temperatures as functions of horizontal distance along CuO pellet in Figure 2.4.

Figure 2.6 shows the experimental and simulation side-view temperature distributions of the pellet. To verify the temperature profile, the temperature variations along two lines in the directions of the vertical and horizontal axes, respectively, were examined, as shown in Figure 2.7. The temperature distribution along the vertical line was observed not to agree with the power density distribution in Figure 2.4. Whereas the highest power density occurred at both the top and bottom of the pellet in Figure 2.3, Figure 2.7(a) shows that the temperature gradually decreased with decreasing height along the side of the pellet, due to heat transfer from the pellet to the quartz glass, which has a higher thermal conductivity than CuO powder. However, the temperature distribution along the horizontal line in Figure 2.7(b) is similar to the power density distribution, with the temperature monotonously decreasing from the side of the pellet closer to the microwave inlet to the outlet side. The deviations between the measured and simulation temperature profiles along the vertical and horizontal lines were 11.8% and 10%, respectively. This confirms the fair accuracy of the numerical simulation.

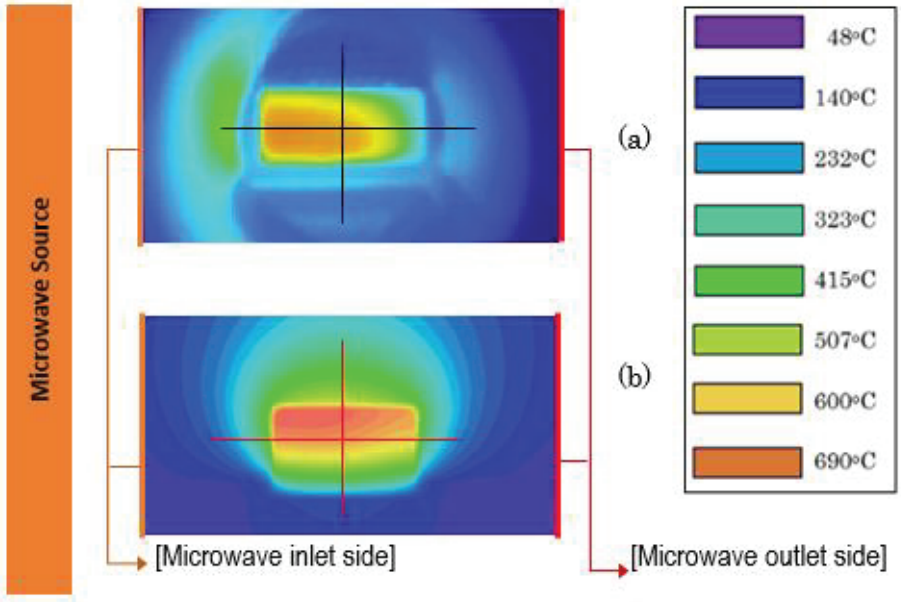

Figure 2.6 Side-view temperature distribution in CuO pellet during microwave heating. (a) Experiment, (b) Simulation.

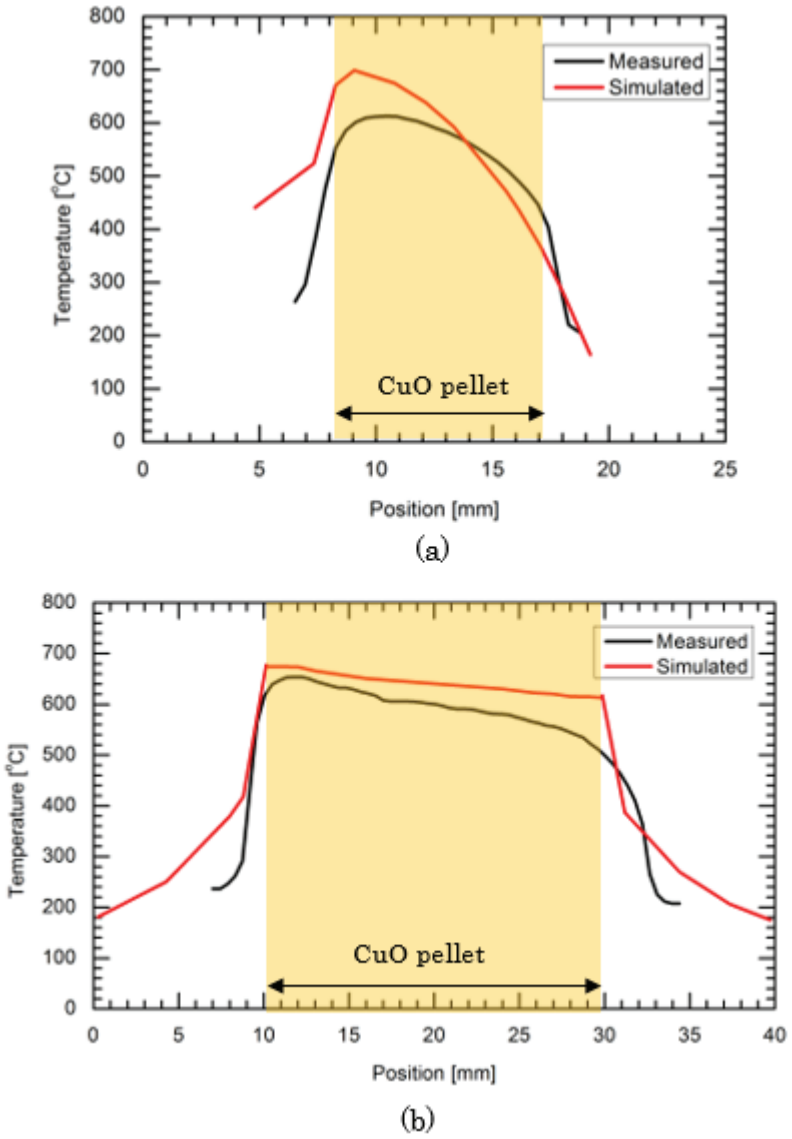

Figure 2.7 Measured and simulated temperatures as functions of (a) vertical and (b) horizontal distances along CuO pellet in Figure 2.6.

The effects of the pellet thickness on the heat generation and temperature distribution during the microwave heating were also numerically investigated using CuO pellets of different thicknesses. Figure 2.8 shows the simulated temperature distributions for pellets of thicknesses 6, 9, and 12 mm, respectively. The same current density j_o used to obtain the results in Figure. 4 was employed. The top-view temperature distribution tendencies for all the pellets were observed to be similar, although the actual temperatures differed. Furthermore, the side-view distributions indicate that the hottest spot on the top side of the pellet closer to the inlet was independent of the pellet thickness.

The amount of generated heat, however, increased with increasing pellet thickness, and this also increased the volumetric average temperature. This indicates that the microwave heating efficiency is also dependent on the volume of the sample material[23].

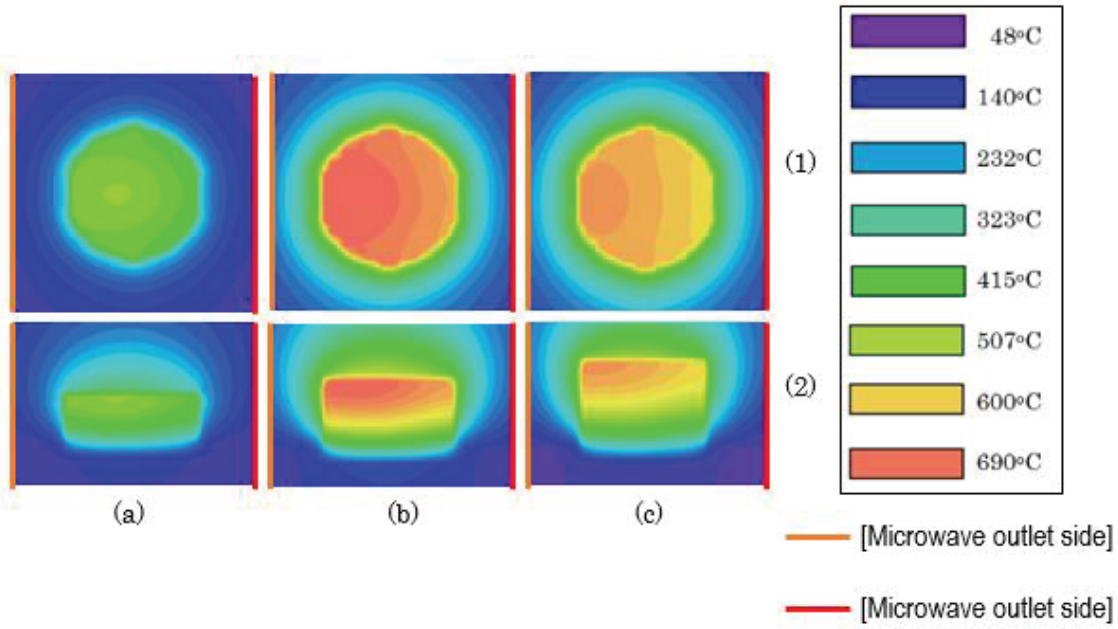

Figure 2.8 Simulated temperature distributions in CuO pellets of thicknesses (a) 6 mm, (b) 9 mm, and (c) 12 mm.

2.3.2 Mass measurement

Figure 2.9 shows the ignition loss of a CuO pellet heated by the present microwave heating apparatus, as well as that of the CuO powder measured by thermogravimetric-differential thermal analysis (TG-DTA) system (TG-DTA 8121; Rigaku Corp., Tokyo). The TG-DTA data revealed that the mass of the CuO powder did not change during heating from room temperature to 800 °C. This was because the CuO powder was not involved in any reaction. In the case of heating using the MWTG apparatus, the mass was constant up to 600 °C, after which it began to decrease very gradually up to 800 °C, to 98.5% of the original mass. The mass reduction was possibly caused by the convectively generated air flow and buoyancy in the high temperature condition by the microwave irradiation.

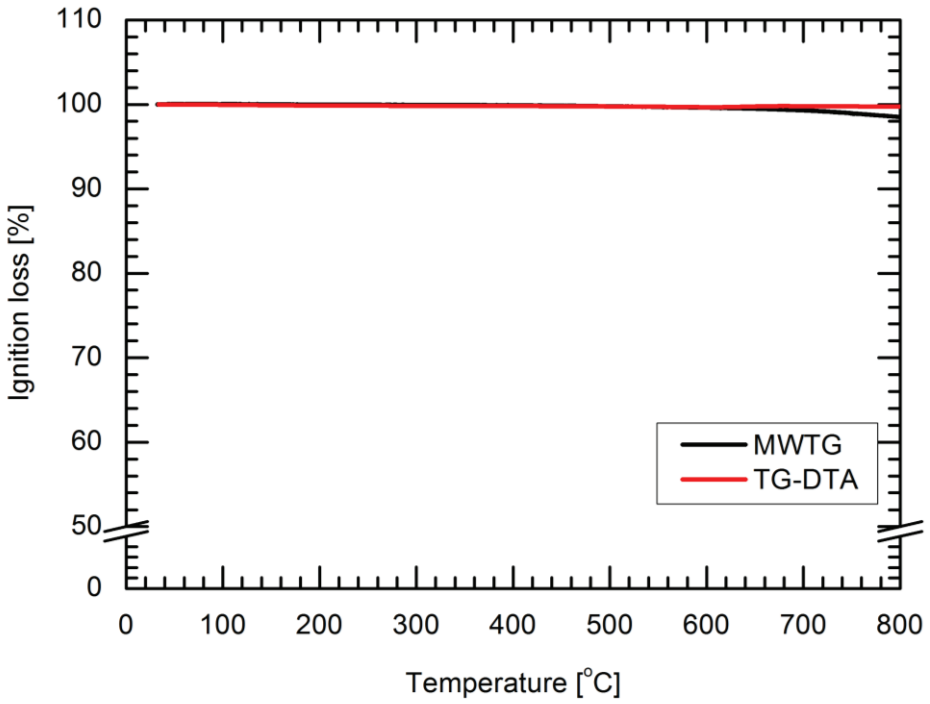

Figure 2.9 Ignition loss of CuO measured by the microwave heating apparatus (MWTG) and TG-DTA

To investigate the mass measurement that involve the reaction mechanism by microwave heating, $Cu(NO_3)_2$ solution has been used as the sample material. Figure 2.10 shows the ignition loss of $Cu(NO_3)_2$ solution measured by MWTG apparatus and TG-DTA analysis. By investigate the ignition loss by both method, the reaction can be divided into 3 steps. The first step is the evaporation of solvent water. The reaction temperature of reaction 1 by MWTG and TG-DTA are from room temperature until 180°C and 200°C, respectively. The reaction 2 is the desorption of hydrate water and formation of intermediate product. In this step, the reaction temperature for both method is the same, that is 260°C. This mechanism of intermediate product has a good agreement with Fukui et al.[8], which the intermediate product of $Cu(NO_3)_2$ solution was formed at this reaction temperature. The last reaction is the completion of denitration reaction, from the intermediate product to the CuO product. From the comparison of ignition loss and mechanism reaction for MWTG and TG-DTA, it can be conclude that MWTG has a good agreement with TG-DTA analysis.

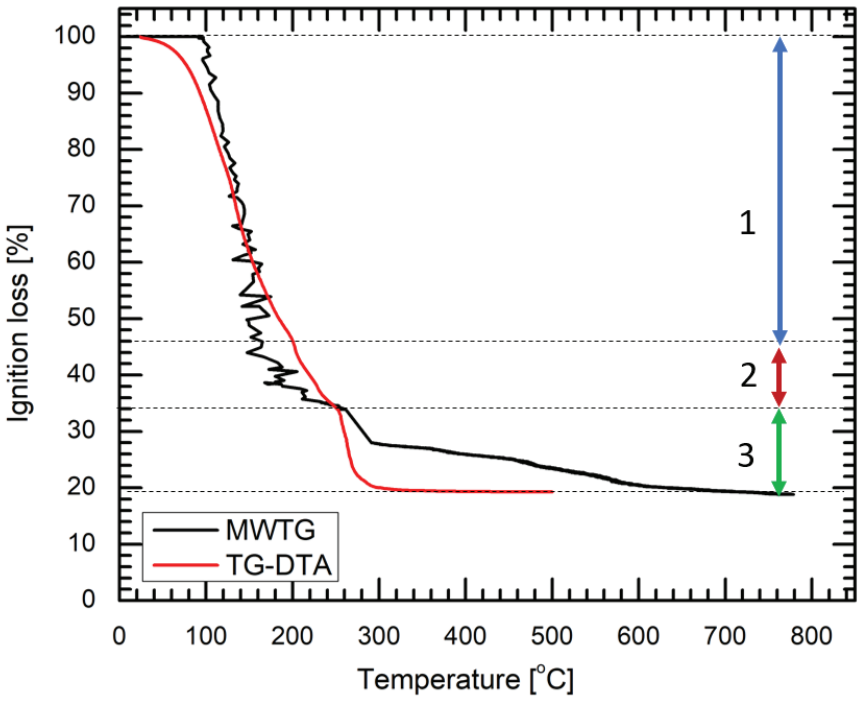

Figure 2.10 Ignition loss of $Cu(NO_3)_2$ measured by the microwave heating apparatus (MWTG) and TG-DTA

2.3.3 Estimation of the dielectric properties

Generally, the permittivity ε' and permittivity loss ε'' of a material vary with the temperature[24]. Because the microwave power density p is determined by these dielectric properties, as described by equation (2.10), the microwave absorption efficiency η of the sample material also varies with the temperature. To confirm whether numerical simulation could be used to estimate the microwave absorption efficiency in the newly developed apparatus at various temperatures, the measured absorption efficiency was compared with that determined by simulation. The simulated microwave absorption efficiency η_{calc} was calculated using the same physical constants as those of the experiment. The work of Samouhos *et al*. was referenced for the dependence of the dielectric properties of CuO[25]. The present results are shown in Figure 2.11, which reveals that the measured microwave absorption efficiency η_{exp} was maximum at a temperature of 475 °C, and thereafter decreased. Likewise, the simulated microwave absorption efficiency η_{calc} increased with increasing temperature, reaching the maximum value at about 400–540 °C. The maximum values of the measured and simulation microwave absorption efficiencies, η_{exp} and η_{calc}, were 0.16 and 0.15, respectively, which

are almost the same. This confirms the reliability of the numerical simulation for estimating the microwave absorption efficiency in the new apparatus at different temperatures.

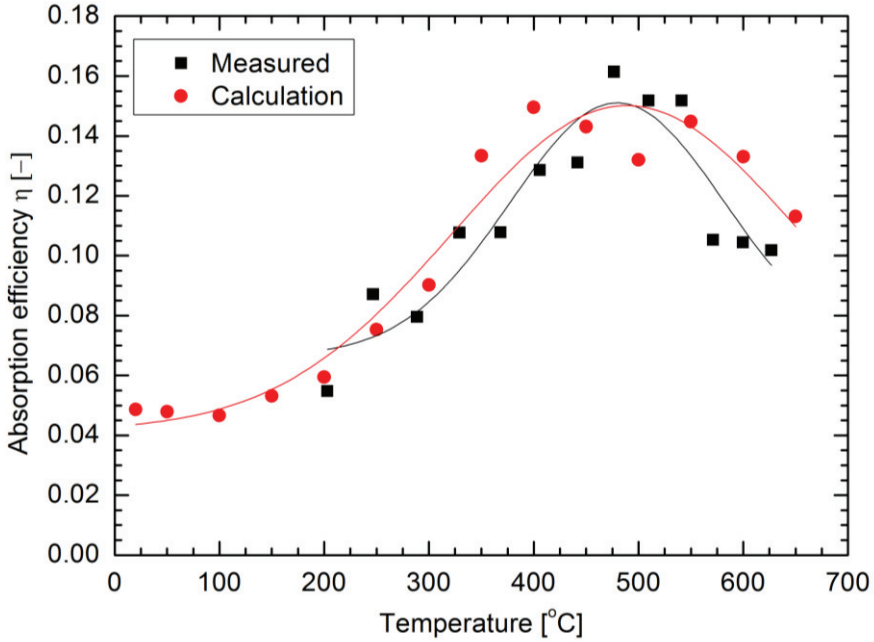

Figure 2.11 Relationship between microwave absorption efficiency and temperature.

Considering that the dielectric properties of the sample material determined the microwave absorption efficiency, it was supposed that the dielectric properties could be estimated by numerically determining the microwave absorption efficiency. As an example, Figure 2.12 shows the numerically determined relationship between the microwave absorption efficiency and the permittivity loss of the sample material for various permittivity values. As can be observed, for a given permittivity, the absorption efficiency increases with increasing permittivity loss, with the relationship being almost proportional. This means that the permittivity loss for a given permittivity can be uniquely determined from the microwave absorption efficiency. This can be used to compensate for the lack of comprehensive data on the permittivity losses of materials.

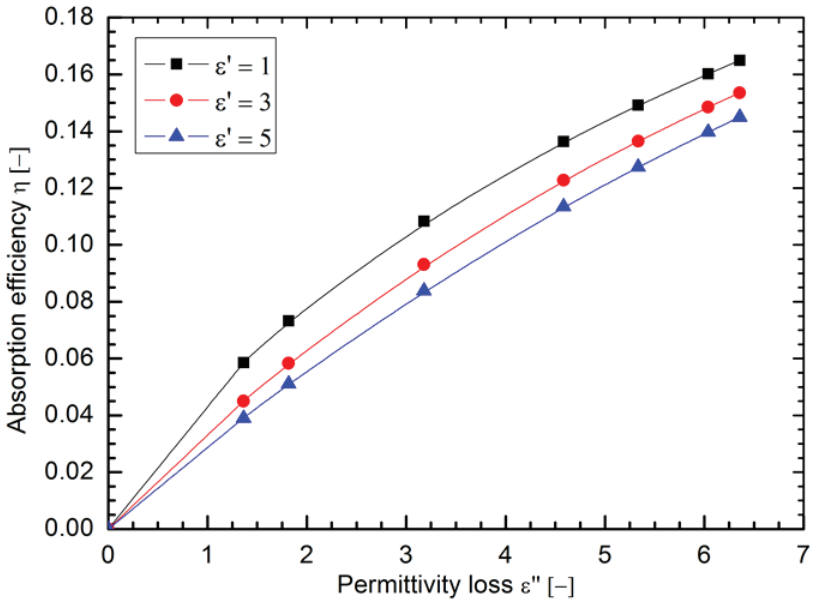

Figure 2.12 Relationship between calculated absorption efficiency and permittivity loss for various permittivity values.

The dependence of the permittivity loss of CuO on the temperature was also estimated based on the microwave absorption efficiency values in Figure 2.11 using the above method. The results are shown in Figure 2.13, together with those of Samouhos *et al.*[25]. It can be seen that the dependence of the present estimated permittivity loss ε'' on the temperature agrees well with that of the previous study. In both cases, the permittivity loss increases with increasing temperature, reaching a maximum value of about 7.25 at 475 °C, and thereafter begins to decrease. However, at temperatures above about 500 °C, certain parts of the CuO pellet are overheated, with a resultant decrease in the permittivity loss of such parts[26].

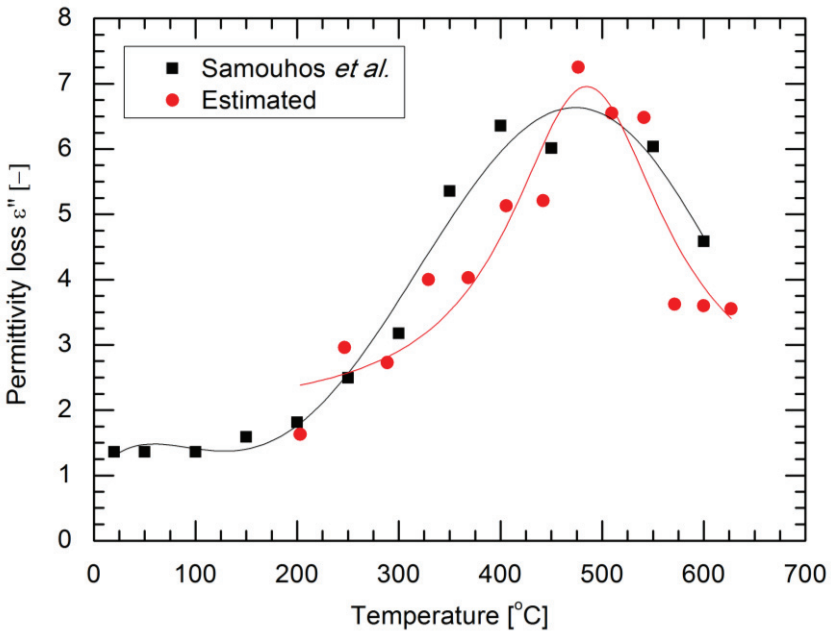

Figure 2.13 Comparison of previously published and presently estimated permittivity losses of CuO.

Furthermore, to confirm the accuracy of the permittivity losses estimated using the developed microwave heating apparatus, the permittivity losses of other materials ($Ni_3(NO_3)_2(OH)_4$ and C_4H_8O) were estimated by the same method and the results were compared with those previously obtained by other methods. Table 2.1 lists the measured microwave absorption efficiencies and the estimated permittivity losses of several materials at room temperature. The presently estimated ε'' of $Ni_3(NO_3)_2(OH)_4$ was particularly compared with that measured by the cylindrical cavity resonator method[27]. The value of the estimated ε'' of $Ni_3(NO_3)_2(OH)_4$, which is an intermediate product of the denitration of nickel nitrate, is almost twice the value measured by the cavity resonance method. However, the estimated ε'' of ethyl acetate ($C_4H_8O_2$) is in relatively good agreement with a previously determined value[28]. These results suggest that there is a larger error in the estimation of the permittivity loss of a material with a lower microwave absorption efficiency using the present method. The deviation may be due to measurement error in the microwave absorption efficiency of a material with a relatively low microwave absorption efficiency.

Table 2.1 Measured absorption efficiencies and estimated and measured permittivity losses of different materials at room temperature

Material	η_{exp}	ε'' **(Estimated)**	ε'' **(Literature)**	**Error**
	[-]	**[-]**	**[-]**	**[%]**
$Ni_3(NO_3)_2(OH)_4$	0.007	0.065	0.036	80
$C_4H_8O_2$	0.083	0.45	0.354	27

2.4 Conclusions

A single-mode-type microwave heating thermogravimetry apparatus was developed, and its validity was investigated by comparing the measured temperature distribution and microwave absorption efficiency of a CuO pellet that was heated in the apparatus with those determined by simulation. The dielectric properties of different materials determined using the new apparatus were also compared with published values. Following is a summary of the findings of this chapter:

1. The maximum temperature of the CuO pellet heated by the developed microwave heating thermogravimetry apparatus occurred on the side closer to the microwave inlet, with the temperature decreasing monotonously in the direction of the outlet.
2. The temperature distribution in the CuO pellet was accurately reproduced by a three-dimensional numerical simulation of the electromagnetic field and revealed one-way travel of the microwave in the microwave thermogravimetry apparatus.
3. The microwave absorption efficiencies of the CuO at different temperatures determined by numerical simulation agreed well with the measured values.
4. Numerical calculations revealed an approximately direct variation of the permittivity loss at a given permittivity with the absorption efficiency, indicating that the permittivity loss could be uniquely determined from the microwave absorption efficiency.
5. The temperature dependence of the permittivity loss of CuO estimated from the measured microwave absorption efficiency agrees well with previously published results.
6. The estimation error of the permittivity loss was large for a material with a low microwave absorption efficiency, possibly due to the measurement error of the absorption efficiency of such a material

2.5 References

[1] R. Vadivambal, D.S. Jayas, Non-uniform temperature distribution during microwave heating of food materials-A review, Food Bioprocess Technol. 3 (2010) 161–171. doi:10.1007/s11947-008-0136-0.

[2] A. Idris, K. Khalid, W. Omar, Drying of silica sludge using microwave heating, Appl. Therm. Eng. 24 (2004) 905–918. doi:10.1016/j.applthermaleng.2003.10.001.

[3] L.Y. Yu, P.S. Li, Thermogravimetric analysis of coal and sludge co-combustion with microwave radiation dehydration, J. Energy Inst. 87 (2014) 220–226. doi:10.1016/j.joei.2014.03.009.

[4] T. Segawa, K. Kawaguchi, K. Ishii, M. Suzuki, N. Arimitsu, H. Yoshida, K. Fukui, Nickel oxide powder synthesis from aqueous solution of nickel nitrate hexahydrate by a microwave denitration method, Adv. Powder Technol. 26 (2015) 983–990. doi:10.1016/j.apt.2015.04.004.

[5] K.-M. Huang, Z. Lin, X.-Q. Yang, Numerical Simulation of Microwave Heating on Chemical Reaction in Dilute Solution, Prog. Electromagn. Res. 49 (2004) 273–289. doi:10.2528/PIER04042803.

[6] B. Adnadjevic, J. Jovanovic, The Effect of Microwave Heating on the Isothermal Kinetics of Chemicals Reaction and Physicochemical Processes, Adv. Induction Microw. Heat. Miner. Org. Mater. (2011) 391–421. http://www.intechopen.com/source/pdfs/13453/InTech-The_effects_of_microwave_heating_on_the_isothermal_kinetics_of_chemicals_reactions_and_physicochemical_processes.pdf.

[7] D.R. Baghurst, D.M.P. Mingos, Application of microwave heating techniques for the synthesis of solid state inorganic compounds, J. Chem. Soc. Chem. Commun. (1988) 829–830. doi:10.1039/c39880000829.

[8] K. Fukui, Y. Igawa, N. Arimitsu, M. Suzuki, T. Segawa, K.I. Fujii, T. Yamamoto, H. Yoshida, Mechanism of synthesis of metallic oxide powder from aqueous metallic nitrate solution by microwave denitration method, Chem. Eng. J. 211–212 (2012) 1–8. doi:10.1016/j.cej.2012.09.032.

[9] K. Fukui, M. Katoh, Y. Saeki, T. Yamamoto, H. Yoshida, Effect of packing fraction on indium tin oxide powder synthesis via a solid-phase reaction with

microwave heating, Chem. Eng. Sci. 98 (2013) 17–24. doi:10.1016/j.ces.2013.05.012.

[10] H. Wang, J.Z. Xu, J.J. Zhu, H.Y. Chen, Preparation of CuO nanoparticles by microwave irradiation, J. Cryst. Growth. 244 (2002) 88–94. doi:10.1016/S0022-0248(02)01571-3.

[11] H. Oshima, Development of Microwave Heating Method for Co-Conversion of Plutonium-Uranium Nitrate to MOX Powder, J. Nucl. Sci. Technol. 26 (1989) 161–166. doi:10.1080/18811248.1989.9734282.

[12] Y. Kato, T. Kurita, T. Abe, Dielectric properties of uranium and plutonium nitrate solution and the oxide compounds formed in the de-nitration process by the microwave heating method, J. Nucl. Sci. Technol. 41 (2004) 857–862. doi:10.1080/18811248.2004.9715557.

[13] G.M.B. Parkes, H.M. Williams, Development of a microwave thermogravimetric analyser based on a multimode oven, Rev. Sci. Instrum. 76 (2005). doi:10.1063/1.1921506.

[14] F. Benaskar, N.G. Patil, V. Engels, E. V. Rebrov, J. Meuldijk, L.A. Hulshof, V. Hessel, A.E.H. Wheatley, J.C. Schouten, Microwave-assisted Cu-catalyzed Ullmann ether synthesis in a continuous-flow milli-plant, Chem. Eng. J. 207–208 (2012) 426–439. doi:10.1016/j.cej.2012.06.147.

[15] S. Marinel, E. Savary, M. Gomina, Sintering of CuO and ZnO in a single mode microwave cavity with shrinkage control., J. Microw. Power Electromagn. Energy. 44 (2010) 57–63. http://www.ncbi.nlm.nih.gov/pubmed/21721329.

[16] J. Fukushima, K. Kashimura, S. Takayama, M. Sato, Microwave-energy Distribution for Reduction and Decrystallization of Titanium Oxides, Chem. Lett. 41 (2012) 39–41. doi:10.1246/cl.2012.39.

[17] M.R. Hossan, D. Byun, P. Dutta, Analysis of microwave heating for cylindrical shaped objects, Int. J. Heat Mass Transf. 53 (2010) 5129–5138. doi:10.1016/j.ijheatmasstransfer.2010.07.051.

[18] P. Rattanadecho, The simulation of microwave heating of wood using a rectangular wave guide: Influence of frequency and sample size, Chem. Eng. Sci. 61 (2006) 4798–4811. doi:10.1016/j.ces.2006.03.001.

[19] V.V. Komarov, V.A. Kolomeytsev, Peculiarities of dominant mode

transformation in rectangular T-septum waveguide with inhomogeneous dielectric loading, Int. J. RF Microw. Comput. Eng. 14 (2004) 201–205. doi:10.1002/mmce.10132.

[20] B. Nanthakumar, C.A. Pickles, S. Kelebek, Microwave pretreatment of a double refractory gold ore, Miner. Eng. 20 (2007) 1109–1119. doi:10.1016/j.mineng.2007.04.003.

[21] T. Santos, L.C. Costa, M. Valente, J. Monteiro, J. Sousa, 3D Electromagnetic Field Simulation in Microwave Ovens : a Tool to Control Thermal Runaway, Proc. COMSOL Conf. (2010) 1–7.

[22] E.C.M. Sanga, A.S. Mujumdar, G.S. V Raghavan, Simulation of convection-microwave drying for a shrinking material, Chem. Eng. Process. 41 (2002) 487–499. doi:10.1016/S0255-2701(01)00170-2.

[23] D.E. Clark, W.H. Sutton, Microwave Processing, Annu. Rev. Mater. Sci. 26 (1996) 299–331.

[24] Z.-Y. Cheng, R. Katiyar, X. Yao, A. Bhalla, Temperature dependence of the dielectric constant of relaxor ferroelectrics, Phys. Rev. B. 57 (1998) 8166–8177. doi:10.1103/PhysRevB.57.8166.

[25] M. Samouhos, R. Hutcheon, I. Paspaliaris, Microwave reduction of copper(II) oxide and malachite concentrate, Miner. Eng. 24 (2011) 903–913. doi:10.1016/j.mineng.2011.03.026.

[26] V. Komarov, S. Wang, J. Tang, Permittivity and Measurements, Encycl. RF Microw. Eng. (2005) 19. doi:10.1002/0471654507.eme308.

[27] M. Kinoshita, H. Kinouchi, M. Shaiful, B. Abdul, K. Wakino, T. Kitazawa, A Method of Evaluating High-Permittivity and Lossy Materials Using a Cylindrical Cavity Based on Hybrid Electromagnetic Theory, Jpn. J. Appl. Phys. 51 (2012) 1–5.

[28] M. Larhed, C. Moberg, A. Hallberg, Microwave-accelerated homogeneous catalysis in organic chemistry, Acc. Chem. Res. 35 (2002) 717–727. doi:10.1021/ar010074v.

CHAPTER 3

Utilization of incineration fly ash from biomass power plants for zeolite synthesis from coal fly ash by microwave hydrothermal treatment

3.1 Introduction

The use of renewable energy sources for the generation of electric power in Japan is being promoted by the Feed-in Tariff Scheme for Renewable Energy, which was established in 2012 [1-3]. Using woody biomass for electricity generation can give a stable supply of electricity that is not influenced by the weather while also contributing to the suppression of carbon dioxide emissions and the conservation of forests. Therefore, the idea of a boiler power plant using woody biomass as a fuel has been attracted attention in recent years [4]. In Japan, the ash generated during biomass incineration is discharged from power plants and transferred to a final disposal site as industrial waste without any further use [5]. Since the costs of conveying and landfilling is particularly high (about 20,000 JPY/t), this appears to be sufficient to inhibit the spread of boiler power plants using woody biomass as a fuel, and so the development of a suitable scheme for the utilization of biomass incineration ash is necessary [6]. It has been reported that the incineration ash discharged after the combustion of biomass could be utilized for a variety of purposes, for example as a soil improving agent [7,8], a fertilizer [9,10], or an adsorbent material [11].

One potential way of utilizing biomass incineration ash is in the preparation of potassium-type zeolites (K-zeolites) from coal fly ash using extracted solutions of the biomass incineration ash, which exhibit pH values ranging from 11.5–13.0 and contain high concentrations of potassium [12,13]. Although several studies have reported zeolite formation from coal fly ash using hydrothermal treatment methods [14-21], a potential problem with these systems is that they require a large quantity of highly concentrated alkaline agent for the dissolution of the ions necessary for zeolite synthesis. Thus,

aqueous solutions extracted from biomass incineration ash could potentially be employed as alkali sources to reduce the quantity of alkaline agent required.

From our previous work, we reported the synthesis of K-zeolites from coal fly ash via an external heating method using woody biomass incineration ash as an alkali source [22]. The zeolites were successfully prepared at a KOH concentration that was much lower than the concentration required to synthesize K-zeolite using a KOH solution alone as the alkaline source. However, long thermal treatment times were necessary to synthesize the zeolite. Therefore, shortening the thermal treatment time is necessary for practical use. Microwaves are capable of heating matter rapidly, directly, and selectively. In our previous studies, we have investigated the effect of microwave irradiation on zeolite synthesis from coal fly ash using pure chemicals as alkali agents. The microwave heating reduced the treatment time necessary for the reaction to go to completion [23-25].

In this chapter, we investigated the effect of microwave heating on the rate of zeolite synthesis from coal fly ash in an extracted solution of biomass incineration ash. Furthermore, the zeolite crystal synthesis rates achieved using the microwave and external heating methods were compared based on the investigation and an empirical equation.

3.2 Materials and Method

Table 3.1 lists the properties of the coal fly ash and biomass incineration ash in this work. Coal fly ash (JIS Z8910, No. 10) with a median diameter of 3.4 μm was used for preparation of the zeolite framework as a source of Si and Al. Biomass incineration ash, which had a potassium concentration of 57.6 mass%, was also used. The ash was collected from the bag filter dust collector following combustion of dry sawdust, bark, and wood chips of Japanese cedar using a fluidized bed furnace in the Chugoku Mokuzai woody biomass power plant in Hiroshima, Japan.

Table 3.1 Properties of coal fly ash and biomass incineration ash

		Coal fly ash		Biomass incineration ash
Component [mass%]	SiO_2	52.1	SiO_2	1.8
	Al_2O_3	22.3	Al_2O_3	1.5
	CaO	2.3	CaO	32.4
	K_2O	<1	K_2O	57.6
	Fe_2O_3	5.2	Fe_2O_3	<1
	Others	18.1	Others	6.7
Median diameter [μm]	3.36		4.4	

The X-ray diffraction (XRD) patterns of the biomass incineration ash before and after extraction with deionized water are shown in Figure 3.1. The crystalline phases of the biomass incineration ash were KCl and K_2CO_3, both of which are readily soluble in water. The residue contained almost no potassium, it expected to be a suitable for use as a raw material for cement (N.B., potassium degrades the quality of cement). In addition, following the extraction process, the mass of the biomass incineration ash decreased by ~40%. Therefore, our reported method of using biomass incineration ash helped to both reduce the mass of biomass incineration ash and produce useful byproducts while reducing the quantities of waste materials produced. Prior to zeolite synthesis, the coal fly ash and biomass incineration ash (before extraction) were dried at 100 °C for 24 h.

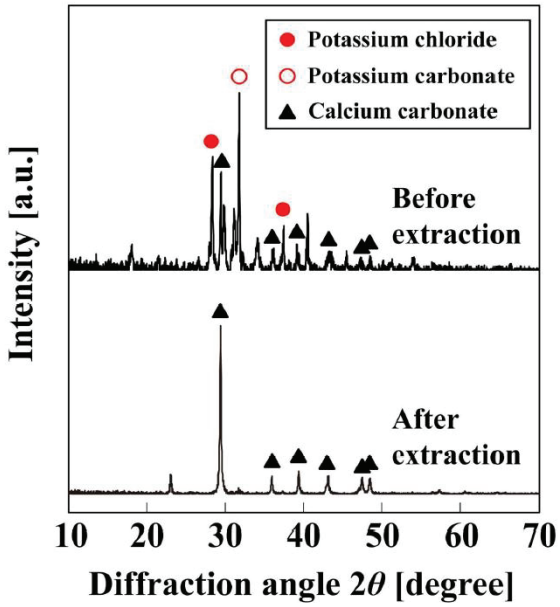

Figure 3.1 XRD pattern of incineration ash before and after extraction process

To confirm the effectiveness of using biomass incineration ash as an alternative to KOH, the following starting suspensions for hydrothermal treatment were prepared:

(i) Initial suspension using only KOH as a source of alkali and potassium (conventional suspension):

An aqueous solution of potassium hydroxide (1.5 mol/L) was prepared by dissolving KOH (4.21 g, 86.0%, Kanto Chemical Co., Inc., Japan) in deionized water (50.0 mL, SWG203, SANSYO, Japan). Then, coal fly ash (10.0 g) was dispersed in this KOH solution and used as the starting suspension.

(ii) Initial suspension using the extracted solution obtained from the biomass incineration ash as a source of alkali and potassium:

Biomass incineration ash (3.0–15.0 g) was dispersed in the deionized water (50 mL), and the resulting mixture was stirred for 10 min. A solution containing alkali and potassium was obtained by filtration. Table 3.2 shows the potassium ion concentration and pH of the obtained solution. The potassium ion concentration and pH increased upon increasing the mass of biomass incineration ash. In our previous work, we have found that pH of more than 13.5 is necessary for stable zeolite synthesis. Therefore, to adjust the pH of this solution to be more than 13.5, KOH (0.842 g, final concentration of 0.3 mol/L) was dissolved in the extracted solution. Finally, coal fly ash (10.0 g) was added as a source of Si and Al.

Table 3.2 Potassium ion concentrations and pH values of extracted solutions obtained from various masses of biomass incineration ash before and after KOH addition

Mass of biomass incineration ash [g]	**Potassium ion concentration [mol/L]**		**pH [-]**	
	Before KOH addition	**After KOH addition**	**Before KOH addition**	**After KOH addition**
3	0.35	0.65	12.94	13.54
5	0.56	0.86	13.02	13.59
10	1.17	1.47	13.18	13.67
15	1.76	2.06	13.31	13.71

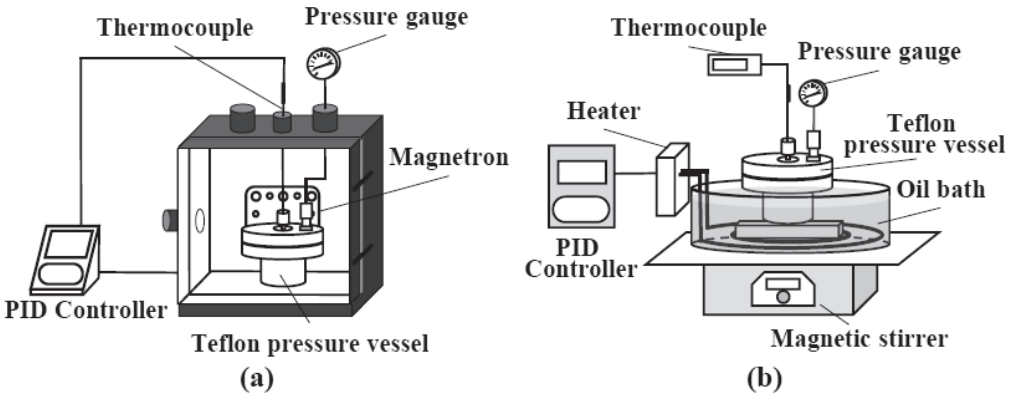

Figure 3.2 Schematics diagram of experimental apparatus; (a) Microwave heating (b) Oil bath heating

A schematic diagram of the microwave heating equipment is shown in Figure 3.2(a). Microwaves (2.45 GHz) generated by a magnetron reach the vessel via a waveguide. The prepared starting suspension was irradiated and heated by the microwaves. The temperature of the suspension was held at 413 K and was controlled by varying the output of the microwaves with a PID controller. The thermal treatment time was 2–32 h. The treatment pressure was maintained at atmospheric pressure (1.013×10^5 Pa), and the rotational speed of the stirrer was set to 100 rpm. After the hydrothermal treatment, the desired product was isolated by filtration (Büchner funnel) and washed with deionized water thoroughly prior to drying at 373 K for 24 h to give the powdered product.

As a control experiment, the prepared starting suspension was treated hydrothermally under the same conditions using a conventional electric heater, shown in Figure 3.2(b). The prepared starting suspensions were then loaded into a 100 mL Teflon reaction vessel, and the suspensions were heated in an oil bath (OHB-1000G, EYELA, Japan) at 413 K with constant stirring at 450 rpm (RCX-1000D, EYELA, Japan) to promote hydrothermal treatment.

The ammonium adsorption capacities of the powdered products were evaluated by a breakthrough experiment. Aqueous solutions of NH_4Cl (200 mg/L, 99.0%, Sigma-Aldrich) were used to permeate the powdered product (0.2 g), which was packed into a cylindrical column (diameter = 8 mm). The adsorption capacity was estimated using a

breakthrough curve calculated from the variation in ion concentration in the permeated solution. The concentration of ammonium ions was measured using an ion meter (F-53, Horiba, Japan). Moreover, the concentrations of elemental Al, Si, and K in the suspension and the extracted solution were also measured using an inductively coupled plasma atomic emission spectrometer (ICP, SPS3000, Seiko, Japan). The crystalline phases were identified by XRD (RINT-2000, Rigaku, Japan), and the surface morphologies of the products were observed by scanning electron microscopy (SEM, S-5200, Hitachi, Japan). The elemental compositions of the products were determined using energy-dispersive X-ray spectrometry (EDX, EDX-800, Shimadzu, Japan).

3.3 Results and Discussion

Figure 3.3 shows the XRD patterns of the powdered products obtained by microwave hydrothermal treatment using extracted solutions obtained from various amounts of biomass incineration ash. As shown, when the quantity of the biomass incineration ash extracted into the solution was ≥ 3.0 g, signals corresponding to the newly generated zeolite phases (i.e., phillipsite) were observed in addition to peaks corresponding to quartz present in the unreacted coal fly ash. However, when 0.3 mol/L of KOH was used without the extracted biomass incineration ash solution, only signals corresponding to the starting material were observed. These results indicate that for zeolite synthesis to be successful, at least 3.0 g of biomass incineration ash must be extracted into solution when using 0.3 mol/L of KOH.

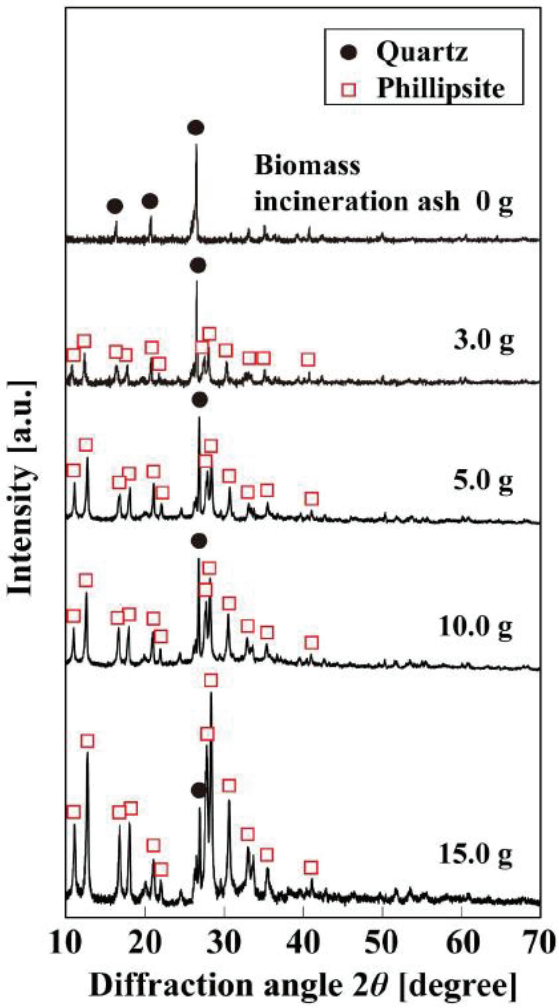

Figure 3.3 XRD pattern of products synthesized by microwave hydrothermal treatment using extracted solution of biomass incineration ash.

Figure 3.4 shows the relationship between the ammonium adsorption capacities of the products synthesized by the two different heating methods and the amount of biomass incineration ash used to prepare the extracted solutions. The hydrothermal treatment time and temperature were fixed at 24 h and 413 K, respectively, for both heating methods. As shown, the ammonium adsorption capacities increased for both methods until the quantity of ash reached 10.0 g. At ash quantities of above 10.0 g, the ammonium adsorption capacities remained constant at ~50 mg/g regardless of the heating method. This value was similar to that seen for products generated by microwave hydrothermal treatment using KOH (1.5 mol/L) without the extracted solution of biomass incineration ash, indicating that zeolite synthesis went to completion when biomass

incineration ash was used. These results reveal that the ammonium adsorption capacity of the product powder does not depend on the heating method, provided that the treatment time is sufficient. Hereafter, the quantity of biomass incineration ash used was fixed at 10.0 g.

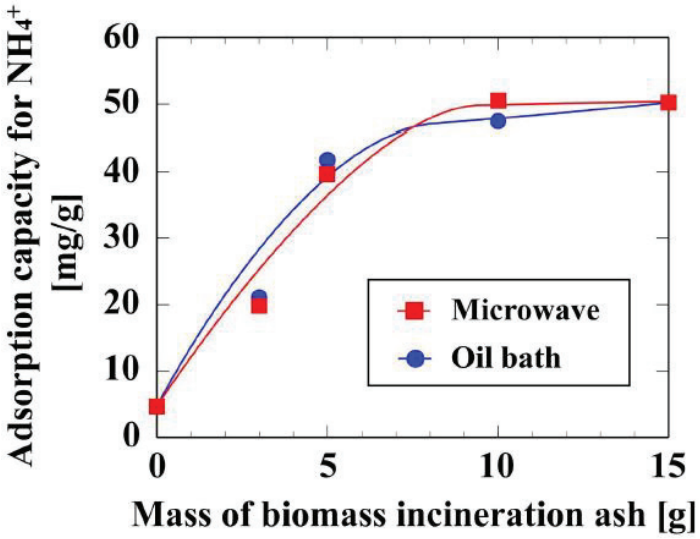

Figure 3.4 Relationships between ammonium adsorption capacities of the product and the amount of biomass incineration ash present in the extracted solutions for microwave and oil-bath

The SEM images of the powdered products prepared by microwave or oil-bath hydrothermal treatment of coal fly ash using extracted solution obtained from 10.0 g of biomass incineration ash are shown in Figure 3.5. In our previous work, large zeolite crystals were observed on the surface of the coal fly ash after oil bath hydrothermal treatment using only KOH without extracted solutions of biomass incineration ash. In contrast, when extracted solutions of biomass incineration ash were employed, relatively small zeolite crystals were observed [22]. As shown in Figure 3.5, small zeolite crystals were observed on the surface of the coal fly ash regardless of the heating method. It should be noted that no noticeable differences between the morphologies of the products fabricated by the different heating methods could be found.

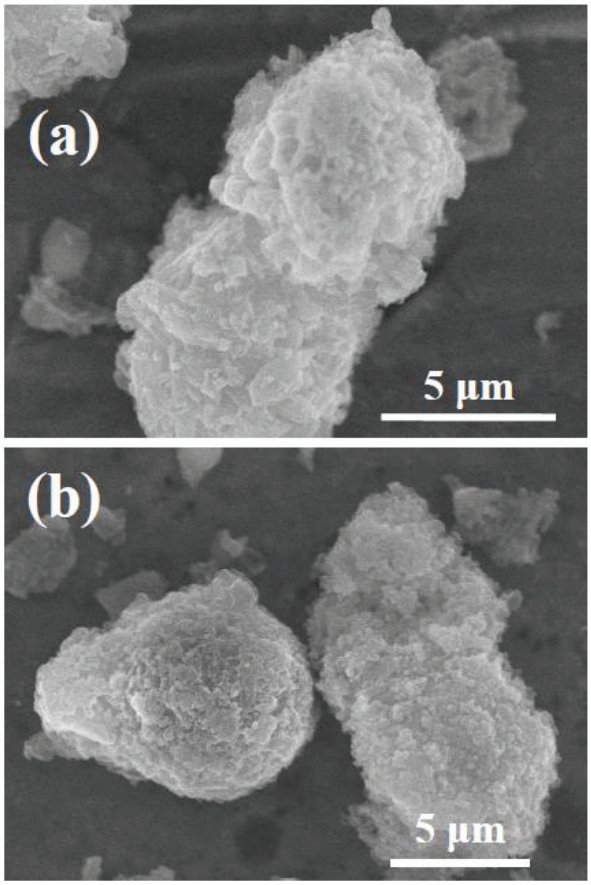

Figure 3.5 Microstructure of the products obtained from coal fly ash with 10 g of biomass incineration ash extract synthesized by (a) oil-bath and (b) microwave heating

The effect of thermal treatment time on the ammonium adsorption capacity of the product powder were examined for the both heating methods. The changes in the ammonium adsorption capacities of the product powders with treatment time are shown in Figure 3.6. For the microwave heating method, the ammonium adsorption capacity gradually increased until a treatment time of ~16 h was reached. After this point it remained almost constant, indicating that the zeolite synthesis was complete. A similar tendency was seen in our previous work, which reported zeolite synthesis from fly ash by a hydrothermal treatment method in a microwave using pure chemicals [23-25].

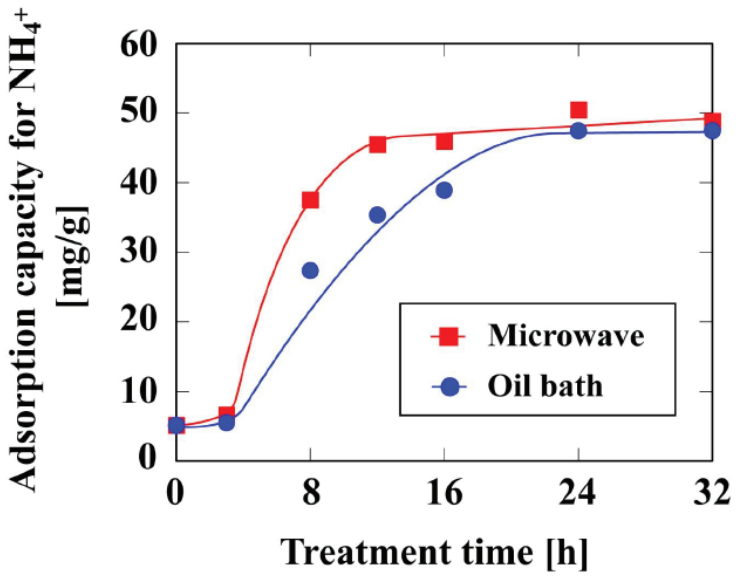

Figure 3.6 Changes in the ammonium adsorption capacities of the products with increasing treatment time for microwave and oil bath heating

For oil-bath heating, the ammonium adsorption capacity increased with the treatment time until approximately 24 h, after which it remained almost constant. As the rate of increase in the ammonium adsorption capacity corresponds to the zeolite generation rate, the rate obtained for microwave heating was larger than that seen for oil-bath heating. However, the ammonium adsorption capacity stable at ~50 mg/g regardless of the heating method, indicating that the amount of zeolite obtained was almost identical regardless of the heating method if the treatment time is sufficient.

Figure 3.7 shows the change in the phillipsite XRD peak intensity with increasing treatment time, where the peak intensity was normalized using the intensity of the crystal quartz peak as the reference. Here, it should be noted that the peak of the crystal quartz did not significantly decrease under the experimental conditions. These XRD peak intensity ratios reflect the progress of the zeolite crystallization. In the case of microwave heating, the phillipsite peak was not detected until 3 h, indicating that there was no crystallization of zeolite before this time. After this, the peak intensity increased with treatment time until 16 h, after which it remained almost constant. These results are similar to those seen for the change in the ammonium adsorption capacity with treatment time, as shown in Figure 3.6. This indicates that the crystallization of zeolite occurred at treatment times of 3–16 h and was completed thereafter. On the other hand, during oil-

bath heating, the phillipsite peak was not detected until a time of 3 h and then increased in intensity until a treatment time of 24 h. This result agrees well with the ammonium adsorption capacity, as shown in Figure 3.6. In order to investigate the effect of microwave heating on the zeolite generation rate, the changes in the concentrations of aluminate and silicate ions over time were measured.

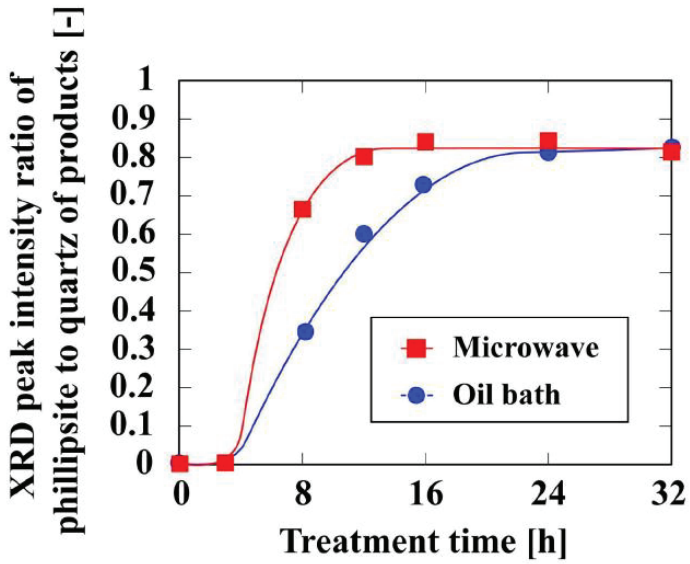

Figure 3.7 Relationships between ratio of phillipsite to silica XRD peak intensities and treatment time for microwave and oil bath heating

As shown in figure 3.8, In both heating methods, the concentration of aluminate ions increased rapidly during the early stages then decreased to a constant concentration after reaching a maximum at 30 min. On the other hand, the concentration of silicate ions gradually increased with time in both cases, plateauing at ~4 h. Similar behavior regarding the concentrations of aluminate and silicate ions during the hydrothermal zeolite synthesis from coal fly ash has been reported previously [14,23-25].

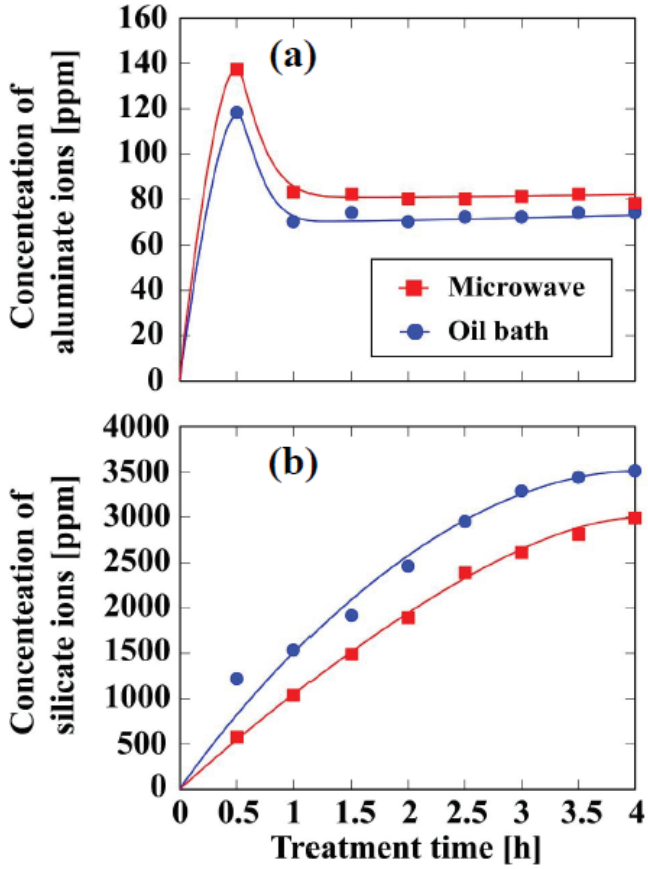

Figure 3.8 Changes in the concentrations of (a) aluminate and (b) silicate ions in the hydrothermal solutions as treatment time for microwave and oil bath heating

As shown in Figure 3.8, there was no difference between the dissolution behaviors of aluminum and silicate ions from coal fly ash when using the microwave and the oil-bath heating methods. The changes in the potassium contents of the product powders with increasing treatment time were also measured for microwave and oil-bath heating, as shown in figure 3.9. Here, the potassium content reflects the total amount of aluminosilicate gel, amorphous zeolite, and crystalline zeolite contained in the product powder. In both cases, the potassium content increased with time until approximately 12 h. After that, it remained almost constant. It should be note that both the time is taken for the potassium content to reach a plateau and the value of said plateau hardly depended on the heating method, although the rate of the increase in the potassium content of the powder obtained by microwave heating was slightly greater than that seen for the powder

obtained by oil bath heating. It is thought that the synthesis of zeolite from coal fly ash takes place primarily through the following heterogeneous reaction processes [24,26]:

(i) aluminate and silicate ions dissolve from the coal fly ash into the hydrothermal solution,

(ii) dissolved ions and potassium ions form aluminosilicate gel on the surface of the coal fly ash, and amorphous zeolite is generated, and

(iii) amorphous zeolite crystallizes to form crystalline zeolite.

From the results shown in Figure 3.7 to 3.9, it can be concluded that the zeolite crystallization rate was higher during microwave heating than during oil-bath heating; however, the peak intensity ratios obtained after long treatment times (more than 24 h) were almost the same regardless of the heating method.

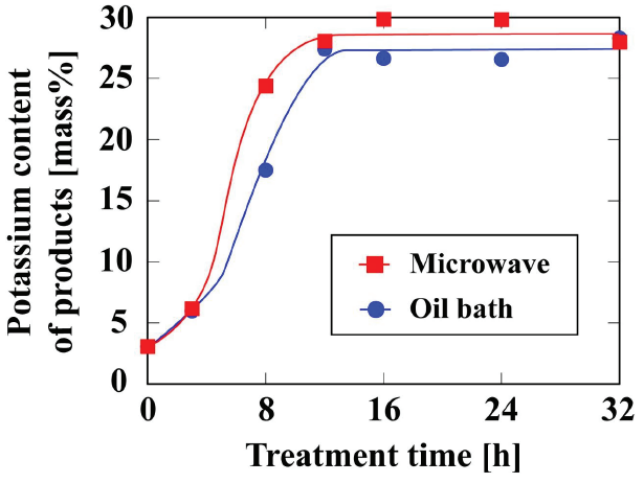

Figure 3.9 Relationship between potassium content and treatment time of product synthesized by microwave and oil bath heating.

In order to investigate the effect of microwave heating on the rate of crystalline zeolite synthesis, we attempted to compare the rate of crystalline zeolite synthesis via microwave heating and external heating using the Avrami equation [27,28]:

$$\alpha(t) = 1 - e^{(-k \cdot t^n)} \tag{3.1}$$

where $\alpha(t)$ and t are the fractions of crystallized zeolite and the treatment time, respectively, and the constant k represents the reaction rate (rate constant). The value of the exponent n provides some information on the crystallization pattern (Avrami index) [29-31]. The Avrami equation has been used by many researchers to explain the synthesis of crystalline zeolite [29,30,32-37], and the equation could provide an empirical way to

describe the kinetic process, although it is difficult to discuss the synthesis process rigorously since the equation has no fundamental derivation [33,35,36,38].

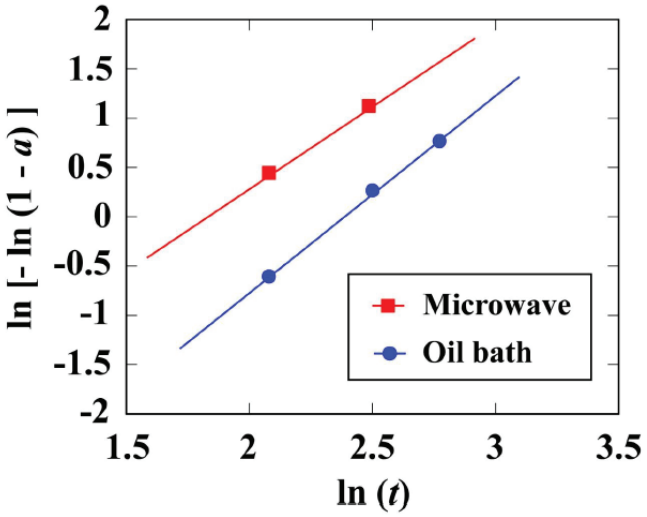

Figure 3.10 Relationship between the fractions of crystallized zeolite and the treatment time for microwave and oil-bath heating.

In Figure 3.10, the XRD results from Figure 3.7 have been replotted as a function of treatment time, where the fraction of crystallized zeolite $\alpha(t)$ was defined by normalizing the XRD peak intensity ratio of phillipsite to quartz in the products to the XRD peak intensity ratio of phillipsite to quartz at the end of crystallization. Crystallization was defined to have finished at treatment times of 16 h and 24 h for microwave heating and external heating, respectively (see Figure 3.7). The Avrami indices (n) and rate constants (k) as obtained from the linear plots in Figure 3.10 are listed in Table 3.3. The Avrami index for microwave heating was slightly smaller than that seen for external heating. Several studies that have examined the effect of treatment temperature on zeolite crystallization have reported that the Avrami index decreases with increasing treatment temperature [34,36]. As microwave heating results in a slightly smaller value of n, it is suggested that there was a higher temperature in the synthetic region compared to that obtained in external heating, even though the bulk temperature was 413 K in both heating methods. This is due to the effect of local heating in the microwave heating method. On the other hand, k was more than five times higher when using microwave heating than when using external heating, indicating that microwave heating led to a higher zeolite crystal generation rate.

Table 3.3 Avrami indices and rate constants

		Microwave	Oil bath
Avrami index	n	1.63	1.99
Rate constant	k	5.21×10^{-2}	0.88×10^{-2}

3.4 Conclusion

We synthesized zeolite by microwave hydrothermal treatment of coal fly ash using extracted solutions of biomass incineration ash. The effect of microwave heating on the crystalline zeolite synthesis rate was investigated by comparison with oil-bath heating (external heating). The zeolite crystal formation rate obtained by microwave heating was larger than that seen for oil-bath heating. This is considered to be due to the local heating in the microwave heating method. The microwave heating method employed higher temperatures in the synthetic region compared to external heating, even though the bulk temperature was set at 413 K in both heating methods. On the other hand, the adsorption capacities of the ammonium ions and the phillipsite-to-quartz peak intensity ratios obtained after long treatment times (>24 h) were almost the same regardless of the heating method, indicating that the heating method did not affect the properties of the obtained zeolite.

3.5 References

[1] P. Sun, P. Nie, A comparative study of feed-in tariff and renewable portfolio standard policy in renewable energy industry, Renew. Energy 74 (2015) 255–262.

[2] K. Sasauchi, Selection of technical systems suitable for small scale biomass power generation under the FIT scheme, J. Jpn. Inst. Energy 94 (2015) 1188–1193.

[3] T. Kimura, Status of, and issues concerning, biomass power generation in the framework of FIT, J. Jpn. Inst. Energy 94 (2015) 1204–1209.

[4] T. Miura, Current status of biomass energy utilization, J. Waste Resour. Recycl. 21 (2010) 11–17.

[5] N. Tanigaki, Y. Ishida, M. Osada, A case-study of landfill minimization and material recovery via waste co-gasification in a new waste management scheme, Waste Manage. 37 (2015) 137-146.

[6] N. Maeda, T. Katakura, T. Fukasawa, A.N. Huang, T. Kawano, K. Fukui, Morphology of woody biomass combustion ash and enrichment of potassium components by particle size classification, Fuel Process. Technol. 156 (2017) 1-8.

[7] A. Demeyer, J.C.V. Nkana, M.G. Verloo, Characteristics of wood ash and influence on soil properties and nutrient uptake: an overview, Bioresour. Technol. 77 (2001) 287-295.

[8] B.B. Park, R.D. Yanai, J.M. Sahm, D.K. Lee, L.P. Abrahamson, Wood ash effects on plant and soil in a willow bioenergy plantation, Biomass Bioenergy 28 (2005) 355–365.

[9] C. Maschowski, M.C. Zangna, G. Trouvé, R. Gieré, Bottom ash of trees from Cameroon as fertilizer, Appl. Geochem. 72 (2016) 88-96.

[10] H. Nurmesniemi, M. Mäkelä, R. Pöykiö, K. Manskinen, O. Dahl, Comparison of the forest fertilizer properties of ash fractions from two power plants of pulp and paper mills incinerating biomass-based fuels, Fuel Process. Technol. 104 (2012) 1–6.

[11] Q. Feng, Q. Lin, F. Gond, S. Sugita, M. Shoya, Adsorption of lead and mercury by rice husk ash, J. Colloid Interface Sci. 278 (2004) 1–8.

[12] A. Peys, H. Rahier, Y. Pontikes, Potassium-rich biomass ashes as activators in metakaolin-based inorganic polymers, Appl. Clay Sci. 119 (2016) 401–409.

[13] S.V. Vassilev, D. Baxter, L.K. Andersen, C.G. Vassileva, An overview of the composition and application of biomass ash. Part 1. Phase–mineral and chemical composition and classification, Fuel 105 (2013) 40-76.

[14] T. Fukasawa, A.D. Karisma, S. Shibata, A.-N. Huang, K. Fukui, Synthesis of zeolite from coal fly ash by microwave hydrothermal treatment with pulverization process, Adv. Powder Technol., 28 (2017) 798-804.

[15] C. Belviso, F. Cavalcante, S. Fiore, Synthesis of zeolite from Italian coal fly ash: Differences in crystallization temperature using seawater instead of distilled water, Waste Manage., 30 (2010) 839-847.

[16] V.K. Jha, M. Nagae, M. Matsuda, M. Miyake, Zeolite formation from coal fly ash and heavy metal ion removal characteristics of thus-obtained Zeolite X in multi-metal systems, J. Environ. Manage., 90 (2009) 2507-2514.

[17] H. Tanaka, A. Fujii, S. Fujimoto, Y. Tanaka, Microwave-Assisted Two-Step Process for the Synthesis of a Single-Phase Na-A Zeolite from Coal Fly Ash, Adv. Powder Technol., 19 (2008) 83-94.

[18] M. Inada, H. Tsujimoto, Y. Eguchi, N. Enomoto, J. Hojo, Microwave-assisted zeolite synthesis from coal fly ash in hydrothermal process, Fuel, 84 (2005) 1482-1486.

[19] K. Fukui, H. Yoshida, H. Sakaguchi, M. Arita, Zeolite Synthesis from Coal Fly Ash Prepared by Hydro-thermal Treatment Method and Effect of Particle Size on its Reaction Mechanism, Kagaku Kogaku Ronbun, 25 (1999) 987-992.

[20] G.G. Hollman, G. Steenbruggen, M. Janssen-Jurkovičová, A two-step process for the synthesis of zeolites from coal fly ash, Fuel, 78 (1999) 1225-1230.

[21] X. Querol, A. Alastuey, A. López-Soler, F. Plana, J.M. Andrés, R. Juan, P. Ferrer, C.R. Ruiz, A Fast Method for Recycling Fly Ash: Microwave-Assisted Zeolite Synthesis, Environ. Sci. Technol., 31 (1997) 2527-2533.

[22] T. Fukasawa, A. Horigome, T. Tsu, A.D. Karisma, N. Maeda , A.-N. Huang, K. Fukui, Utilization of incineration fly ash from biomass power plants for zeolite synthesis from coal fly ash by hydrothermal treatment, Fuel Process. Technol. 167 (2017) 92-98.

[23] K. Fukui, M. Katoh, T. Yamamoto, H. Yoshida, Utilization of NaCl for phillipsite synthesis from fly ash by hydrothermal treatment with microwave heating, Adv. Powder Technol., 20 (2009) 381-393.

[24] K. Fukui, K. Kanayama, T. Yamamoto, H. Yoshida, Effects of microwave irradiation on the crystalline phase of zeolite synthesized from fly ash by hydrothermal treatment, Adv. Powder Technol., 18 (2007) 381-393.

[25] K. Fukui, K. Arai, K. Kanayama, H. Yoshida, Phillipsite synthesis from fly ash prepared by hydrothermal treatment with microwave heating, Adv. Powder Technol., 17 (2006) 369-382.

[26] E.G. Derouane, S. Determmerie, Z. Gabelica, N. Blom, Synthesis and characterization of ZSM-5 type zeolites I. physico-chemical properties of precursors and intermediates, Appl. Catal. 1 (1981) 201-224.

[27] M. Avrami, Kinetics of Phase Change. I General Theory, J. Chem. Phys., 7 (1939) 1103-1112.

[28] M. Avrami, Kinetics of Phase Change. II Transformation-Time Relations for Random Distribution of Nuclei, J. Chem. Phys., 8 (1940) 212-224.

[29] C. Chen, T. Cheng, Application of Avrami equation to kinetics analysis of fly ash based Linde F (K) zeolite, Asian J. Chem., 25 (2013) 1811-1813.

[30] M.L.G. Castillo, F.D. Renzo, F. Fajula, J. Bousquet, Crystallization kinetics of zeolite omega, the synthetic analog of mazzite, Micropor. Mesopor. Mat., 90 (2006) 221-228.

[31] J. Yang, B.J. McCoy, G. Madras, Distribution kinetics of polymer crystallization and the Avrami equation, J. Chem. Phys., 122 (2005) 064901.

[32] P.M. Budd, G.J. Myatt, C. Price, S.W. Carr, An empirical model for the nucleation and growth of zeolites, Zeolites, 14 (1994) 198-202.

[33] R.W. Thompson, Analysis of zeolite crystallizations using Avrami transformation methods, Zeolites, 12 (1992) 680-684.

[34] P.N. Joshi, G.N. Rao, A.N. Kotasthane, V.P. Shiralkar, Influence of template on crystallization of ZSM-5 zeolites, J. Inclus. Phenom. Mol., 9 (1990) 91-99.

[35] R.W. Thompson, A. Dyer, Mathematical analyses of zeolite crystallization, Zeolites, 5 (1985) 202-210.

[36] S.B. Kulkarni, V.P. Shiralkar, A.N. Kotasthanc, R.B. Borade, P. Ratnasamy, Studies in the synthesis of ZSM-5 zeolites, Zeolites, 2 (1982) 313-318.

[37] J. Ciric, Kinetics of zeolite A crystallization, J. Colloid Interf. Sci., 28 (1968) 315-324.

[38] P.T. Cardew, R.J. Davey, A.J. Ruddick, Kinetics of polymorphic solid-state transformations, J. Chem. Soc., Faraday Trans. 2, 80 (1984) 659-668.

CHAPTER 4

Synthesis of NiCuZn ferrite nanoparticles from metallic nitrate solutions using the microwave direct denitration method

4.1 Introduction

A multilayer chip inductor (MLCI) has a laminated-type passive surface mount design (SMD) equipped with magnetic shielding characteristic that does not produce significant electromagnetic interference[1]. This component is suitable for high-density packaging of electrical circuits and permits the miniaturization of electronic devices such as cameras, mobile phones, and notebook computers.

NiCuZn ferrites are one of the functional materials that have shown promise for MLCI applications due to their high electrical resistivity, high permeability, and low sintering temperature[2–5]. Conventionally, NiCuZn ferrite is prepared from a mixture of metallic oxide powders using a solid-state reaction process and a subsequent calcination process at a high temperature[1]. However, some disadvantages such as poor compositional control, chemical inhomogeneity, and contamination during ball milling may be encountered in this method[6]. The NiCuZn ferrite powders have also been successfully synthesized previously by the combustion synthesis[7], sol-gel[8], co-precipitation[9], and hydrothermal method[10]. It has been reported that the ferrite spinel powders obtained by these methods are much finer than those obtained by the conventional solid-state reaction method. However, these methods also show limitations such as the requirement for relatively long reaction time and the complicated multiple-step pathways involved in the process.

Some researchers have attempted to apply microwave heating to the preparation of NiCuZn ferrite. A microwave heating offers some of advantages such as it can heat an object directly, rapidly, and selectively[11]. Microwave generates heat through its interactions with the dipoles and charges in the object[12]. Because of these characteristics, the microwave heating method can reduce the required reaction time,

while inhibiting the synthesis of byproducts. Therefore, it is one of the most promising candidate methods for clean and energy-efficient heating.

Recently, NiCuZn ferrite powders have been successfully obtained using the solid-state reaction method by the microwave heating of a mixture of NiO, CuO, ZnO, and Fe_2O_3 powders. Additionally, this work reported that a small amount of additive material served to reduce the activation energy and bulk density of the sintered material[4]. It has also been found that the NiCuZn ferrite product prepared from commercial ferrite materials by microwave sintering has a higher density than that obtained by conventional sintering[13].

Our previous studies have reported that CuO and NiO powders can be synthesized from $Cu(NO_3)_2 \cdot 3H_2O$ and $Ni(NO_3)_2 \cdot 6H_2O$ aqueous solutions, respectively, by the microwave direct denitration (MDD) reaction method[14]. The mechanism of this reaction was also clarified[15]. From our prior work, the nitrates and oxides of Cu and Ni have been found to exhibit very high microwave absorptivities. We therefore believe that the NiCuZn ferrite powder may be easily and efficiently obtained by the MDD method from metallic nitrate aqueous solutions; such an approach has not been reported thus far. Further, since this method requires only simpler and shorter steps, it will likely help simplify the synthesis of NiCuZn ferrite powders.

In this chapter, the synthesis of nanoparticles of NiCuZn ferrite using the MDD method from a mixture of solutions of metal nitrate hydrates as the raw material were studied. The reaction mechanism and influence of reaction temperature on the morphology of the obtained powder product were examined. Furthermore, the magnetic properties of the powder product and sintered product materials with a Bi_2O_3 additive agent were also investigated.

4.2 Materials and Method

A NiCuZn ferrite powder having the chemical composition $Ni_{0.5}Cu_{0.1}Zn_{0.4}Fe_2O_4$ was synthesized from an aqueous mixture of metal nitrate hydrate reagents by the microwave direct denitration (MDD) method. Analytical grade $Ni(NO_3)_2 \cdot 6H_2O$, $Cu(NO_3)_2 \cdot 3H_2O$, $Zn(NO_3)_2 \cdot 6H_2O$, and $Fe(NO_3)_2 \cdot 9H_2O$ reagents (Sigma-Aldrich) were used as the raw materials. The reagents were dissolved in 20.0 mL of distilled water. The

mass (4.8, 0.8, 4.0, and 12.1 g, respectively) of each reagent was adjusted according to the chemical stoichiometric ratio of the ferrite $Ni_{0.5}Cu_{0.1}Zn_{0.4}Fe_2O_4$.

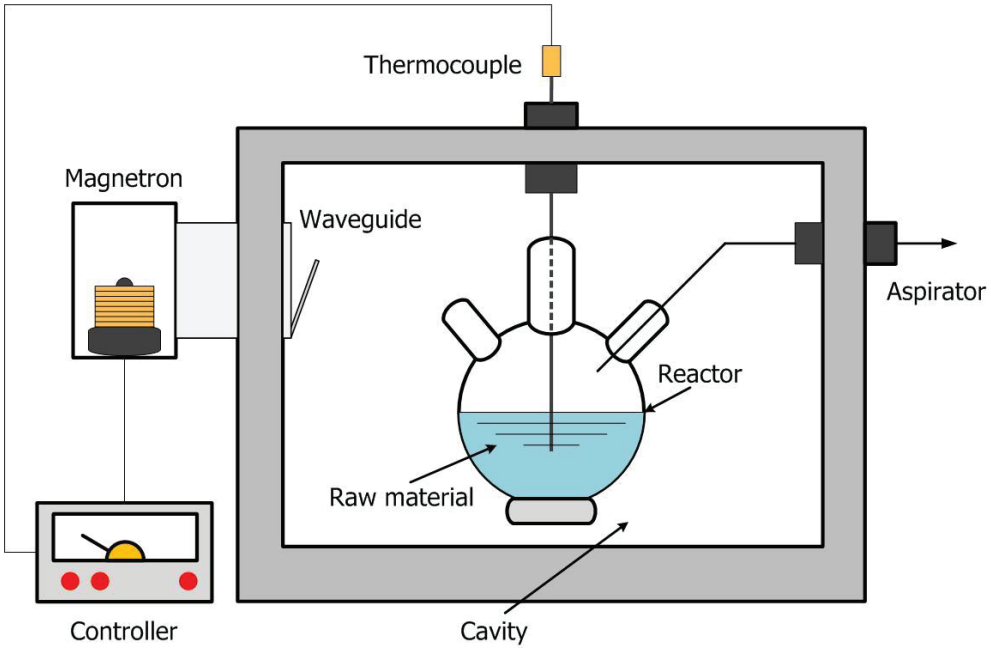

Figure 4.1 Schematic of the multimode microwave heating set-up.

Figure 4.1 shows a schematic diagram of the multi-mode microwave synthesis apparatus, which contains a magnetron, waveguide, PID controller, K-type thermocouple, and aspirator. The starting material solution in the three-necked quartz flask reactor was irradiated using a 2.45 GHz microwave and heated to the target temperature rapidly using a constant output power of 700 W. The temperature in the reactor was measured using a K-type thermocouple. The temperature was kept constant at 500–1000 ºC for 1 h using a PID controller. To prevent the accumulation of exhaust water vapor and nitrogen oxide gas generated by the denitration of the starting solution, the air was drawn into the reactor by a circulating aspirator which absorbed the vapor and the nitrogen oxide gas. The obtained product powder was dried in an oven at 60 ºC for 24 h. Then it was loosened and crushed by a ball mill for 1 h to obtain the dispersed powder.

As a control experiment, the NiCuZn ferrite powder was also synthesized by the solid-state reaction (SSR) method in accordance with the procedure described by Zhu et al.[4]. For the preparation of the raw material, analytical grade NiO, ZnO (Nacalai Tesque Inc.), CuO, and Fe_2O_3 (Sigma Aldrich) powder reagents were weighed according

to the stoichiometric ratio of the NiCuZn ferrite. The mixture of reagents was wet-milled at 300 rpm for 4 h using a planetary ball mill (Fritsch, Pulverisette 6) and dried at 60 ^{o}C for 12 h. The product powder was then obtained by heating at 500–1000 ^{o}C in an electric furnace. The subsequent procedures were the same as that employed in the above mentioned MDD method.

The ferrite powder of mass 0.8 g obtained by each method was pressed into a cylindrical pellet of diameter 13.0 mm and height 1.75 mm by a 2.94 MPa uniaxial hand press. The pellet was then sintered using an electric furnace (Nitto Kagaku Co., LTD) at 1000 ^{o}C for 4 h. Furthermore, to investigate the effect of the additive material, Bi_2O_3, on the densification of the pellet by the sintering process, 1.0 mass % of Bi_2O_3 powder reagent was mixed in the obtained powder using a rotary mixer for 1 h. The sintered pellet was also prepared from the mixture of NiCuZn ferrite with Bi_2O_3 as described earlier.

The crystalline phases of the products were identified using an X-ray diffractometer with a Cu-Kα source (XRD; Rigaku, MiniFlex 600). The crystal grain size was calculated by the Scherrer equation[16]:

$$L = \frac{K\lambda}{\beta cos\theta} \tag{4.1}$$

Here, L is the crystal grain size, K the dimensionless shape factor (=0.9), λ the X-ray source wavelength (=0.15418 nm), β the full width at half maximum (FWHM), and θ the Bragg angle. Further, the morphology of the product was observed by scanning electron microscopy (SEM; Hitachi, S-5200) and the specific surface area was measured by BET analysis (Microtrac Bel Corp., Belsorp-mini II). The magnetic properties were acquired using a superconducting quantum interference device (SQUID, Quantum Design MPMS-5s). The magnetization was measured from 1.0 to 10.0 kOe as a function of the magnetic field at room temperature.

3. Result and discussion

Figure 4.2 shows the XRD patterns of the powders obtained at a reaction temperature of 500 ^{o}C using the microwave direct denitration (MDD) and the solid-state reaction (SSR) methods. Figure 4.2(a) indicates that the NiCuZn ferrite, which had much higher peak intensities than other compounds, was formed from the aqueous mixture of metal nitrate hydrate reagents by microwave irradiation. However, by-products of the

denitration reaction such as ZnO and Fe_2O_3 were also formed at this reaction temperature. This suggests that the NiCuZn ferrite was directly produced from the mixture of metal nitrate hydrate reagents without the synthesis of intermediate crystalline oxides. It can be also observed that all peaks of the compounds in the product powder acquired by the MDD method at 500^{o}C were relatively broad, which suggests that most of the compounds still existed as the amorphous phase. On the other hand, as shown in Figure 4.2(b), the peak intensity of Fe_2O_3 was higher than that of the others component. The peaks corresponding to unreacted ZnO and NiO were also detected. Therefore, in the case of the SSR method, we believe that the crystalline NiCuZn ferrite was formed by the gradual solid phase diffusion of NiO, CuO, and ZnO phases into the crystalline Fe_2O_3[17]. Further, we believe that the NiCuZn ferrite formed by the solid phase diffusion displays high crystallinity due to the high crystallinity of the Fe_2O_3 matrix.

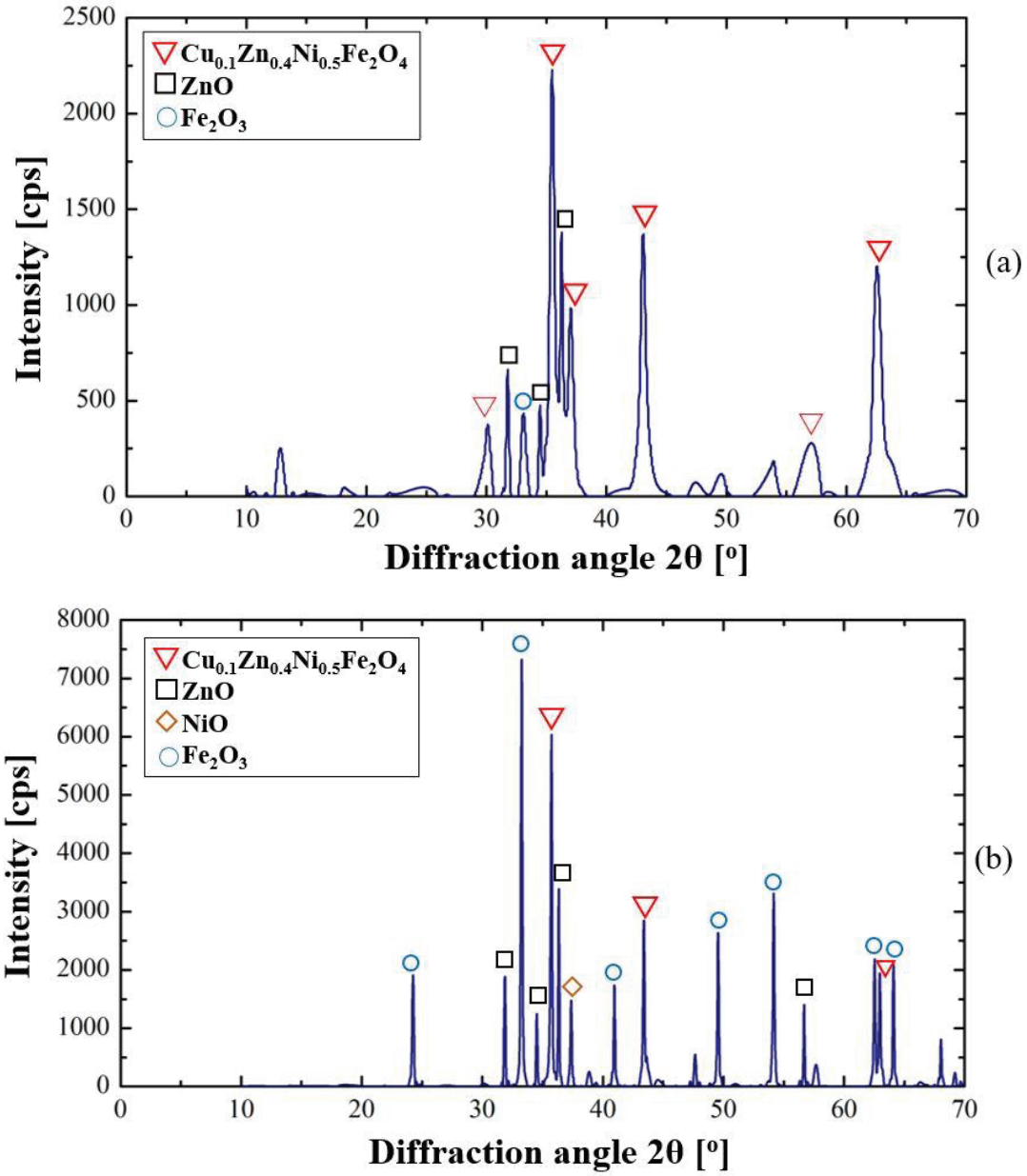

Figure 4.2 XRD patterns of the powders synthesized at 500ºC by the (a) microwave denitration and (b) solid state reaction methods.

The effect of reaction temperature on the crystalline content of the powders obtained by both synthesis methods was investigated. Figure 4.3 shows the XRD patterns of the product powders acquired at various reaction temperatures for both methods. Figure 4.3(a) shows that the MDD method was able to provide a NiCuZn ferrite with a single crystalline phase at reaction temperatures greater than 900 ºC. As the reaction temperature increased, the by-products of ZnO and Fe_2O_3 phase decreased due to the

thermal decomposition[18]. On the other hand, as shown in Figure 4.3(b), the intensity of unreacted raw materials, Fe_2O_3 and NiO phases, was decreased with increasing reaction temperature from 800 to 1000 ºC. Even when the reaction temperature attained to 900 ºC, the peaks of the Fe_2O_3 and NiO phases were still observed when using the SSR method. The NiCuZn ferrite composed of a single crystalline phase could be acquired using the SSR method only at temperatures above 1000 ºC.

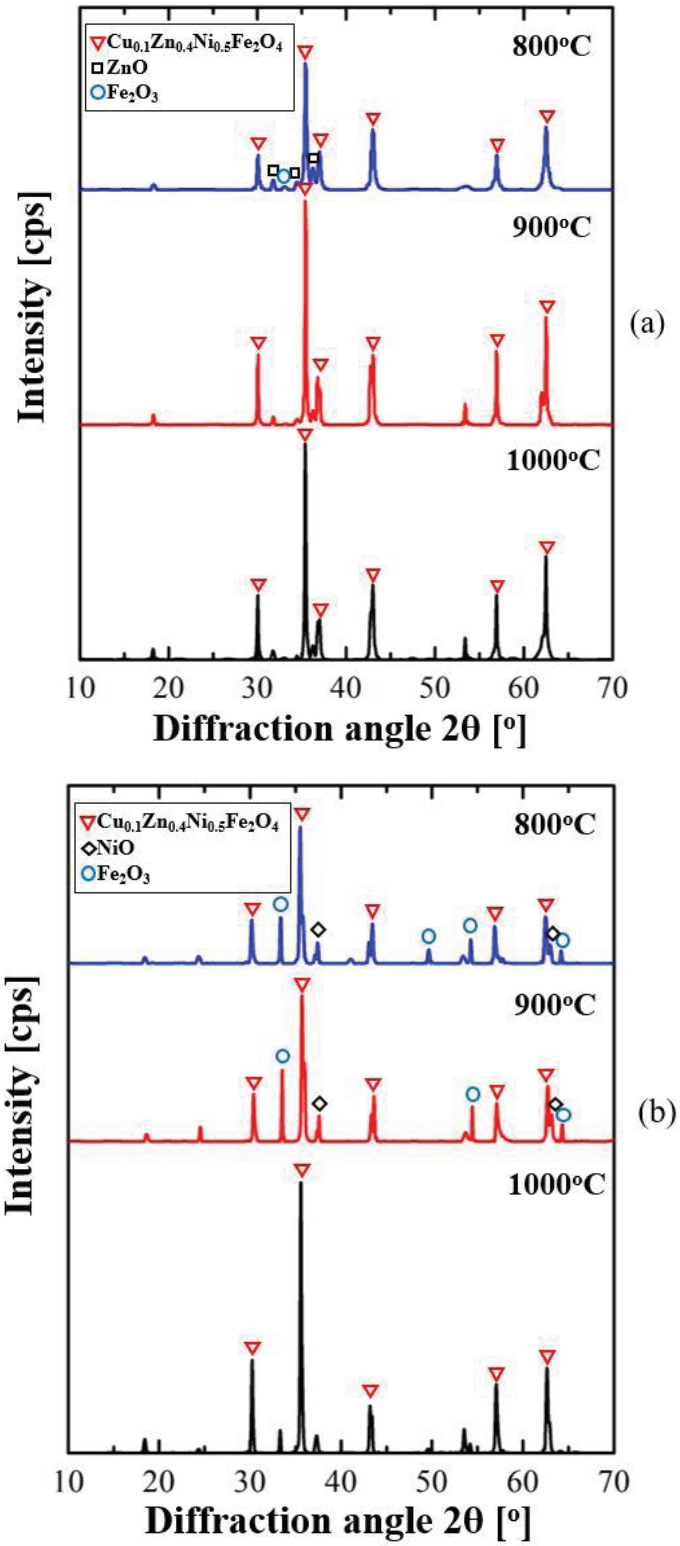

Figure 4.3 XRD patterns of the powders synthesized at 800–1000 °C by (a) microwave denitration and (b) solid state reaction methods.

Figure 4.4 shows the relationship between the reaction temperature and the crystal grain size of generated NiCuZn ferrite in the product powders. Here, the crystal grain size was calculated from the peak at $2\theta = 35.4^{o}$ using Scherrer equation shown in Eq. (1). The crystal grain size of the NiCuZn ferrites obtained by the MDD and SSR methods remained constant at about 25 nm and 60 nm, respectively, at reaction temperatures lower than 650 ^{o}C. At higher temperatures, the crystal grains from the MDD method monotonically increased to a maximum size of 62.55 nm at 900 ^{o}C. Above 900 ^{o}C, the grain size decreased slightly. On the other hand, the crystal grain obtained by the SSR method decreased gradually to about 40 nm when using reaction temperatures greater than 650 ^{o}C. This result indicates that the SSR method formed the NiCuZn ferrite by the gradual solid phase diffusion of the additive elements into the highly crystalline Fe_2O_3 matrix structure [17]. These results also confirmed that above 800 ^{o}C the MDD method could provide NiCuZn ferrite particles with larger crystal grain sizes than the SSR method.

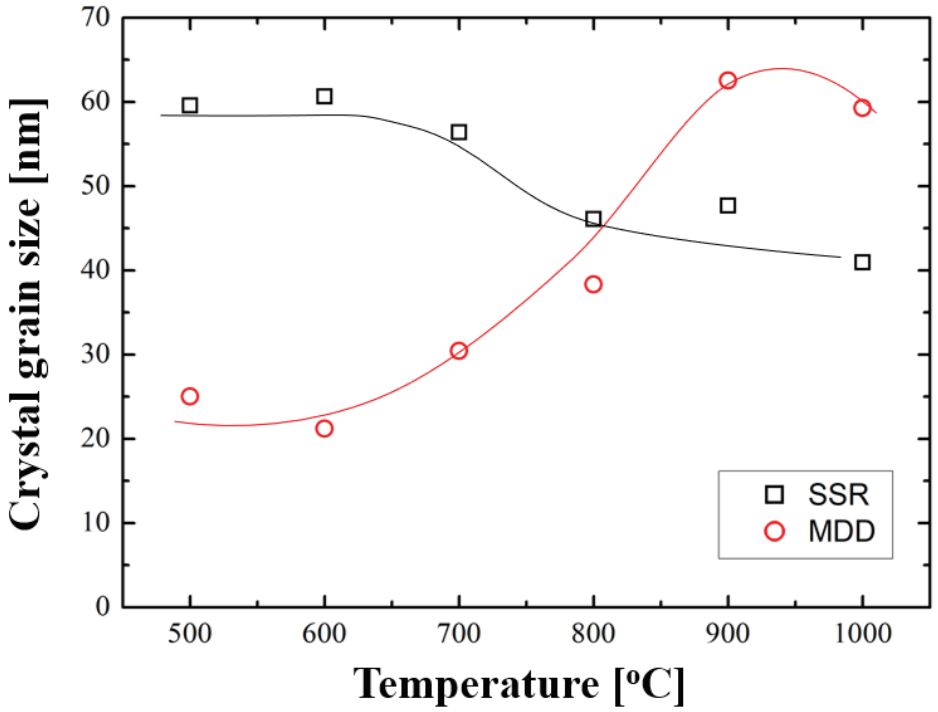

Figure 4.4 Crystal grain size of the NiCuZn ferrite powder as a function of reaction temperature for the microwave denitration and solid state reaction methods.

Furthermore, the morphology and particle size of the NiCuZn ferrite powders obtained from both methods were analyzed. Figure 4.5 shows the SEM images of NiCuZn ferrite product powders synthesized at 700 ^{o}C. The size of the primary particles constituting the NiCuZn ferrite product powder was quite different for the two methods. While the size of primary particles obtained by the MDD method was less than 100 nm, that of the SSR method was larger than 250 nm. While both types of primary particles existed in an aggregated state, in the case of the SSR method, the primary particles were randomly and irregularly aggregated, whereas with the MDD method, the aggregates consisted of thin layers of primary particles laminated in the form of Mille-feuille-like or petal-like structures. We surmise that this structure was formed by the interaction of the electromagnetic field induced by the microwave radiation and the magnetic NiCuZn ferrite. However, further details of this aspect will be addressed in a future study.

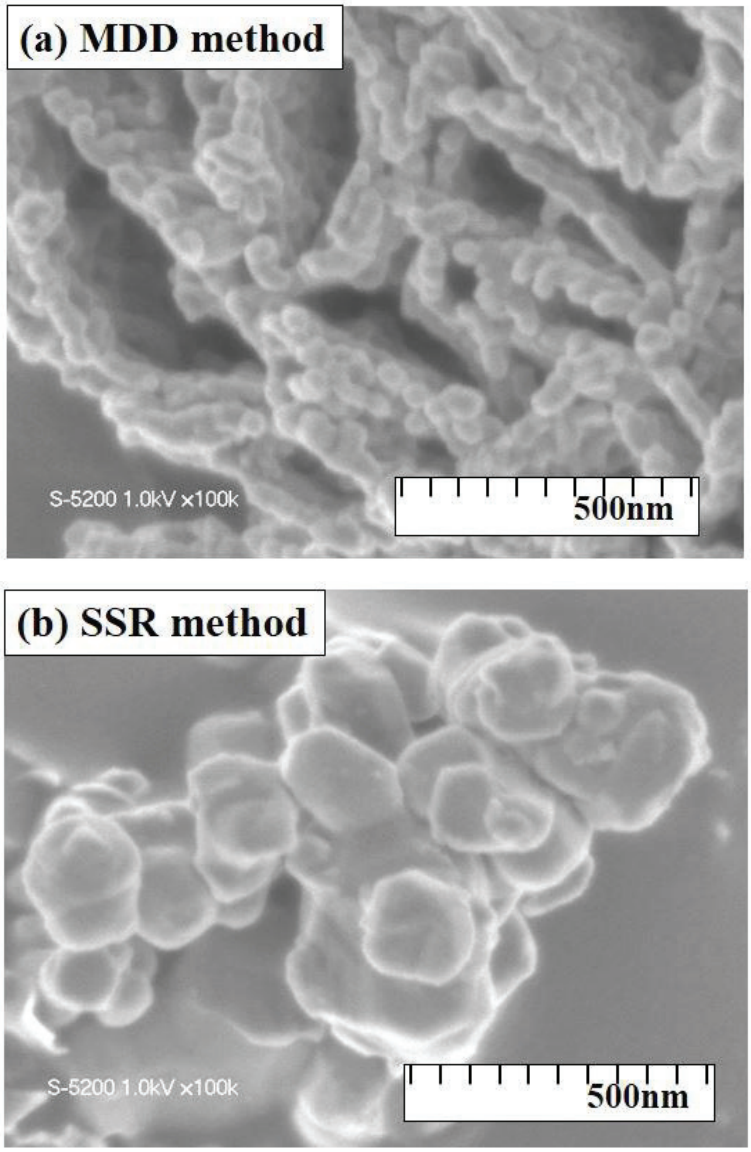

Figure 4.5 Microstructures of a NiCuZn ferrite powder synthesized at 700 ^{o}C by the (a) microwave denitration and (b) solid state reaction methods.

Figure 4.6 shows the relationship between the reaction temperature and average particle size of the product powder, which can be calculated from the specific surface area measured by BET analysis. An increase in the reaction temperature raised the average size of the particles obtained by the SSR method. Then, the size remained constant in the range between 600 and 800 ^{o}C. Above 800 ^{o}C, it rapidly increased again. Accordingly, it is thought that this rapid increase is due to the sintering activation of the as-synthesized primary particles at temperatures greater than 800 ^{o}C. On the other hand,

independent of the reaction temperatures in the 500–800 ºC range, the average size of the particles obtained by the MDD method remained constant at around 30–40 nm. The particle size began to increase from 800 ºC and reach the maximum particle size of 117.5 nm at 900 ºC. Then it kept constant above 1000 ºC. This result indicates that the microwave heating could enhance the grain growth and particle diameter size with the increasing reaction temperature. It has been reported that NiCuZn ferrite synthesized by various other methods could provide the comparable particle size. NiCuZn ferrite powder synthesized by thermal decomposition of an oxalate precursor had 350 nm in diameter after calcination at 750 ºC [19]. Roy et al. [20] also has reported NiCuZn ferrite synthesized by nitrate citrate gel auto combustion method was about 19-22 nm. Comparing the particle sizes of the product powders obtained from MDD and SSR methods, it is observed that the MDD method provided NiCuZn ferrite particles which were less than 1/5th the size of the particles obtained by the SSR method. This result suggests that the MDD method can contribute to the miniaturization of electronic components. To further verify the applicability of the NiCuZn ferrite product in electronics, the magnetic properties of the product were also investigated.

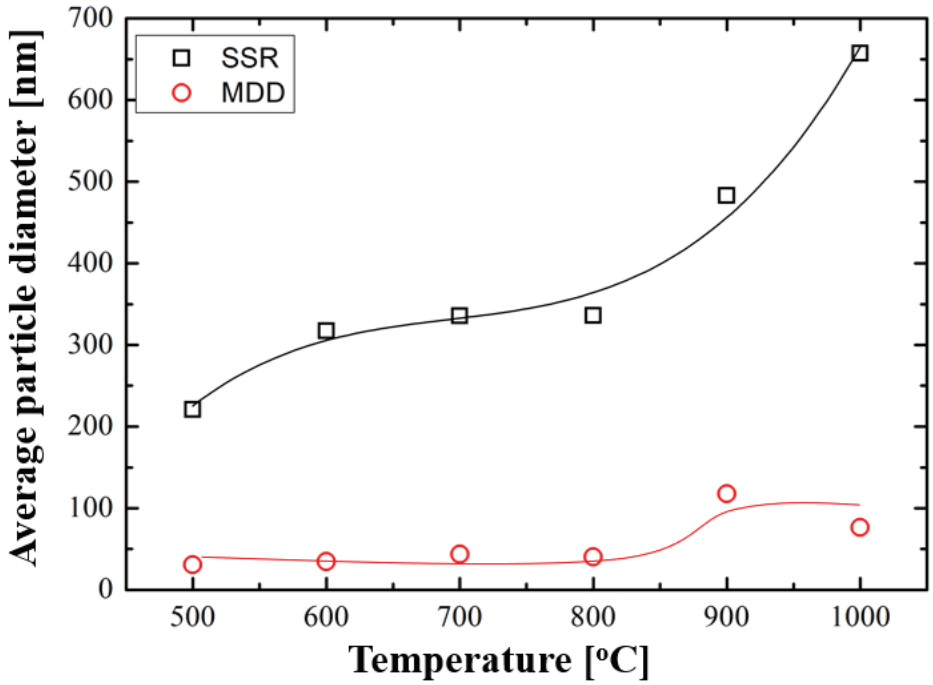

Figure 4.6 Average particle size of the product powder calculated from BET analysis as a function of reaction temperature for the microwave denitration and solid state reaction methods.

The magnetization characteristic of the spinel material depends on the composition, the additive material, and its microstructure[21]. The magnetization of soft ferrite is induced by domain rotation and wall motion, which are affected by particle size and the sintered particle density[15]. Moreover, the porosity of the material, which is inversely proportional to the density parameter, also plays a role in controlling the magnetization properties of the material. However, porosity hinders the domain wall motion[17]. To address these factors, the effect of the sintering treatment on the densification and the magnetic properties of the product was investigated. Table 1 shows the relative densities of the sintered pellets produced from ferrite powders obtained by both methods under various reaction temperatures. The relative density was defined as the ratio of bulk density to true density. The bulk density of the pellet was determined by an Archimedes method and the true density value of the NiCuZn ferrite is 5.38 g/m^3 [24]. The relative density of the sintered pellet obtained by the MDD method was higher than that from the SSR method, irrespective of the reaction temperature. This may be because the primary particle size obtained by the MDD method is much smaller than that by SSR method as shown in Figure 4. 6. In summary, the NiCuZn ferrite product powder synthesized by MDD method facilitates the production of pellets with higher density.

Table 4.1 Relative densities of the sintered NiCuZn ferrite pellets without the additive Bi_2O_3 powder prepared by the microwave direct denitration and solid-state reaction methods under various reaction temperatures.

Synthesis method		**MDD**		**SSR**	
Reaction temperature	[°C]	700	1000	700	1000
Relative density	[-]	0.73	0.69	0.62	0.65

To enhance the sinterability of the product powder and increase the bulk density of the pellet, 1.0 mass% of the sintering additive compound, Bi_2O_3, was added to the NiCuZn ferrite product powder, and pelletized. It was reported that the grain growth and bulk density of ferrite material could be enhanced by adding Bi_2O_3, substituting Bi^{3+} ions for Fe^{3+} ions of NiCuZn ferrite[22]. Figure 4.7 shows the relationship between the reaction temperature and the relative density of the sintered NiCuZn ferrite pellet with the Bi_2O_3 additive. For both synthesis methods, the relative density of the pellet increased

and reached the maximum at 700 ºC, and thereafter decreased gradually with increasing reaction temperature. The pellet produced from the product powder synthesized by the MDD method had a higher density than that obtained by the SSR method, except at a reaction temperature of 1000 ºC. These results also suggest that the MDD method provides product-powders having higher sinterability than those synthesized by the SSR method.

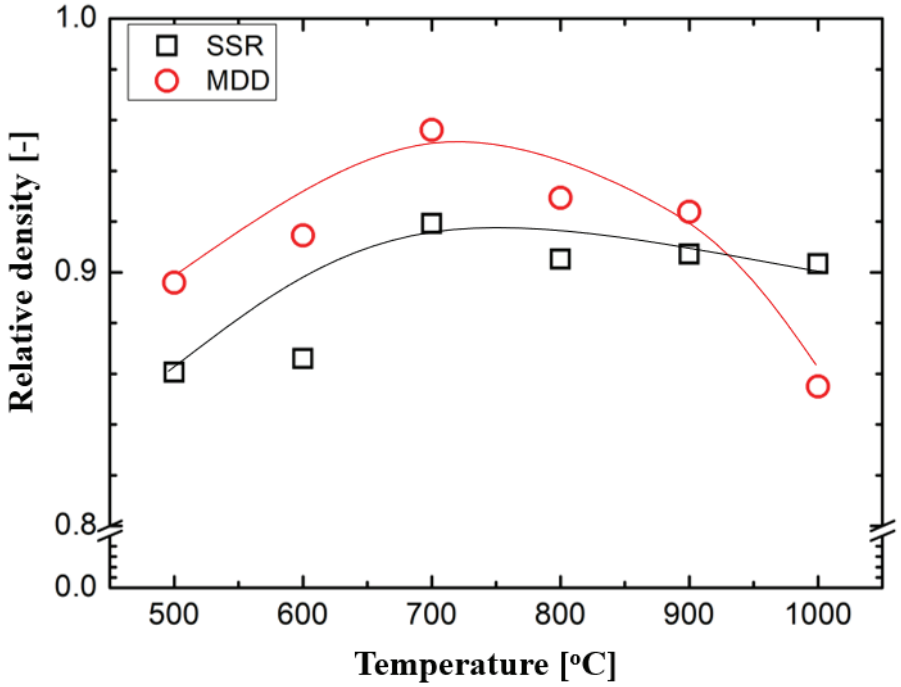

Figure 4.7 Relative density of the sintered NiCuZn ferrite pellet with an additive Bi_2O_3 powder as a function of the reaction temperature for the microwave denitration and solid state reaction methods.

Figure 4.8 shows the SEM images of the sintered pellet with the additive Bi_2O_3, fabricated from NiCuZn ferrite powders synthesized by the two methods at 700 ºC. In both cases, the grain size displayed a wide distribution with an average value of about 20 nm, which is much larger than the primary NiCuZn ferrite particle size shown in Figures 4.5 and 4.6. Almost no difference in the grain size between the two powder synthesis methods could be found. Therefore, we believe that product materials with nearly the same structure are obtained by the sintering treatment of NiCuZn ferrite powders, irrespective of the synthesis method.

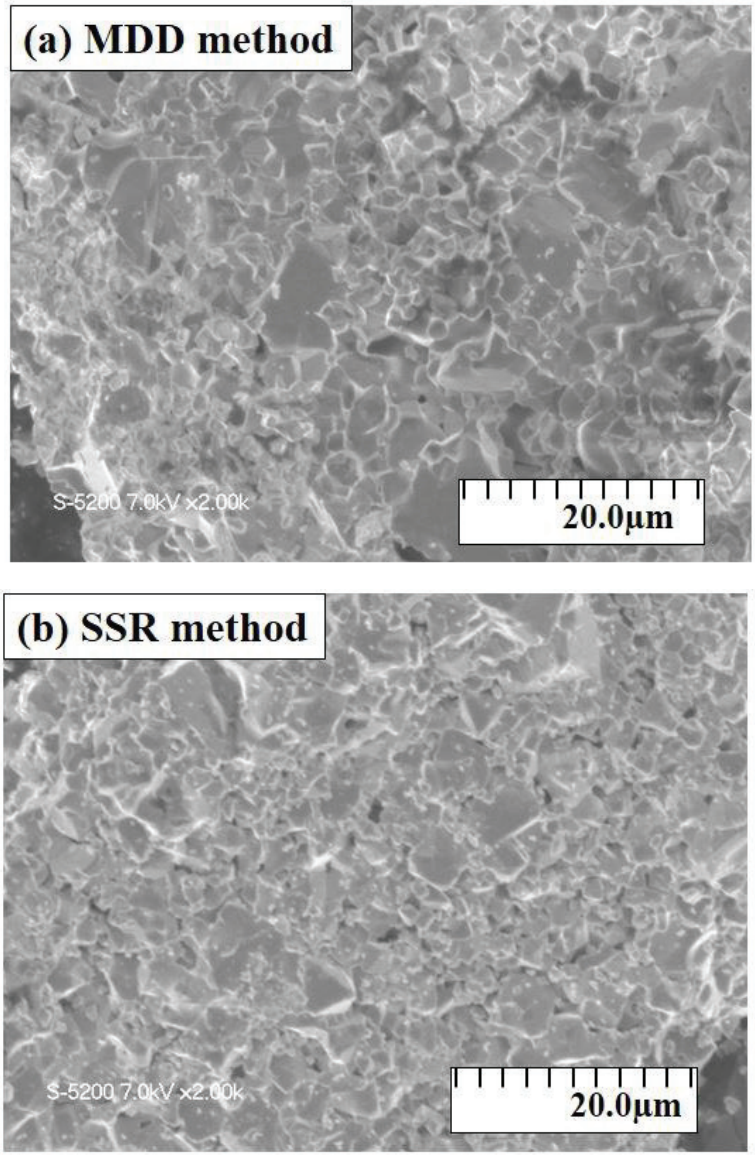

Figure 4.8 Microstructures of sintered NiCuZn ferrite pellets with the additive Bi_2O_3 powder produced by the (a) microwave denitration and (b) solid state reaction methods (reaction temperature: 700 ^oC).

Figure 4.9 shows the XRD patterns of the sintered pellets with 1.0 mass % of additive Bi_2O_3 fabricated from the NiCuZn ferrite powders synthesized using both methods at 700 ^oC. It can be observed that the sintered pellets fabricated from the powders produced by both synthesis methods contain only the crystalline phase of NiCuZn ferrite. Different with Figure 4.3, at the reaction temperature of 800^oC, the secondary phases of NiO, ZnO, and Fe_2O_3 could be obtained in XRD pattern. It was

thought that the sintering process could provide the pure spinel ferrite due to the completion of the NiCuZn ferrite reaction synthesis. Further, the additives Bi_2O_3 could not be detected due to the small amount of the addition. Little difference in the degree of crystallinity of the NiCuZn ferrite also could be found between the two methods. The crystal grain sizes were also similar at about 4.8 nm. Consequently, it can be surmised that sintered NiCuZn ferrite materials having the same crystallinity and structure were obtained from ferrite product nanoparticles synthesized by the different methods.

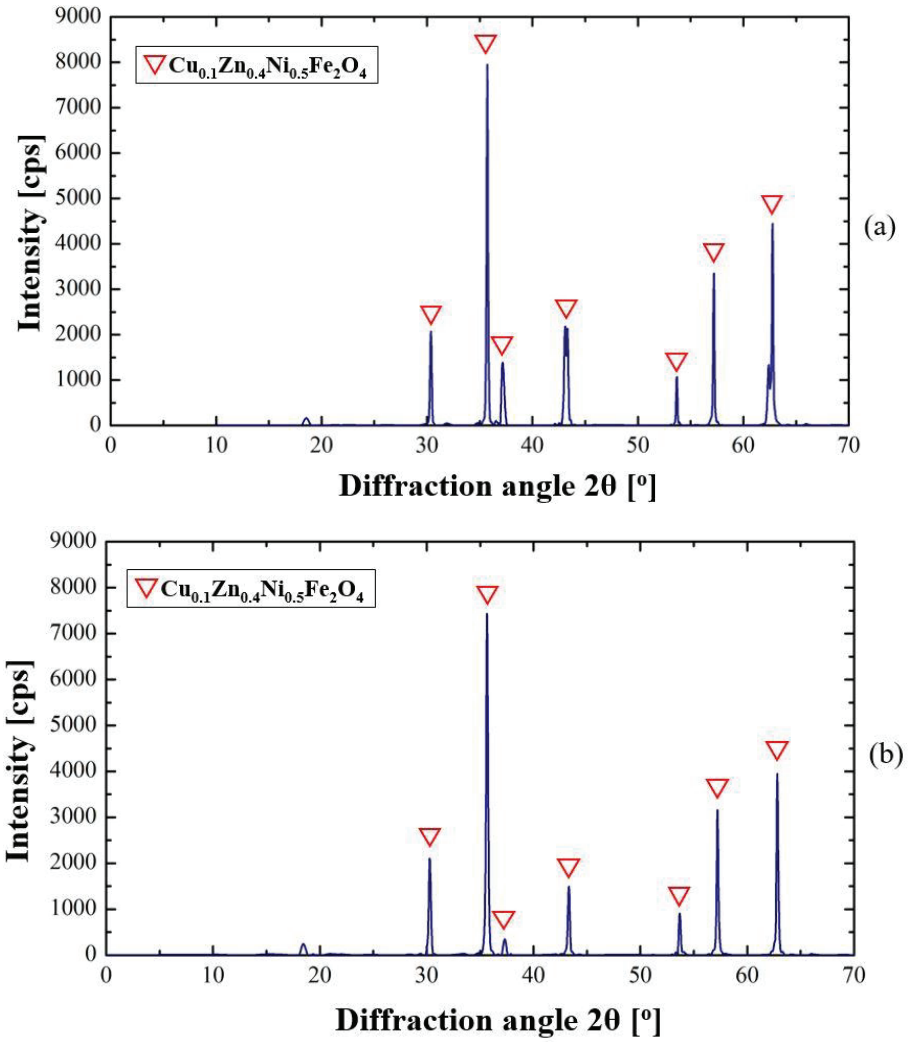

Figure 4.9 XRD patterns of sintered NiCuZn ferrite pellets with an additive Bi_2O_3 powder produced by the (a) microwave denitration and (b) solid state reaction methods (reaction temperature: 700 ^oC).

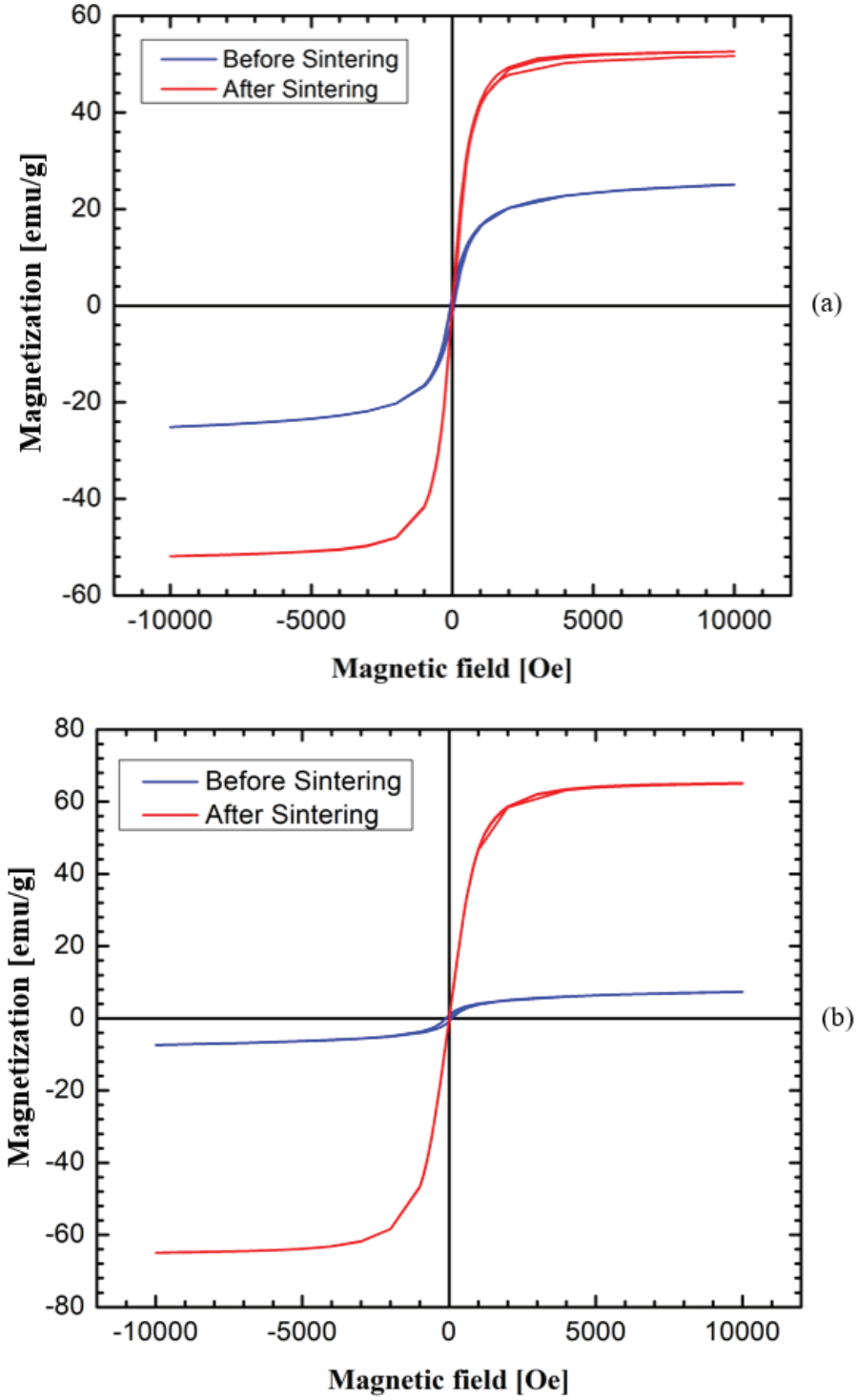

Figure 4.10 Magnetic hysteresis loops of the NiCuZn ferrite product powders and sintered product materials prepared at 700℃ by the (a) microwave direct denitration and (b) solid state reaction methods.

The hysteresis loop in Figure 4.10 shows the magnetic behaviors of the NiCuZn ferrite powders and the sintered product materials prepared by the MDD and SSR methods. Since little hysteresis loss (i.e., a narrow hysteresis loop) was observed, all the NiCuZn ferrite powders and sintered products were categorized as soft ferromagnetic materials[25]. The sintering treatment and additive Bi_2O_3 compound significantly improved the magnetic properties of the products obtained by both synthesis methods. Table 4.2 summarizes the saturation magnetization, remanence, and coercivity of the NiCuZn ferrite product powders and sintered product materials. The NiCuZn ferrite powder synthesized by the MDD method had a saturation magnetization that was more than three times larger than that of the powders produced by the SSR method. The saturation magnetization properties of soft ferromagnetic are influenced by the microstructure factor of the materials[26]. The materials having smaller grain size expected to have the higher saturation magnetization[23]. Therefore, with the smaller grain size of NiCuZn ferrite product powder synthesized by MDD method as shown in Figure 4.4, its saturation magnetization is higher than that by the SSR method. More preferable soft-magnetic properties, that is, higher saturation magnetization and lower coercivity could be obtained by reducing the impurity content in the NiCuZn ferrite product [21]. The coercivity of NiCuZn ferrite powder synthesized by the MDD was about half of that of the powder produced by the SSR method. This shows that the MDD method provides more attractive magnetic characteristics to the product powder as compared to the SSR method. This may be because more unreacted oxides such as NiO, Fe_2O_3 remained as impurities in the product powder by the SSR method than in that obtained by the MDD method. On the other hand, the sintering treatment provides better soft-magnetic properties due to the densification and high purity of NiCuZn ferrite product materials. With regards to the sintered NiCuZn ferrite products, the MDD method provided a saturation magnetization of about 80% that of powders obtained by the SSR method. The saturation magnetization of the sintered NiCuZn ferrite synthesized by MDD method was 51.69 emu/g and it was comparable with other previous studies, which is higher than the value of the saturation magnetization of sintered NiCuZn ferrite reported by He et al., 48 emu/g [21] and Rahman et al., 40.9 emu/g [27] , and almost the same value as the result by Reddy et al., 55.25 emu/g [28]. On the other hand, the sintered NiCuZn ferrite synthesized by both methods has relatively low coercivity. This may be

due to the similarity in the structures of sintered NiCuZn ferrite materials between the MMD and SSR methods, as revealed in Figures 4.8 and 4.9. Moreover, since the sintering treatment remarkably increased the grain size, both magnetic properties parameters were much improved. The number of domain walls is higher in larger grains. With the increase in number of walls, the contribution to magnetization or demagnetization due to wall movement and domain rotation increases. It is expected to have a low coercivity [29]. Consequently, it can be concluded that a NiCuZn ferrite product material with nearly the same magnetic characteristics as those obtained by existing synthesis methods could be produced by the MDD method.

Table 4.2 Magnetic properties of the NiCuZn ferrite product powders and sintered product materials prepared by the microwave direct denitration (MDD) and solid-state reaction (SSR) methods at 700 °C.

Synthesis Method	Condition	Saturation magnetization [emu/g]	Remanence magnetization [emu/g]	Coercivity [Oe]
MDD	Before sintering	25.08	2.14229	55.21
	After sintering	51.69	0.12629	1.66
SSR	Before sintering	7.36	0.9217	99.04
	After sintering	65.01	0.24648	2.26

4.4 Conclusions

Nanoparticles of NiCuZn ferrite were successfully synthesized by the MDD method from an aqueous mixture of metal nitrate hydrate reagents. The morphology and magnetic properties of the product powder and sintered pellets were investigated.

1. A single-phase NiCuZn ferrite powder could be obtained by the MDD method at a reaction temperature greater than 900 ^{o}C, which was lower than the reaction temperature (1000 ^{o}C) required for the same result when using the SSR method.
2. The average particle size of NiCuZn ferrite powder synthesized by the MDD method is 30 nm, which was less than one-fifth the particle size obtained by the SSR method.

3. The primary particles of its materials had a characteristic aggregated structure with thin layers consisting of primary particles laminated in the form of Mille-feuille like or petal-like structures.
4. The NiCuZn ferrite powder synthesized by the MDD method had a higher sinterability than that obtained by the SSR method since the particle size of the former was much smaller than that of latter.
5. The sintered NiCuZn ferrite materials with similar crystallinity and structure could be obtained from the NiCuZn ferrite powders synthesized by the MDD and SSR methods.
6. The saturation magnetization of the NiCuZn ferrite powder synthesized by the MDD method was more than three times that of the powders obtained by the SSR method, and its coercivity was also about half of that obtained by the SSR method.
7. The MDD method yielded about 80% of saturation magnetization and almost the same coercivity as the SSR method with respect to the sintered NiCuZn ferrite materials.

4.5 References

[1] H.M. Sung, C.J. Chen, W.S. Ko, H.C. Lin, Fine Powder Ferrite for Multilayer Chip Inductors, IEEE Trans. Magn. 30 (1994) 4906–4908. doi:10.1109/20.334261.

[2] T. Nakamura, Low-temperature sintering of Ni-Zn-Cu ferrite and its permeability spectra, J. Magn. Magn. Mater. 168 (1997) 285–291. doi:10.1016/S0304-8853(96)00709-3.

[3] M. Penchal Reddy, W. Madhuri, G. Balakrishnaiah, N. Ramamanohar Reddy, K. V. Siva Kumar, V.R.K. Murthy, R. Ramakrishna Reddy, Microwave sintering of iron deficient Ni-Cu-Zn ferrites for multilayer chip inductors, Curr. Appl. Phys. 11 (2011) 191–198. doi:10.1016/j.cap.2010.07.005.

[4] J. Zhu, C. Ouyang, S. Xiao, Y. Gao, Microwave sintering versus conventional sintering of NiCuZn ferrites. Part I: Densification evolution, J. Magn. Magn. Mater. 407 (2015) 308–313. doi:10.1016/j.jmmm.2016.01.099.

[5] C. Ouyang, S. Xiao, J. Zhu, W. Shi, Microwave sintering versus conventional

sintering of NiCuZn ferrites. Part II: Microstructure and DC-bias superposition characteristics, J. Magn. Magn. Mater. 407 (2016) 182–187. doi:10.1016/j.jmmm.2016.01.081.

[6] P.S. Anil Kumar, J.J. Shrotri, S.D. Kulkarni, C.E. Deshpande, S.K. Date, Low temperature synthesis of Ni0.8Zn0.2Fe2O4 powder and its characterization, Mater. Lett. 27 (1996) 293–296. doi:10.1016/0167-577X(96)00010-9.

[7] Y. Li, J. Zhao, J. Han, X. He, Combustion synthesis and characterization of NiCuZn ferrite powders, Mater. Res. Bull. 40 (2005) 981–989. doi:10.1016/j.materresbull.2005.02.018.

[8] W.C. Kim, S.I. Park, S.J. Kim, S.W. Lee, C.S. Kim, Magnetic and structural properties of ultrafine Ni–Zn–Cu ferrite grown by a sol–gel method, J. Appl. Phys. 87 (2000) 6241–6243. doi:10.1063/1.372667.

[9] J.S. Kim, C.W. Ham, The effect of calcining temperature on the magnetic properties of the ultra-fine NiCuZn-ferrites, Mater. Res. Bull. 44 (2009) 633–637. doi:10.1016/j.materresbull.2008.06.021.

[10] Z. Ma, C. Mang, X. Weng, Q. Zhang, The Influence of Different Metal Ions on the Absorption Properties of Nano-Nickel Zinc Ferrite, (2018). doi:10.3390/ma11040590.

[11] J. Sun, W. Wang, Q. Yue, Review on microwave-matter interaction fundamentals and efficient microwave-associated heating strategies, Materials (Basel). 9 (2016). doi:10.3390/ma9040231.

[12] K. Fukui, K. Kanayama, M. Katoh, T. Yamamoto, H. Yoshida, Synthesis of indium tin oxide powder by solid-phase reaction with microwave heating, Adv. Powder Technol. 20 (2009) 488–492. doi:10.1016/j.apt.2009.05.007.

[13] C.Y. Tsay, K.S. Liu, T.F. Lin, I.N. Lin, Microwave sintering of NiCuZn ferrites and multilayer chip inductors, J. Magn. Magn. Mater. 209 (2000) 189–192. doi:10.1016/S0304-8853(99)00684-8.

[14] K. Fukui, Y. Igawa, N. Arimitsu, M. Suzuki, T. Segawa, K.I. Fujii, T. Yamamoto, H. Yoshida, Mechanism of synthesis of metallic oxide powder from aqueous metallic nitrate solution by microwave denitration method, Chem. Eng. J. 211–212 (2012) 1–8. doi:10.1016/j.cej.2012.09.032.

[15] T. Segawa, K. Kawaguchi, K. Ishii, M. Suzuki, N. Arimitsu, H. Yoshida, K. Fukui,

Nickel oxide powder synthesis from aqueous solution of nickel nitrate hexahydrate by a microwave denitration method, Adv. Powder Technol. 26 (2015) 983–990. doi:10.1016/j.apt.2015.04.004.

[16] K. Mohit, V.R. Gupta, S.K. Rout, Microwave Dielectric Properties of Ni0.2CuxZn0.8–xFe2O4 for Application in Antenna, Prog. Electromagn. Res. B. 57 (2014) 157–175.

[17] S. Bid, S.K. Pradhan, Characterization of crystalline structure of ball-milled nano-Ni-Zn-ferrite by Rietveld method, Mater. Chem. Phys. 84 (2004) 291–301. doi:10.1016/j.matchemphys.2003.08.012.

[18] C.W. Kim, J.G. Koh, A study of synthesis of NiCuZn-ferrite sintering in low temperature by metal nitrates and its electromagnetic property, J. Magn. Magn. Mater. 257 (2003) 355–368. doi:10.1016/S0304-8853(02)01234-9.

[19] J. Mürbe, J. Töpfer, High permeability Ni-Cu-Zn ferrites through additive-free low-temperature sintering of nanocrystalline powders, J. Eur. Ceram. Soc. 32 (2012) 1091–1098. doi:10.1016/j.jeurceramsoc.2011.11.021.

[20] P.K. Roy, J. Bera, Characterization of nanocrystalline NiCuZn ferrite powders synthesized by sol-gel auto-combustion method, J. Mater. Process. Technol. 197 (2008) 279–283. doi:10.1016/j.jmatprotec.2007.06.027.

[21] X.M. He, S.M. Yan, Z.W. Li, X. Zhang, X.Y. Song, W. Qiao, W. Zhong, Y.W. Du, Structure, morphology, and magnetic properties of high-performance NiCuZn ferrite, Chinese Phys. B. 24 (2015) 1–6. doi:10.1088/1674-1056/24/12/127502.

[22] L. Jia, H. Zhang, X. Wu, T. Li, H. Su, B. Liu, Microstructures and magnetic properties of Bi-substituted NiCuZn ferrite, J. Appl. Phys. 111 (2012). doi:10.1063/1.3677651.

[23] X. Qi, J. Zhou, Z. Yue, Z. Gui, L. Li, Effect of Mn substitution on the magnetic properties of MgCuZn ferrites, J. Magn. Magn. Mater. 251 (2002) 316–322. doi:10.1016/S0304-8853(02)00854-5.

[24] A. Barba, C. Clausell, C. Felíu, M. Monzó, Sintering of (Cu0.25Ni0.25Zn0.50)Fe2O4Ferrite, J. Am. Ceram. Soc. 77 (2004) 571–577.

[25] S.M. Kabbur, U.R. Ghodake, D.Y. Nadargi, C.K. Rahul, S.S. Suryavanshi, Effect of Dy3+ substitution on structural and magnetic properties of nanocrystalline Ni-Cu-Zn ferrites, J. Magn. Magn. Mater. 451 (2018) 665–675.

doi:doi.org/10.1016/j.jmmm.2017.12.006.

[26] S. Yonatan Mulushoa, N. Murali, M. Tulu Wegayehu, S.J. Margarette, K. Samatha, Influence of Cu-Cr substitution on structural, morphological, electrical and magnetic properties of magnesium ferrite, Results Phys. 8 (2018) 772–779. doi:10.1016/j.rinp.2017.12.062.

[27] K.R. Rahman, F.U.Z. Chowdhury, M.N.I. Khan, Structural, morphological and magnetic properties of Al3+substituted Ni0.25Cu0.20Zn0.55AlxFe2−xO4ferrites synthesized by solid state reaction route, Results Phys. 7 (2017) 354–360. doi:10.1016/j.rinp.2016.12.045.

[28] M. Penchal Reddy, W. Madhuri, M. Venkata Ramana, N. Ramamanohar Reddy, K. V. Siva Kumar, V.R.K. Murthy, K. Siva Kumar, R. Ramakrishna Reddy, Effect of sintering temperature on structural and magnetic properties of NiCuZn and MgCuZn ferrites, J. Magn. Magn. Mater. 322 (2010) 2819–2823. doi:10.1016/j.jmmm.2010.04.036.

[29] A. Verma, T.C. Goel, R.G. Mendiratta, P. Kishan, Magnetic properties of nickel zinc ferrites prepared by the citrate precursor method, J. Magn. Magn. Mater. 208 (2000).

CHAPTER 5

Synthesis of Cu-Ce-Zr oxide catalyst nanoparticles by microwave denitration method

5.1 Introduction

$CeO_2.ZrO_2$ has been widely used as an automotive catalyst called TWC (three-way catalyst) to remove the NOx emission, CO, and HC simultaneously[1]. In this catalyst, ceria is an essential component in important roles. Firstly, it stabilizes the refractory oxide, called washcoat. Secondly, it interacts with precious metals and provides a support for them. Finally, it stores oxygen during lean phases, and release it during rich phases of facilitating the simultaneous conversion of those harmful gas substances [2]. While the introducing of a foreign cation such as Zr into the ceria oxide can enhance oxygen ion mobility within the crystal lattice [3]. As the result, the oxygen storage capacity (OSC), as well as thermal stability of the catalyst could be enhanced [4,5]. Recently, the Cu-Ce-Zr mixed oxide catalyst is prepared to improve the catalytic performance of TWC system. The CuO species has a strong synergetic interaction with CeO_2 and significantly can decrease the operation temperature (~250^{o}C) [6].

The performance of Cu-Ce-Zr oxide catalyst was affected by its preparation method and conditions. The Cu-Ce-Zr oxide catalyst has been prepared by some methods, such as impregnation method[7], sol-gel method [8], citric acid method [9], and co-precipitation method [10–12]. However, Cu-Ce-Zr oxide prepared by co-precipitation method usually suffer the contamination of alkaline metals as well as the environmental wastes (salts from hydrolysis and washing water) [13].

In the previous chapter, the NiCuZn ferrite powder has been successfully synthesized by microwave direct denitration method from the mixture of metal nitrate hydrate solution as a raw material. The microwave heating which has a high heating rate can synthesize the ferrite powder easily and efficiently with shorter and simpler steps. Moreover, the microwave heating also enhanced the microstructure of the powder product. Thus, we believe that the microwave denitration method can be implemented in the synthesis of Cu-Ce-Zr oxide from the mixture of metal hydrate nitrate solution.

In this chapter, the Cu doped Ce-Zr oxide catalyst ($Ce_{0.6}Zr_{0.4}O_2$:Cu, CCZ catalyst) nanoparticles synthesized by microwave denitration method was studied. The characteristic of the catalyst product and catalyst performance such as OSC was investigated and compared with CCZ catalyst synthesized by the citric acid method.

5.2 Materials and Method

As the raw material, the aqueous solution mixture of high purity metallic nitrate reagents (Reagent grade 98%, Sigma-Aldrich, Germany), i.e. copper (II) nitrate trihydrate ($Cu(NO_3)_2 \cdot 3H_2O$), zirconyl nitrate ($ZrO(NO_3)_2 \cdot 2H_2O$), and cerium (III) nitrate hexahydrate ($Ce(NO_3)_3 \cdot 6H_2O$) were used. The composition of the raw material was adjusted according to the chemical stoichiometric ratio of CCZ catalyst, $Ce_{0.6}Zr_{0.4}O_2$:Cu. The doping ratio of Cu, which was defined as the atomic molar ratio of Cu element to all metallic elements, Cu, Ce, and Zr, was varied in the range of 10 – 30 %.

The multi-mode type microwave oven consisted of the magnetron, waveguide, PID controller, and thermocouple, as shown in the previous chapter in figure 4.1, was used for the experiment. A 2.45 GHz microwave generated by the magnetron was introduced into the cavity by the waveguide. The mixed aqueous solution in the reactor, the three-neck 100 mL pyrex flask, was irradiated and heated up by 720 W constant output of the microwave until the temperature attained to the reaction temperature of 600^{o}C. Then, the temperature was kept constant for 2 hours at the set point with adjusting 40-770 W of the microwave output by PID controller. Here, the temperature was measured by a K-type thermocouple at the center of the reactor. During the increase in the temperature, the progress of the reaction, water was evaporated from the solution and then nitrogen oxide gas was generated by the denitration reaction. To prevent the accumulation of these exhausted gas components, 100 mL/min of the compressed air was fed, and they were absorbed by a circulating aspirator.

As the control experiment, the CCZ catalyst was synthesized by citric acid method[9]. The CCZ catalyst was prepared from the aqueous mixture of metallic nitrate reagents with the same composition as microwave denitration method and added to the aqueous citric acid solution. The molar ratio of the total metal components (the sum of Cu, Ce, and Zr) to citric acid was kept to 1.0:1.0. The mixture was stirred at room temperature and dried at 120 ^{o}C for 10 h resulting in porous foam-like solid. This

precursor was calcined at 500 ºC for 5 hours in an electric furnace (Nitto Kagaku Co., LTD). Finally, the sample products were crushed and sieved prior to use for analysis.

The crystalline phases of the products were identified using an X-ray diffractometer (XRD; Rigaku, MiniFlex 600). The morphology of the product was observed by scanning electron microscopy (SEM; Hitachi, S-5200) and the specific surface area was measured by BET analysis (Microtrac Bel Corp., Belsorp-mini II). The elemental composition of the material was measured by X-ray photoelectron spectroscopy (XPS; Shimadzu, ESCA-3400). The thermogravimetric analysis of raw materials was carried out using TG-DTA (Rigaku, TG-8120).

5.3 Result and discussion

Figure 5.1 shows the temperature change of raw material with various composition of Cu doping ratio during microwave heating process. For the raw material without Cu content, the temperature can be reached the maximum temperature of 487 ºC for 7 min, then decreased as time elapsed. It shows that the mixture solution in this condition has a low microwave absorptivity. On the other hand, the raw material with Cu contents can heat up by microwave irradiation to reach over the denitration reaction temperature. For the Cu 10 and 20 mol%, the temperature of raw material can be attained 600 ºC for 5 min and kept constant for 20 min. For Cu composition of 30 mol%, the reaction temperature of 600 ºC can be reached for 4 min, which shows that it has a higher heating rate. Figure 5.2 shows the microwave absorption efficiency of the material, with and without Cu content measured by MWTG apparatus. It was confirmed that Cu content enhanced the microwave absorption efficiency of the raw material from 13% to 22%. The microwave absorptivity characteristic of each substance in the mixture solution can be the factor of its microwave heating rate. The higher composition of Cu corresponds to the higher heating rate of the raw material because the $Cu(NO_3)_2 \cdot 3H_2O$ solution has a high microwave absorptivity[14].

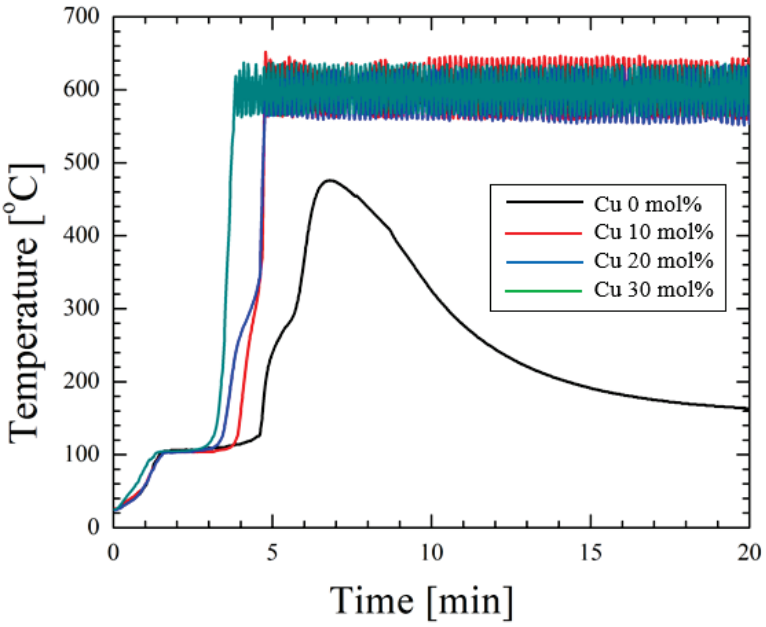

Figure 5.1 The temperature change of raw material with various composition of Cu doping ratio during microwave heating treatment

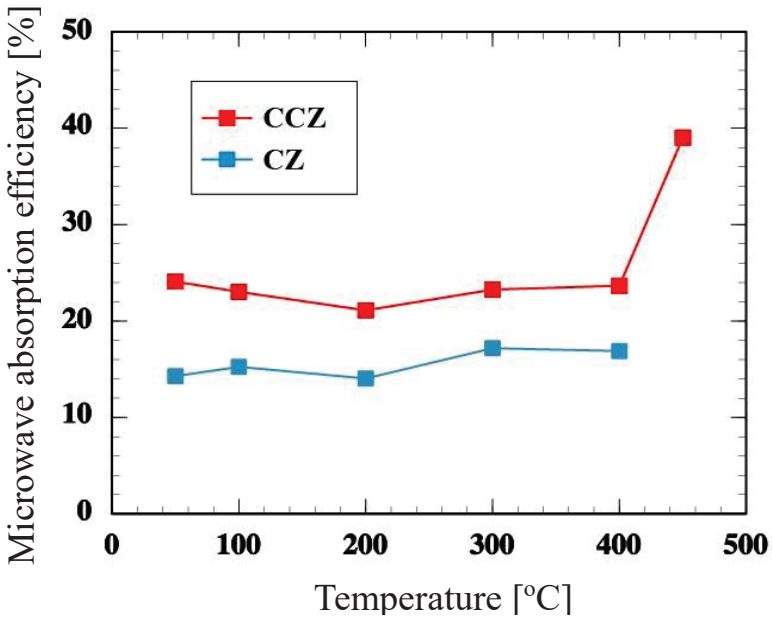

Figure 5.2 Microwave absorption efficiency of raw material measured by MWTG

Figure 5.3 shows the XRD pattern of the products synthesized by microwave denitration method and citric acid method. It shows that the single crystalline phase of CCZ catalyst nanoparticle could be synthesized by both methods with the 20%, or less, of the Cu doping ratio at the temperature treatment of 600 ^{o}C. However, for the Cu composition of 30%, the diffraction peak of CuO could be observed at the diffraction degree 2θ of 36^{o} and 39^{o}. It is indicated that the CuO was formed from the denitration reaction of $Cu(NO_3)_2 \cdot 3H_2O$. The similar result also was obtained by Fu et al., which at the 33% of Cu content, the CuO phase in the synthesized CCZ catalyst was detected by XRD. The presence of bulk CuO indicates that the aggregation of excessive CuO species on the support surface[15].

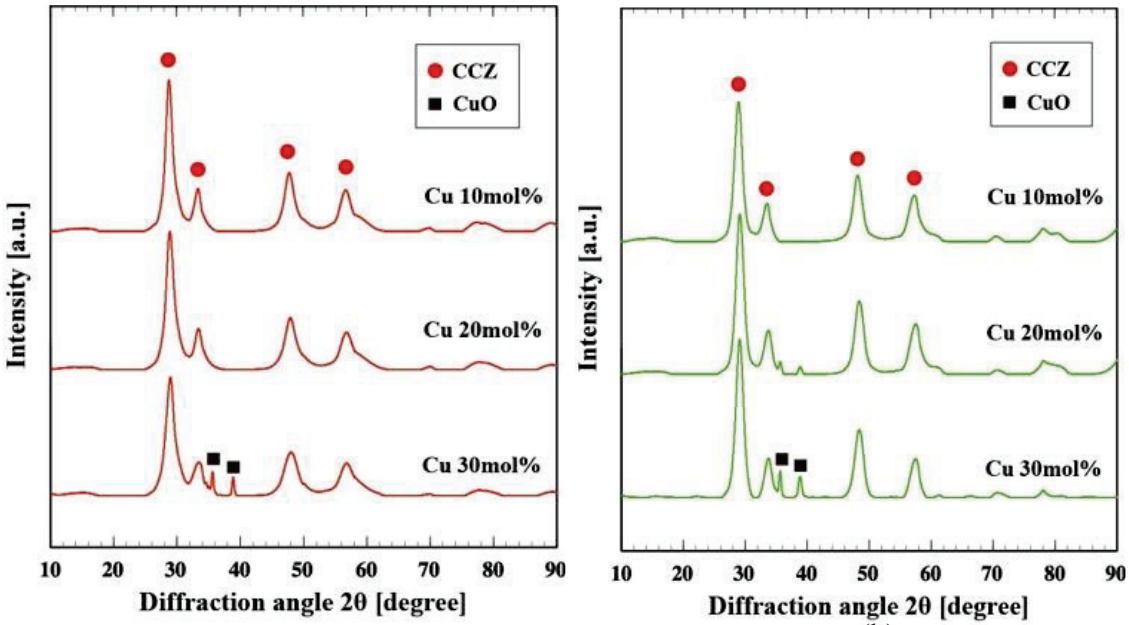

Figure 5.3 XRD pattern of the products synthesized by (a) microwave denitration method and (b) citric acid method

The BET analysis was used to investigate the surface area of the CCZ nanoparticle. Figure 5.4 shows the specific surface area of CCZ nanoparticle synthesized by both methods at various Cu content. The specific surface area of CCZ nanoparticles synthesized by microwave denitration and citric acid methods is decreased with the increasing of Cu content. It is indicated that the Cu dispersed on the support surface and may be block part of pores. For the microwave denitration method, the highest specific

surface area was acquired 68.0 m^2/g at 10 % of the Cu doping ratio. On the other hand, the specific surface area of CCZ nanoparticles synthesized by the citric acid method at same Cu content was around 20-30 m^2/g, which was only less than a half of that by microwave denitration method. This result shows that microwave denitration method can provide the higher surface area of the CCZ catalyst material than citric acid method. The high surface corresponds to the high contact area between the catalyst material and gas. Further, it is expected to improve the gas decomposition performance of the catalyst.

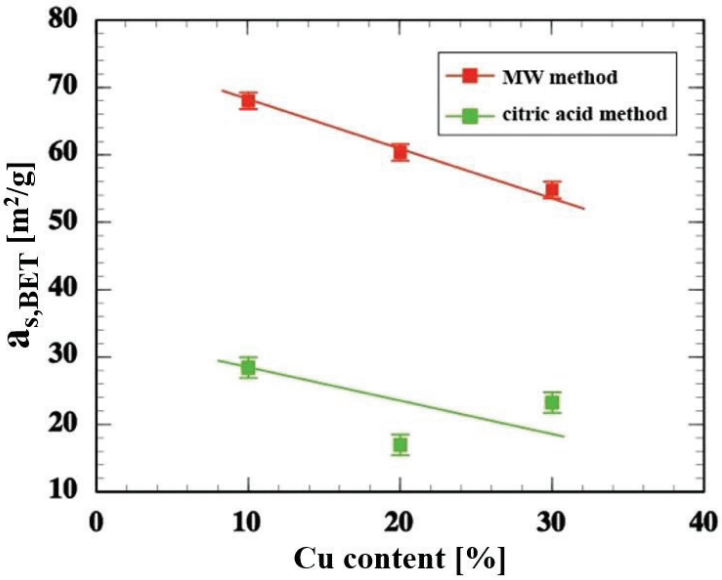

Figure 5.4 Specific surface area of CCZ nanoparticle product at various %mol Cu content

Figure 5.5 shows the microstructure of CCZ nanoparticle product synthesized by microwave denitration and citric acid method at 10 mol% Cu contents from SEM image analysis. It revealed that the aggregates of CCZ nanoparticle could be formed as a final product by both methods. From figure 5.5(a), the particle of the product is existing on the aggregates formation with small size of primary particles. The pores also can be found in the particle of CCZ product synthesized by microwave denitration. It was thought that the microwave heating can generate the NOx gas rapidly, so that the pores was formed. Otherwise, as can be observed in figure 5.5(b), the CCZ product synthesized by citric acid is in the bulk body form and do not have pores in the particle. It also confirmed the BET analysis result that the specific surface area of CCZ nanoparticle product

synthesized by microwave denitration method is higher than those by a citric acid method due to the particle size and the existence of pores.

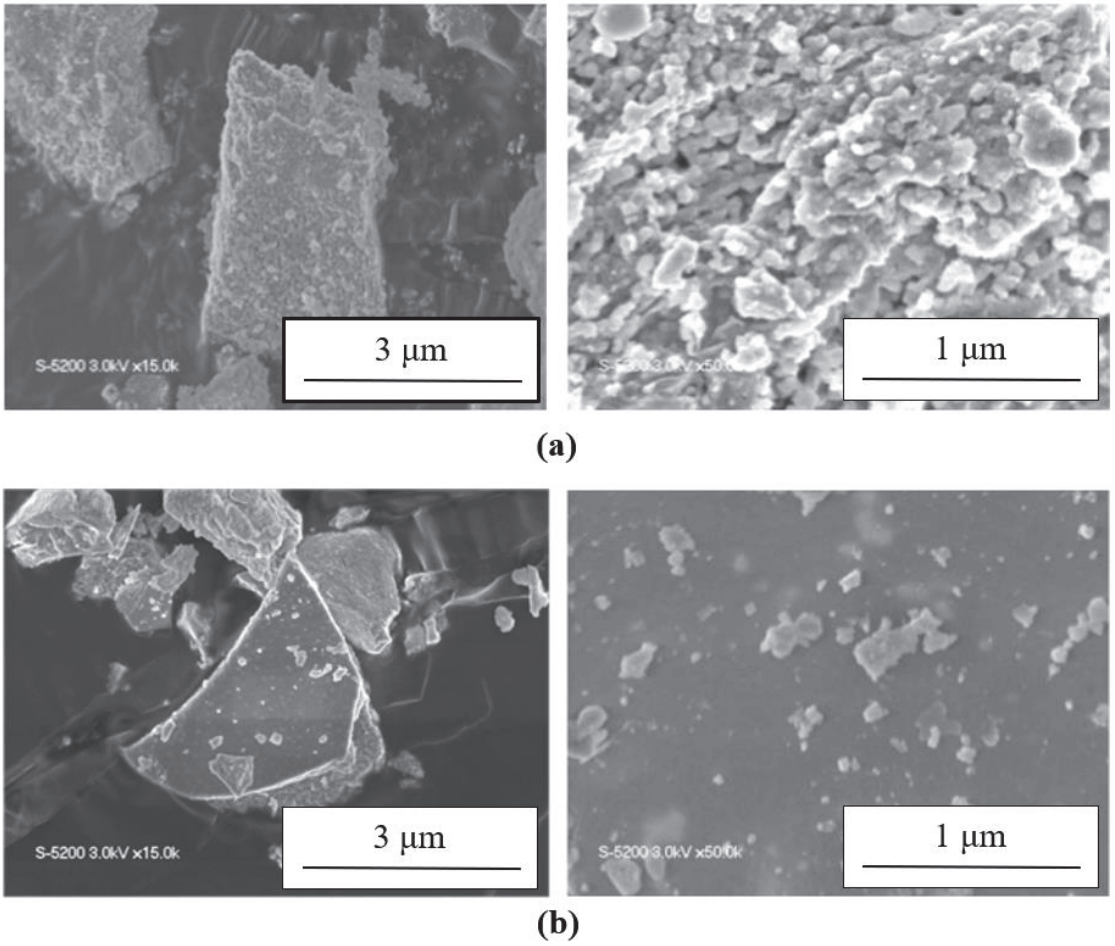

Figure 5.5 Microstructure of CCZ nanoparticle synthesized by (a) microwave denitration and (b) citric acid method (Cu content=10 mol%)

The Oxygen Storage Capacity (OSC) is defined as the maximum amount of oxygen which can be stored inside the catalyst[2]. The OSC was measured by thermogravimetric OSC conventional method[16] at the temperature condition of 200ºC using oxygen gas for the oxidation reaction, and hydrogen gas for the reduction reaction. Figure 5.6 shows the TG profile of the CuCeZr oxide product contained 20 mol% Cu. TG profiles represent the oxygen release/storage performance of the sample product at 200ºC. The OSC (μmol-O_2/g) can be obtained by the equation (5.1) as follows,

$$\mathrm{OSC} = \frac{\Delta w / 16.0 \times 10^{-6}}{m} \tag{5.1}$$

Where Δw is the mass change (g) of the sample during the oxidation process, 16.0×10^{-6} g/ μmol is a molar mass of oxygen gas value, and m is the total mass sample. On the other hand, the OSC rate can be obtained from equation (5.2). OSC rate (%/s) is the rate of the sample to storage the oxygen during catalytic process.

$$\text{OSC rate} = \frac{\Delta ignition\ loss}{\Delta t} \tag{5.2}$$

From the thermogravimetric analysis method, the OSC and OSC rate of the CCZ nanoparticles catalyst synthesized by microwave denitration method with Cu composition of 20 mol% was obtained 12,303 μmol-O_2/g and 0.012 %/s.

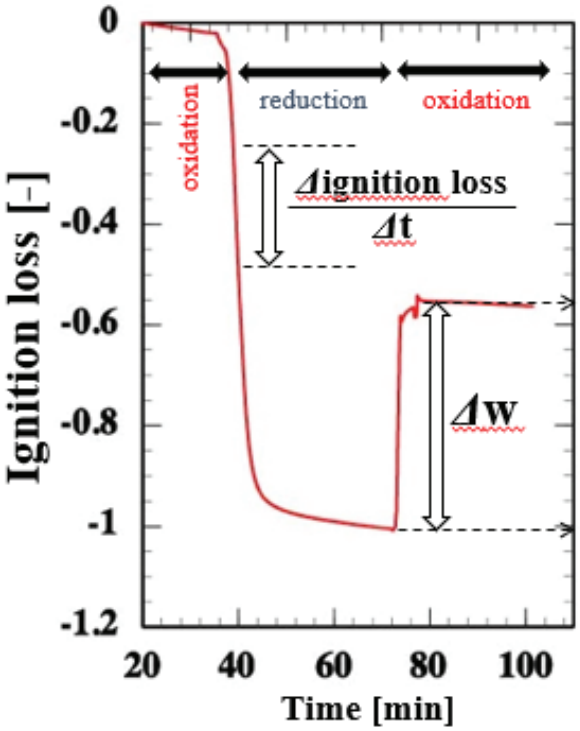

Figure 5.6 TG profiles during measurement of OSC at 200ºC for CCZ catalyst synthesized by microwave denitration method with Cu content 20 mol%

The OSC and OSC-rate also were carried out for the CCZ catalyst product at the various composition. Figure 5.7 shows the oxygen storage capacity of CCZ nanoparticle synthesized by both methods, at various mol% Cu content. The OSC of CCZ nanoparticle is increased with the increasing of Cu content. It has been reported that the OSC of the catalyst depends principally on the amount of Ce element in the mixed oxides and the

surface area affects little to it [17,18]. Although in this case, the Ce content was same between CCZ nanoparticles obtained by both methods, the CCZ nanoparticles synthesized by citric acid method had a little higher OSC value than those by microwave denitration method. This may be because citric acid method could yield CCZ nanoparticles with a higher crystallinity so that it affects the quality and performance of the catalyst.

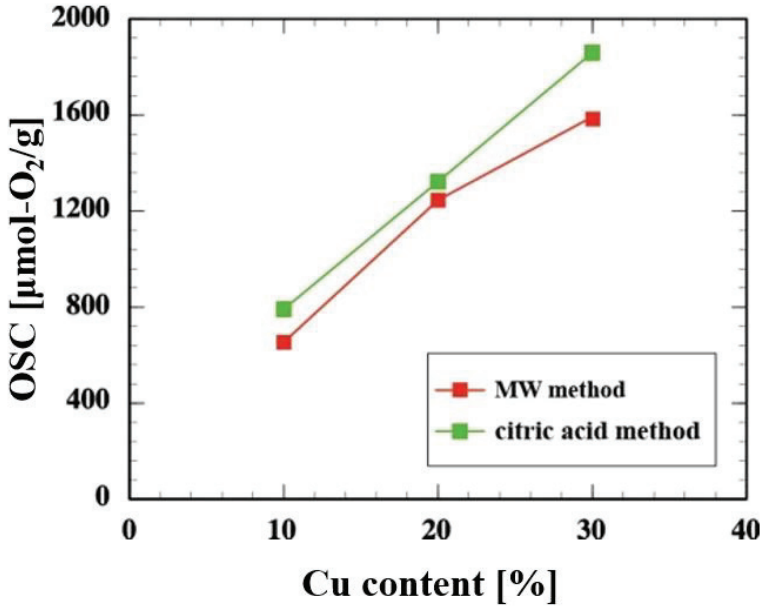

Figure 5.7 Oxygen storage capacity (OSC) of CCZ nanoparticle at various %mol Cu content

Figure 5.8 shows the rate of oxygen storage capacity (OSC) of CCZ nanoparticle synthesized by microwave denitration and citric acid method. The OSC-rate of CCZ nanoparticle is increased with the increasing of mol% Cu content. On the other hand, the OSC-rate of CCZ synthesized by microwave denitration method is relatively higher than citric acid method. As can be observed in figure 5.4, the CCZ synthesized by microwave denitration method has a larger specific surface area, than that by the citric acid method. Accordingly, it was thought that the increase in the surface area of CCZ can enhance the release of the active oxygen easier, as the result, the OSC-rate also increase.

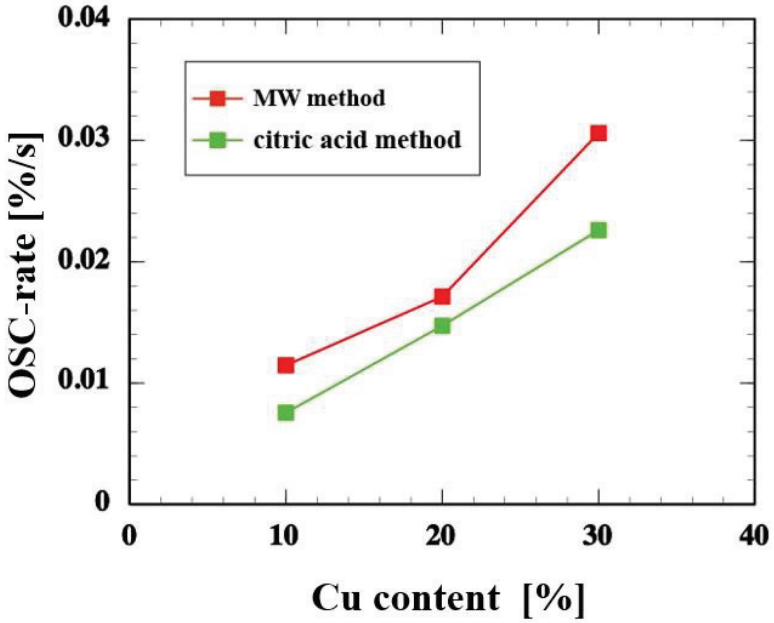

Figure 5.8 Rate of oxygen storage capacity (OSC) of CCZ nanoparticle at various mol% Cu content

Figure 5.9 shows the curves of Ce 3d spectra of CCZ nanoparticle synthesized by microwave denitration method at various %mol Cu content. As seen in figure 5.9, the curves of Ce 3d are composed of eight peaks. Letters *a* and *b* refer to the $3d_{3/2}$ and $3d_{5/2}$ spin-orbit components, respectively. The couple peaks corresponding to the configuration of Ce^{3+} species are *a* (884.1-885.1 eV) and *b* (903.1-903.4 eV). Moreover, the remained of six peaks are corresponded to the Ce^{4+} species. The presence of Ce^{3+} was referred to the generation of oxygen vacancies [19].

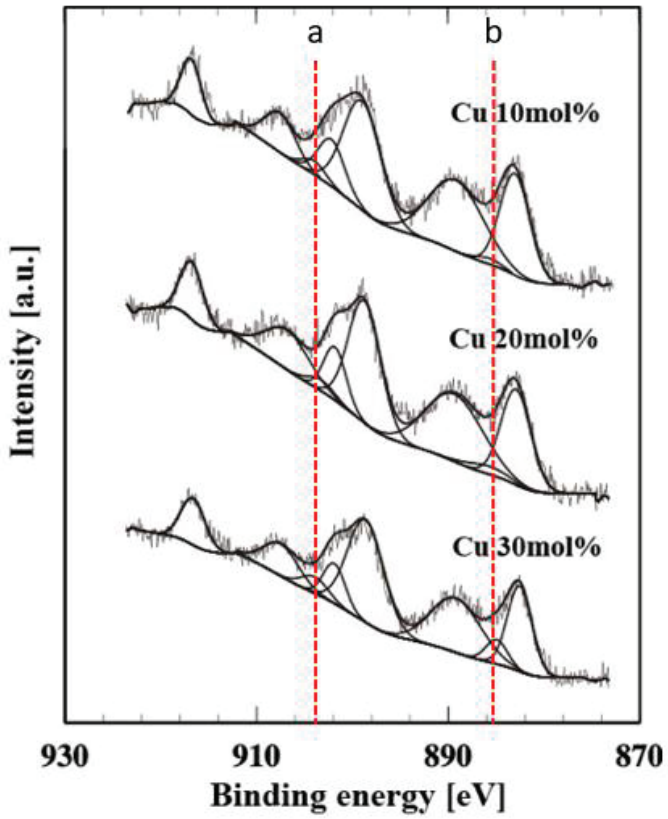

Figure 5.9 XPS spectra of Ce 3d from CCZ nanoparticle synthesized by microwave denitration method

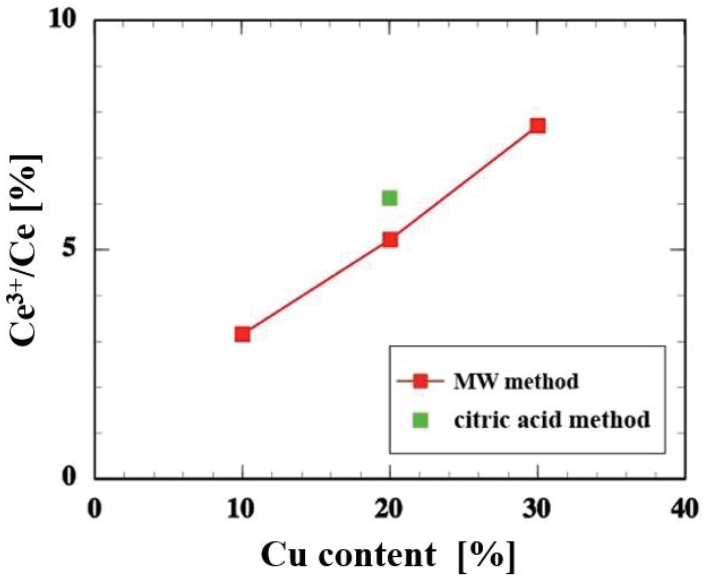

Figure 5.10 Atomic Ce^{3+}/Ce of CCZ nanoparticle product synthesized by microwave denitration and citric acid method

The molar ratio of the surface relative Ce^{3+}/Ce content of the CCZ nanoparticles product was calculated from the normalized peak area of Ce^{3+} and the total peak area in the XPS spectra curves. Figure 5.10 shows the molar atomic ratio of Ce^{3+}/Ce at various Cu content by both methods. It was thought that on the Cu doped in Ce-Zr oxide, the Cu2+ ion is inserted to the crystal lattice of Ce-Zr oxide and substitute Ce3+ ion. The oxygen deficiency occurred in the structure of ceria oxide causes lattice distortion and increasing the Ce3+ ion content. With the increasing of Cu content, the atomic ratio of Ce^{3+}/Ce increase as shown in figure 5.10. This is similar to the results of Ali et. al, that the OSC and ratio the Ce^{3+}/Ce content increased as the Cu doping ratio increased [9]. The redox ability of CCZ catalyst might be also strongly improved by a large amount of Cu[12]. The increasing of Ce^{3+}/Ce content in the catalyst product corresponded to the higher OSC and OSC-rate value of the catalyst in figure 5.7 and 5.8. Further, it was clarified that the Ce^{3+}/Ce content of CCZ nano-particles synthesized by the citric acid method and microwave denitration method were 5.6% and 4.2%, respectively. The Ce^{3+}/Ce content of CCZ nanoparticles synthesized by the citric acid method at the same mol% Cu content is higher than that by microwave denitration method.

5.4 Conclusions

The CCZ catalyst nanoparticle has been successfully synthesized by microwave denitration method from the mixture of metal hydrate nitrate solution. Following is a conclusion of the findings of this chapter:

1. CCZ catalyst nanoparticle with a single crystalline phase of $Ce_{0.6}Zr_{0.4}O_2$ could be obtained below 20% of the Cu doping ratio by microwave denitration method.
2. The specific surface area of CCZ nanoparticles synthesized by citric acid method was around 20-30 m^2/g, which was only less than a half of that by microwave denitration method.
3. The specific surface area of CCZ nanoparticles synthesized by microwave denitration and citric acid methods decreased with increasing the Cu doping ratio.
4. With the same composition of ceria content in the CCZ catalyst product, the citric acid method can produce the CCZ catalyst with a little higher OSC value than those by microwave denitration method, due to its crystallinity phase.

5. From the XPS analysis, the Ce^{3+}/Ce content of CCZ nano-particles synthesized by microwave denitration method has a comparable value than that by the citric acid method, i.e. 4.2% and 5.6%, respectively.

5.5 References

[1] A. Martínez-Arias, M. Fernández-García, V. Ballesteros, L.N. Salamanca, J.C. Conesa, C. Otero, J. Soria, Characterization of high surface area Zr-Ce (1:1) mixed oxide prepared by a microemulsion method, Langmuir. 15 (1999) 4796–4802. doi:10.1021/la981537h.

[2] T. Khossusi, R. Douglas, G. McCullough, Measurement of oxygen storage capacity in automotive catalysts, Proc. Inst. Mech. Eng. Part D J. Automob. Eng. 217 (2003) 727–733. doi:10.1243/09544070360692113.

[3] H. Matsui, M. Motoyama, H2 /, 193 (1993) 298–299.

[4] Y. Nagai, T. Nonaka, A. Suda, M. Sugiura, Structure analysis of CeO2-ZrO2 mixed oxides as oxygen storage promoters in automotive catalysts, R&D Rev. Toyota CRDL. 37 (2002) 20–27. http://www.tytlabs.co.jp/english/review/rev374epdf/e374_020nagai.pdf.

[5] R. Rao, L. Li, F. Li, Effect of Sr on the properties of Ce – Zr – La mixed oxides, 71 (2006) 285–291. doi:10.2298/JSC0603285R.

[6] Z. Qu, Z. Wang, X. Zhang, H. Wang, Role of different coordinated Cu and reactive oxygen species on the highly active Cu–Ce–Zr mixed oxides in NH_3 -SCO: a combined in situ EPR and O_2 -TPD approach, Catal. Sci. Technol. 6 (2016) 4491–4502. doi:10.1039/C5CY02125A.

[7] M. Manzoli, R. Di Monte, F. Boccuzzi, S. Coluccia, J. Kašpar, CO oxidation over CuOx-CeO2-ZrO2catalysts: Transient behaviour and role of copper clusters in contact with ceria, Appl. Catal. B Environ. 61 (2005) 192–205. doi:10.1016/j.apcatb.2005.05.005.

[8] X.F. Dong, H.B. Zou, W.M. Lin, Effect of preparation conditions of CuO-CeO2-ZrO2 catalyst on CO removal from hydrogen-rich gas, Int. J. Hydrogen Energy. 31 (2006) 2337–2344. doi:10.1016/j.ijhydene.2006.03.006.

[9] S. Ali, L. Chen, F. Yuan, R. Li, T. Zhang, S.U.H. Bakhtiar, X. Leng, X. Niu, Y. Zhu, Synergistic effect between copper and cerium on the performance of Cux-

Ce0.5-x-Zr0.5(x = 0.1–0.5) oxides catalysts for selective catalytic reduction of NO with ammonia, Appl. Catal. B Environ. 210 (2017) 223–234. doi:10.1016/j.apcatb.2017.03.065.

[10] H.I. Hsiang, T.H. Chen, Electrical properties of low-temperature-fired ferrite-dielectric composites, Ceram. Int. 35 (2009) 2035–2039. doi:10.1016/j.ceramint.2008.11.004.

[11] Z. Yang, D. Mao, X. Guo, G. Lu, CO oxidation over CuO catalysts supported on CeO2-ZrO2prepared by microwave-assisted co-precipitation: The influence of CuO content, J. Rare Earths. 32 (2014) 117–123. doi:10.1016/S1002-0721(14)60040-5.

[12] S. Dey, D. Mohan, G.C. Dhal, R. Prasad, Copper based mixed oxide catalysts (CuMnCe, CuMnCo and CuCeZr) for the oxidation of CO at low temperature, Mater. Discov. 10 (2017) 1–14. doi:10.1016/j.md.2018.02.001.

[13] L.C. Wang, Y.M. Liu, M. Chen, Y. Cao, H.Y. He, G.S. Wu, W.L. Dai, K.N. Fan, Production of hydrogen by steam reforming of methanol over Cu/ZnO catalysts prepared via a practical soft reactive grinding route based on dry oxalate-precursor synthesis, J. Catal. 246 (2007) 193–204. doi:10.1016/j.jcat.2006.12.006.

[14] K. Fukui, Y. Igawa, N. Arimitsu, M. Suzuki, T. Segawa, K.I. Fujii, T. Yamamoto, H. Yoshida, Mechanism of synthesis of metallic oxide powder from aqueous metallic nitrate solution by microwave denitration method, Chem. Eng. J. 211–212 (2012) 1–8. doi:10.1016/j.cej.2012.09.032.

[15] G. Fu, D. Mao, S. Sun, J. Yu, Z. Yang, Preparation, characterization and CO oxidation activity of Cu-Ce-Zr mixed oxide catalysts via facile dry oxalate-precursor synthesis, J. Ind. Eng. Chem. 31 (2015) 283–290. doi:10.1016/j.jiec.2015.06.038.

[16] Y. Sakamoto, Y. Kizaki, T. Motohiro, New Direct Evaluation of Oxygen Storage / Release Capacity on Millisecond Time Scale, 37 (n.d.) 14–19.

[17] M. Sugiura, Oxygen storage materials for automotive catalysts: Ceria-zirconia solid solutions, Catal. Surv. from Asia. 7 (2003) 77–87. doi:10.1023/A:1023488709527.

[18] Y. Nagai, T. Yamamoto, T. Tanaka, S. Yoshida, T. Nonaka, T. Okamoto, A. Suda, M. Sugiura, X-ray absorption fine structure analysis of local structure of CeO2–ZrO2 mixed oxides with the same composition ratio (Ce/Zr=1), Catal. Today. 74 (2002) 225–234. doi:10.1016/S0920-5861(02)00025-1.

[19] J. Fan, X. Wu, X. Wu, Q. Liang, R. Ran, D. Weng, Thermal ageing of Pt on low-surface-area CeO 2 – ZrO 2 – La 2 O 3 mixed oxides : Effect on the OSC performance, 81 (2008) 38–48. doi:10.1016/j.apcatb.2007.11.022.

CHAPTER 6

Summary

5.1 Summary and Conclusions

The mechanism of microwave heating has been investigated using the developed single mode type of microwave thermogravimetric. The application of microwave heating on the synthesis of some particulate materials also has been carried out. For the conclusion of this dissertation, the major results are summaries as follows:

1. A single mode type microwave heating thermogravimetry apparatus was developed, and its microwave heating mechanism was investigated by measuring the temperature distribution and mass change during microwave heating process of CuO pellet. The maximum temperature of CuO pellet occurred on the side closer to the microwave inlet, with the temperature decreasing monotonously in the direction of the outlet. The temperature distribution in the CuO pellet was accurately determined by three-dimensional numerical simulation of the electromagnetic field and successfully validated with the temperature distribution measured by experimental apparatus. Moreover, the microwave absorption efficiency and the estimated permittivity loss of the CuO powder at various temperature condition during microwave heating process were agreed with the previously published result.
2. The K-zeolite from the coal fly ash and extracted solution of biomass incineration fly ash has been synthesized by microwave hydrothermal treatment. The zeolite crystal generation rate obtained by microwave heating was larger than those by oil-bath heating treatment, with the value of k (rate constant) 5.21×10^{-2} and 0.88×10^{-2}, respectively. It confirmed that microwave heating treatment can shorten the synthesis time of K-zeolite, compared to the required time when using oil-bath heating treatment. On the other hand, the adsorption capacities of the ammonium ions and the phillipsite-to-quartz peak intensity ratios obtained after treatment times more than 24 h were almost the same regardless of the heating method. It is indicating that the heating method did not affect the properties of the obtained zeolite.

3. NiCuZn ferrite nanoparticle were successfully synthesized by microwave direct denitration (MDD) method from an aqueous mixture of metal nitrate hydrate reagents. A single phase of NiCuZn ferrite could be obtained at the reaction temperature of more than 900^{o}C with the average particle diameter about 30 mm. This average particle diameter was less than one-fifth of that NiCuZn ferrite synthesized by solid state reaction (SSR) method. The saturation magnetization of product synthesized by MDD method was found 25.08 emu/g, which was more than three time that by SSR method. On the other hand, the coercivity of the product synthesized by MDD, 55.21 Oe was found about half of that obtained by SSR method. This result suggests that the MDD method could provide more attractive magnetic characteristics of NiCuZn ferrite nanoparticle to the product powder. For further research, the electrical properties of NiCuZn ferrite synthesized by this method is necessary to be investigated as an application of MLCI fabrication.
4. The CCZ nanoparticles catalyst has been synthesized by microwave denitration method from the mixture of metal nitrate hydrate solutions and compared their properties with those by citric acid method. The CCZ nanoparticles could be obtained by both method with %mol doping ratio of Cu content less than 20%. The specific surface area of CCZ nanoparticles synthesized by microwave denitration method was found larger than those by citric acid method, i.e. 68 m^2/g and 30 m^2/g, respectively. The specific surface area of CCZ nanoparticles synthesized by both methods decreased with increasing the Cu doping ratio. With the same composition of ceria content in the CCZ catalyst product, citric acid method can produce the CCZ catalyst with a little higher OSC value than those by microwave denitration method. Further, the Ce^{3+}/Ce content of CCZ nanoparticles synthesized by microwave denitration method has a comparable value than that by citric acid method, i.e. 4.2% and 5.6%, respectively.
5. The present research is expected to be useful for the improvement of particle technology, especially concerned to the application of microwave heating treatment. For the further research, other materials could be used regarding the investigation of reaction mechanism using microwave heating.

Acknowledgement

Praise to ALLAH SWT almighty for HIS merciful blessing.

I am indebted to my supervisor, Professor Kunihiro Fukui for the guidance, advice, and the support during my study in Hiroshima University. I also would like to thank Assistant Professor Tomonori Fukasawa for the help and supports during in laboratory. And special thanks to Professor Manabu Shimada, Professor Nakai Satoshi, and Associate Professor Toru Ishigami for their patience, advice, and support as referee members.

For microwave research team in the laboratory, Dr. Tomoomi Segawa, Hamaba san, Riku san, Horigome san, and Shinokawa san, thank you so much. For my friends, Sunada san and Irwan for the help in daily life. And for all member of Fine Particle Technology Laboratory that I could not mention the name one by one, thank you very much.

I also thank Prof. Sugeng Winardi, Dr. Eng. Siti Machmudah, and Dr. Tantular Nurtono from Institut Teknologi Sepuluh Nopember for their continuous supports, even long before the commencement of my Ph.D.

A special mention to Ministry of Education, Culture, Sports, Science, and Technology of Japan, for the Ph.D. scholarship and to Hosakawa Micron Powder Foundation for the research fund.

Last but not least, I would like to really thank my parents, Sri Sulistiani and Achmad Basuni, my brother, Achmad Arthur Pradana, and my sister, Astri Azizun Nisa', for their prayers, love, support, and motivation. Without them, I might not be able to achieve anything.

Achmad Dwitama Karisma

Higashi Hiroshima, September 2018

List of Publications

1. A.D. Karisma, T. Hamaba, T. Fukasawa, A.-N. Huang, T. Segawa, K. Fukui, Validation of measured microwave absorption and temperature change for development of a single-mode-type microwave heating thermogravimetry apparatus, Rev. Sci. Instrum. 88 (2017) 024101. doi:10.1063/1.4974813.
2. T. Fukasawa, A. Horigome, A.D. Karisma, N. Maeda, A.N. Huang, K. Fukui, Utilization of incineration fly ash from biomass power plants for zeolite synthesis from coal fly ash by microwave hydrothermal treatment, Adv. Powder Technol. 29 (2018) 450–456. doi:10.1016/j.apt.2017.10.022.
3. A.D. Karisma, Y. Shinokawa, T. Fukasawa, A. Huang, K. Fukui, NiCuZn-ferrite nanoparticle synthesis from metallic nitrate solution using microwave denitration method, The 7th Asian Particle Technology Symposium (APT 2017) O2-1 65.
4. A.D. Karisma, R. Nakamura, T. Fukasawa, T. Ishigami, K. Fukui, Synthesis of Cu-Ce-Zr oxide catalyst nanoparticle by microwave denitration method, The 6th International Conference on the Characterization and Control of Interfaces for High Quality Advanced Materials (ICCCI 2018) P-A-09.